Feshbach Resonances in Ultracold Bose-Fermi Mixtures

by

Daniele Carlo Enrico Bortolotti

B.S., Western Michigan University, 2001

M.S., University of Colorado, 2004

A thesis submitted to the

Faculty of the Graduate School of the

University of Colorado in partial fulfillment

of the requirements for the degree of

Doctor of Philosophy

Department of Physics

2007

This thesis entitled:
Feshbach Resonances in Ultracold Bose-Fermi Mixtures
written by Daniele Carlo Enrico Bortolotti
has been approved for the Department of Physics

John L. Bohn

Murray Holland

Date

The final copy of this thesis has been examined by the signatories, and we find that both the content and the form meet acceptable presentation standards of scholarly work in the above mentioned discipline.

Bortolotti, Daniele Carlo Enrico (Ph.D., Physics)

Feshbach Resonances in Ultracold Bose-Fermi Mixtures

Thesis directed by Prof. John L. Bohn

In the wake of successful experiments in Fermi condensates, experimental attention is broadening to include resonant interactions in degenerate Bose-Fermi mixtures. In this thesis we wish to study the equilibrium properties of the fermionic molecules that can be created in such a mixture.

To this end, we first discuss the two body properties of the system, and introduce the model Hamiltonian we use to describe the resonant physics, highlighting its virtues, as well as its limitations. We then proceed by analyzing the mean field solution of this model, by studying both the equilibrium problem, and the non-equilibrium equations of motion, thus developing a powerful language to discuss the system. We then highlight the limitations of the mean-field approach, and develop a numerically tractable generalized version of this theory, which is able to correctly describe the two-body properties of the system in the low-density limit.

Finally, we study the properties of the system using this generalized mean-field theory, by first analyzing the two-body scattering matrix in the many-body environment, assessing its complex poles in order to understand the stability properties of the Feshbach molecules in the gas. Secondly we solve the equilibrium equations self-consistently, to study the molecular populations and density distributions at equilibrium, as a function of external bias magnetic field.

Acknowledgements

First and foremost a huge thanks to John Bohn, who was the greatest advisor anyone can hope for. Aside from teaching me to be a physicist, he has allowed me to pursue my research interests freely, but always keeping me honest about my results. He has also given me a lot of trust and understanding, which helped me work through of some personal challenges throughout the years.

I also wanted to thank Alexandr Avdeenkov, for teaching me most of what I know about many-body physics, and for his patience with many of my trivial questions. I would also like to thank Shai Ronen, Murray Holland and Victor Gurarie for the substantial amount of time they spent helping me. A big thanks to Massimo Inguscio and the LENS cold atoms groups, for letting me spend time there, and for their help throughout these years.

On a more personal note, I would also like to acknowledge the moral support of my good friends Stefano Tonzani and Josh Dunn, who made coffee at JILA a much more pleasant experience, and for their physical insights and suggestions, and Ed Meyer, for helping me release some steam by means of the most terrifying of Horror movies.

Finally I must thank my wife, Khouloud Manai, and my daughters Sara and Nur, for inspiring me and motivating me, and for putting up with me in the harder times. My parents and my brother for their help, and for making me close to home in spite of the many miles.

Support for this work came from the DOE and The Keck foundation.

Contents

Chapter

Figures

Figure

Chapter 1

Introduction

The use of magnetic Feshbach resonances to manipulate the interactions in ultracold quantum gases has enabled the study of an astounding amount of physics. Notable examples, include the study of the crossover between BCS (Bardeen-Cooper-Schrieffer [1]) and BEC (Bose-Einstein Condensate [2, 3]) superfluidity in ultracold Fermi gases [4, 5, 6], and the "Bose Nova" collapse in Bose gases [7]. Recent experimental developments, [8, 9, 10, 11] have enabled the creation of an ultracold mixture of bosons and fermions, with an interspecies Feshbach resonance, opening the ground for what may very well be a new prolific source of physical insight.

From the theoretical point of view, on the other hand, studies of Bose-Fermi mixtures to date have been mostly limited to non resonant physics, focusing mainly on mean field effects in trapped systems [12, 13, 14, 15, 16, 17, 18, 19, 20, 21, 22], phases in optical lattices [23, 24, 25, 26, 27],or equilibrium studies of homogeneous gases, focusing mainly on phonon induced superfluidity or beyond-mean-field effects [28, 29, 30, 31, 32, 33, 34]. Pioneering theoretical work on the resonant gas include [35], whereby a mean-field equilibrium study of the gas is supplemented with a beyond mean-field analysis of the bosonic depletion, and [36], where an equilibrium theory is developed using a separable-potentials model.

The aim of this thesis is to develop and solve a mean-field theory describ-

ing an ultracold atomic Bose-Fermi mixture in the presence of an interspecies Feshbach resonance. This goal appears innocuous enough at first sight, since mean-field theories for resonant Bose-Bose [37, 38] and Fermi-Fermi [39, 40, 41] gases exist, and have studied extensively. In both of these theories, the mean-field approximation consists of considering the bosonic Feshbach molecules as being fully condensed, and this greatly simplifies the treatment, since the Hamiltonian reduces to a standard Bogoliubov-like integrable form [42].

The fundamental difference between these examples and the Bose-Fermi mixtures is that in the latter the Feshbach molecules are fermions, and therefore their center of mass momentum must be included explicitly. The most obvious mean-field approach consists in considering the atomic gas to be fully condensed. However, as we will see in more detail in the body of the thesis, resonant molecules are really composed of two bound atoms, which spend their time together vibrating around their center of mass. It follows that outright omission of the bosonic fluctuations of the atoms, disallows the bosonic constituents to oscillate (i.e. fluctuate) at all, and therefore this leads to an improper description of the the two-body physics of the gas.

This thesis is organized as follows. In chapter 2 we lay the groundwork by briefly introducing the main scattering theory concepts necessary to approach the problem. We then proceed by describing the low-energy resonance physics in general terms, and to introduce the main classes of resonances which exist. An introduction to the physics of magnetic Feshbach resonances in alkali atoms follows, where we outline in detail the nature of the interatomic interaction using the language of ultracold scattering physicists.

In chapter 3 we introduce the field theory model used to study these resonances, describing in detail the paramerization used, and outlining the exact solution of this model in the two-body limit. The chapter ends with a test of

this two-body theory, by comparing the binding and resonance energies predicted by the model and the virtually-exact analogues obtained from two-body close coupling calculations.

Chapter 4 introduces the simplest mean-field many-body theory of the gas, obtained by disregarding all bosonic fluctuations. The solution of the theory is outlined, and its limitations highlighted. We recognize here that, in spite of these limitations, mean-field theory gives us a language useful to deal with the problem, which will persist even beyond the limits of applicability of the theory itself. The chapter then proceeds to describe a non-equilibrium approach to the problem, whereby the beyond mean-field HFB equation of motion are shown to reduce to their mean-field equivalent, highlighting the importance of properly accounting for the bosonic fluctuations.

Finally in chapter 5 we introduce our generalized mean-field theory, which is, in short, similar to the mean-field theory described in chapter 4, but with the notable improvement of using properly renormalized molecules as building blocks, instead of their bare counterparts. This approach is not trivially described in the Hamiltonian formalism, where substituting dressed molecules for free ones would lead to double counting of diagrams. In this chapter we therefore shift to the Green-function/path-integral language, where this double-counting can be avoided quite easily. Finally we proceed to the numerical solution of this theory, and note that for narrow resonances the results are in line with their mean-field equivalents. This encourages us to develop a simple theory to study the molecular formation via magnetic-field ramps, and, using an approach based on the Landau-Zener formalism [43, 44], we derive analytic expressions.

Throughout this thesis, we work with zero temperature gases, in the free space thermodynamic limit. These are limitations which render the results obtained here hard to directly compare with experimental results. One of the main

possible future directions of this work should include solving the same problem in a trap, and generalization to higher temperatures.

This thesis, by its very nature, represents a synthesis of the work of this author during the last few years. We therefore draw heavily from published work which resulted from this effort, and in particular [45] and [46].

Chapter 2

Scattering Theory: The Starting Point

The rich physics of the system we intend to study is in large part due to the exotic nature of the interactions between its various constituents. An understanding of the two-particle dynamics is therefore paramount to any analysis which may follow, and it is the aim of this chapter to introduce this physics, by first providing a general outline of cold collision theory, and in particular resonant scattering theory, and then describing how Feshbach resonances arise in ultracold collisions between alkali atoms.

2.1 Fundamental Concepts

The essence of the two-body physics we are interested in is low energy resonant scattering, in general, and magnetic-field Feshbach resonances in alkali gases in particular. In the following we introduce some of the basic concepts and equations we will need to talk about these resonances; focusing on interactions between distinguishible particles, interacting via a central potential. The conventions we use here are those found in [47].

A prototypical scattering experiment consists of a beam of identical particles incident upon a target, from which they scatter. The beam is assumed to be described as a plane wave of well defined momentum k and from a specific direction, which we will choose as our $\hat{z}$ axis. Furthermore the properties of the scattered

particles are measured far enough away from the target ($r \to \infty$) that interactions with it no longer influence them. Under these circumstances the wavefunction of the incident particles can be written, in center of mass coordinates,

$$\psi(r) = \frac{1}{(2\pi)^{3/2}} \left[e^{ikz} + f(k,\theta) \frac{e^{ikr}}{r} \right]. \tag{2.1}$$

The first term in this expression represents the incoming plane wave, and the second term represents the scattered spherical wave, where $f(\theta)$ is the amplitude of the scattered wave, and is therefore known as "scattering amplitude". The scattering amplitude contains all the physical information about the scattering process, and it can be used to calculate any observable. Also we should point out that the wavefunction is normalized to unity incoming flux.

For central potentials, such as (for the most part) alkali atom collisions, it is often convenient to separate the angular degrees of freedom by expanding the wave function in spherical harmonics, or " partial waves", whereby the scattering amplitude can be written as

$$f(k,\theta) = \sum_l (2l+1) f_l(k) P_l(cos\theta), \tag{2.2}$$

where where P_l is a Legendre polynomial, and f_l are the partial-wave amplitudes. We then expand the incoming plane wave in spherical waves, and take the asymptotic form, obtaining

$$e^{ikz} \to \sum_l (2l+1) P_l(cos\theta) \left[\frac{e^{ikr} - e^{i(kr - l\pi)}}{2ikr} \right] \tag{2.3}$$

Inserting 2.2 and 2.3 into eq. 2.1, and expanding the incoming plane wave in spherical waves, we obtain, after some simplifications,

$$\psi(r) = \frac{1}{(2\pi)^{3/2}} \sum_l \frac{P_l(cos\theta)}{2ik} \left[(1 + 2ikf_l(k)) \frac{e^{ikr}}{r} - \frac{e^{-i(kr - l\pi)}}{r} \right]. \tag{2.4}$$

From this expression we see that the quantity $1 + 2ikf_l(k,\theta)$ determines the physics of the scattering, such that if $f_l \to 0$ the outgoing wave is identical to

the incoming wave, and no scattering occurred. Furthermore if we note that the incoming flux must equal the outgoing flux, then $|1+2ikf_l(k,\theta)|^2 = 1$, and we can therefore define a quantity $\delta_l(k)$, such that $1+2ikf_l(k,\theta) = e^{2i\delta_l(k)}$, and insert into eq. 2.4, the effect of the scattering event is therefore to generate a "phase-shift" $\delta_l(k)$ in the outgoing wave which would vanish, had no scattering occurred.

The quantity

$$S_l = e^{2i\delta_l(k)} = 1 + 2ikf_l(k) \tag{2.5}$$

is so ubiquitous in scattering theory, that it has been dubbed the "scattering (S-) matrix". A close cousin of S_l is the T-matrix, defined as

$$T = \frac{\pi i}{\mu k}(S-1), \tag{2.6}$$

Where μ is the reduced mass. This quantity will be of fundamental importance in the many-body treatment, and the definition in eq.2.6 will be much more convenient for that purpose which is the reason why we will adopt it.

An observable of particular interest in scattering theory is the scattering cross section σ, defined as the number of particles scattered per unit time as a fraction of the number of incident particles per unit area per unit time. From the discussion above about the role of the scattering amplitude we can readily deduce

$$\sigma(k) = \int |f(k,\theta)| d\Omega = \sum_l \frac{4\pi}{k^2}(2l+1)sin^2(\delta_l) = \sum_l 4\pi(2l+1)|f_l(k)|^2. \tag{2.7}$$

It is often useful to define partial cross sections σ_l so that

$$\sigma(k) = \sum_l \sigma_l(k). \tag{2.8}$$

2.2 Low Energies Collisions and Resonances

The physics of low energy collisions is characterized by the fact that the great majority of relevant observables can be characterized universally with a

handful of parameters, by only knowing the features of the long-range physics. This universality is quite remarkable in its own right, and has the useful side effect of allowing one to explore the fundamental scattering properties of very complex systems without the need for sophisticated potential surfaces.

If we could define a length-scale R_0 separating short-range and long-range physics, a collision would be defined as "low energy" if $R_0 << 1/k$, where k is the collision momentum [48], and $2\pi/k$ is the deBroglie wavelength. The use of the conditional here is due to the fact that in the great majority of physically relevant systems, potentials generally asymptote to zero, so that a clear cut definition of R_0 is not available. However if the potentials approach zero fast fast enough (we'll see shortly what "enough" means), then R_0 can be defined heuristically.

In the case of alkali atoms, R_0 is generally identified with the van der Waals length $R_0 = (\mu C_6/8\hbar^2)^{1/4}$ [49], where C_6 is the parameter defining the perturbative long-range van der Waals potential $-C_6/r^6$.

2.2.1 Effective Range Expansion

We will begin with the radial Schrödinger equation for the scattering of two particles (setting $\hbar = 1$)

$$u_l'' + \left(k^2 - 2mV - \frac{l(l+1)}{r^2}\right) u_l = 0, \tag{2.9}$$

where u_l is the radial wavefunction, $k = \sqrt{2\mu E}$ is the collision momentum, V is the interaction potential, and l is the orbital angular momentum quantum number.

Since we here postulate that the energy is low, and $1/k >> R_0$, we can say that if $r << R_0$, then $k^2 << 2mV$, and in this region eq. 2.9 reads

$$u_l'' + \left(-2mV - \frac{l(l+1)}{r^2}\right) u_l = 0. \tag{2.10}$$

On the other hand if $r >> 1/k$ then since $1/k >> R_0$, and by definition of R_0 , $V \to 0$, and eq. 2.9 reads

$$u_l'' + \left(k^2 - \frac{l(l+1)}{r^2}\right) u_l = 0. \tag{2.11}$$

In this region the solution is readily found to be

$$A_l(\cos(\delta_l) j_l(kr) + \sin(\delta_l) n_l(kr)), \tag{2.12}$$

where j and n are the regular and irregular spherical Bessel functions, δ_l, is the scattering phase shift, remarkably the same phase shift described above. This can be verified by plugging eq. 2.5 into 2.4, and expanding the exponentials in spherical Bessel functions. Finally A_l is an unimportant (at least for the purposes of this discussion) flux normalization constant.

Near threshold the short-range solution does not depend significantly on energy, leaving all of the energy dependence in the long-range region. In the intermediate $R_0 < r < 1/k$ region, it turns out that the solution is also energy independent, provided that V approaches zero faster than $1/r^{2l+3}$. This can be verified by guessing the solution $u_l = c_1 r^{l+1} + c_2 r^{-l}$, and checking it by plugging into eq.2.9. In this regime, $r > R_0 >> 1$, therefore both $V u_l$ and $k^2 u_l$ are much smaller than the other terms, and eq.2.9 becomes

$$u_l'' - \frac{l(l+1)}{r^2} u_l = 0. \tag{2.13}$$

Since the solution is virtually energy independent for the range of r's in which V acts, then so is the logarithmic derivative $Y_l = 1/u_l \frac{du_l}{dr}$. The scattering phase shift is in turn found by matching Y with the logarithmic derivative of the long-range solution (eq. 2.12) at some large distance $r = R$, obtaining

$$\cot(\delta_l) = \frac{kRn_l'(kR) - Y_l j_l(kR)}{kRj_l'(kR) - Y_l n_l(kR)}. \tag{2.14}$$

Finally, since the only energy dependence in eq. 2.14 is in k, (and not in Y_l) it is a simple, though tedious, algebraic exercise, using the properties of the spherical Bessel functions, to show that as $k \to 0$, $k^{2l+1}cot(\delta_l) \to const.$, and that only even powers of k appear in the Taylor expansion of this quantity around zero,

$$k^{2l+1}\cot(\delta_l) = F_l(k^2) \approx -\frac{1}{a_l} + \frac{1}{2}r_l k^2 + \cdot. \tag{2.15}$$

In the case of s-wave collisions, ($l = 0$) the quantities a_0 and r_0 are known as "scattering length" and "effective range."

As we saw in section 2.1, the scattering amplitude is a measure of the strength of the scattering. A particularly useful form in which to write this quantity is derived by solving eq. 2.5 for f_l in terms of δ_l, thus obtaining, in combination with equation 2.15

$$f_l(k) = \frac{1}{k\cot(\delta_l) - ik}. \tag{2.16}$$

From this expression we can readily write

$$f_l(k) = \frac{1}{k^{-2l}F_l(k^2) - ik} \approx \frac{1}{k^{-2l}(-1/a_l + r_l k^2) - ik}. \tag{2.17}$$

2.2.2 Resonances at Low energy

It is instructive to write the approximate version of equation 2.17, in terms of the collision energy $E = k^2/2\mu$, where μ is the reduced mass. We then obtain the expression

$$f_l = \frac{1}{k}\frac{\Gamma k^{2l+1}}{(E - E_r) - i\Gamma k^{2l+1}}, \tag{2.18}$$

where we have defined $\Gamma = \frac{1}{2r_l\mu}$, and $E_r = \frac{1}{a_l r_l \mu}$. From equation 2.7, we then get

$$\sigma_l = \frac{4\pi}{k^2}(2l+1)\frac{(\Gamma k^{2l+1})^2}{(E - E_r)^2 + (\Gamma k^{2l+1})^2}. \tag{2.19}$$

This expression is known as a Breit-Wigner profile, in honor of its discoverers.

The most remarkable feature of equation 2.19 if that as $E \to E_r$, the cross section is enhanced, and reaches its maximum possible value. Also in this regime the S-matrix reaches 1, and we say that the systems reaches "unitarity". We call this phenomenon a resonance. Furthermore, if the resonance energy E_r is large enough, and Γ is small enough that over the width of the resonance variations in $1/k^2 l$ are negligible, then we see that the resonance is Lorentzian in shape, with full width at half maximum equal to 2Γ, see fig.2.1. We should also note that the enhancement of the cross-section to unitarity requires that the phase shift $\delta_l = \pi/2$.

To better understand the physics of a resonant state, we turn to equation 2.4, and imagine a scattering event at "negative energy."(i.e. $k \to i\kappa$). We then get

$$\psi \propto A\left(S(\kappa)\frac{e^{-\kappa r}}{r} + \frac{e^{\kappa r}}{r}\right). \tag{2.20}$$

Solutions to the Schrödinger equation in this regime should lead to bound states, with boundary conditions implying exponentially decaying wavefunctions. Therefore, the coefficient A must vanish, as the s-matrix S diverges, such that the product SA is held constant, so that the normalization of the wavefunction is finite. We see in this case that a pole in the s-matrix implies a bound state. At a resonance, we saw above, the scattering amplitude has a (complex) pole, which means that the s-matrix also has one. In this light we can think of poles in the scattering amplitudes as either bound states, if real, or as resonances, if complex.

In somewhat qualitative terms, we may say that resonances indicate the presence of the "shadow" of a bound states (known as a quasi-bound state), whereby when the two particles scatter at this energy they spend an unusually large time close together, in a bound-like state, but eventually come apart. The amount of time they spend together is inversely related to the imaginary part of

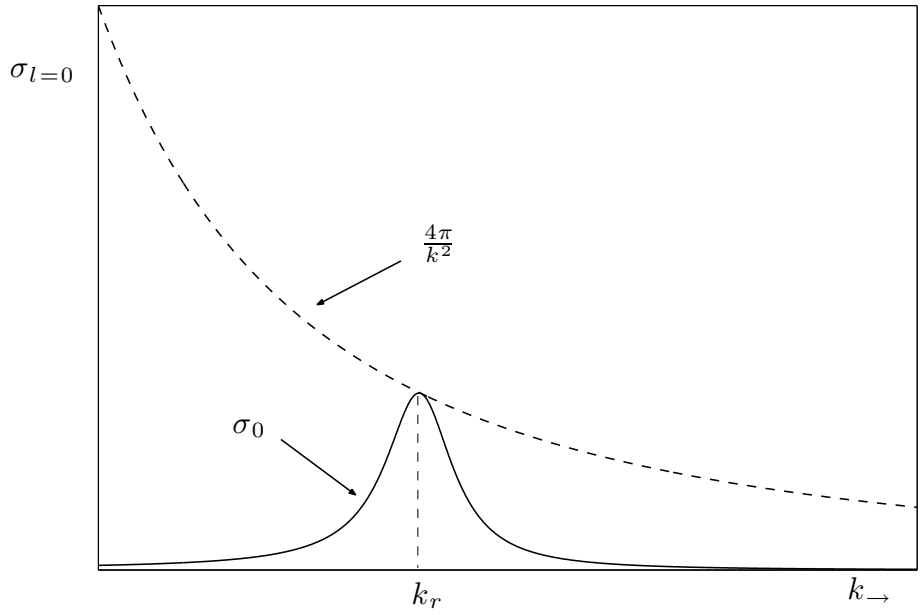

Figure 2.1: Typical $l = 0$ cross-section versus momentum profile near an s-wave resonance (solid line), and its unitarity limit (dashed line).

the resonant energy, or, more precisely, to width of the resonance.

2.3 Types of Resonances

In the previous section we have introduced the concept of scattering resonance by disregarding the internal degrees of freedom of the colliding objects, and thus focusing on the simplest possible example. Here we will briefly introduce other types of resonances, including the Feshbach resonance, complementing the previous discussion by focusing mainly on the phenomenological characteristics of resonant scattering.

2.3.1 Potential Resonances

In section 2.2.2 we mentioned that resonance states are "shadows" of real bound states. Here we would like to better qualify this statement, by introducing the simple example of a "potential resonance", graphically illustrated in fig. 2.2. In this thought experiment we will consider an attractive interparticle potential, and we analyze what the effect on the physics would be if we could tune its depth.

For a perturbative attractive potential, the scattering length is negative. This can be understood by noting that the wavefunction in the absence of this potential is $\sin(kr)$. Since the potential is negative, for small r the deBroglie wavelength will be slightly smaller, and the wavefunction will thus oscillate slightly faster, accumulating a small positive phase. Since for $a_{sc} = -\lim_{k\to 0} \tan(\delta)/k \approx -lim_{k\to 0}\ \delta/k$, then if $\delta > 0$, $a_{sc} < 0$.

As the potential is made deeper, and thus less perturbative, the phase shift increases, and the scattering length becomes more and more negative. The phase shift eventually reaches π, adding a node to the wave function, and causing the scattering length to diverge through negative infinity. This added node is a signature of a new bound-state having appeared. Increasing the potential further

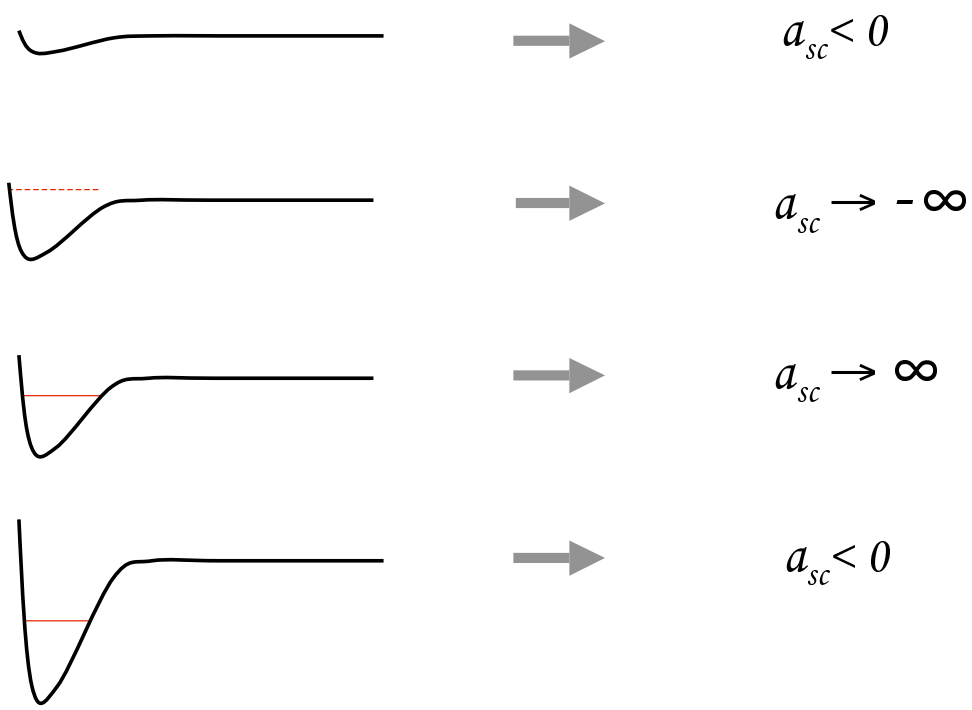

Figure 2.2: Conceptual representation of a potential resonance. A weakly attractive potential with small negative scattering length is represented in the top figure. As the depth of the potential is increased it becomes more and more attractive, and the scattering length increases, as a resonant state approaches threshold. Eventually the resonance crosses threshold, and a bound state is created, as the scattering length remains large, but changes sign abruptly. As the potential becomes deeper, the bound state becomes more deeply bound, and the scattering length decreases, eventually becoming negative once again. The whole process repeats as more and more bound states are created

causes the scattering length to initially change sign abruptly, and subsequently diminish from positive infinity, through zero, and again through negative infinity as another bound-state is added to the potential.

2.3.2 Shape resonances

Another example of single-channel resonance, is the shape resonance. This resonance is characterized by the presence of a potential barrier in the interparticle potential. If we imagined the barrier to be infinitely high, we could easily convince ourselves of the existence of a bound-state behind it. As the barrier becomes finite, tunneling will allow the particles to separate, though the presence of the barrier will cause them to spend a long time close to each other, in correspondence to energies around where the original bound-state was. This phenomenon causes an amplification of the scattering cross-section, causing a resonance.

Examples of shape resonances are ubiquitous in nonzero partial-wave scattering between alkali atoms, where at long range the repulsive centrifugal potential $l(l+1)/2\mu r^2$ is stronger than the (negative) Van der Waals potential $-C_6/r^6$, while at short range the opposite is true.

2.3.3 Feshbach Resonances

Feshbach resonances are different from all other resonances described so far, in that they are an intrinsically multi-channel phenomenon. What this means is that they are the consequence of the complicated interplay between different internal states of the colliding particles.

Using qualitative reasoning similar to that used above, we can think of a two channel scattering problem, for example a spinless particle (particle 1) colliding with a two state particle (particle 2), where state $|1\rangle$ and state $|2\rangle$ are separated by energy Δ, $|2\rangle$ being the higher energy one. There are therefore two distinct ways

in which the two object can interact, namely particle 1 with particle 2 in either of the two states. This implies that there are two distinct interaction potentials, characterizing the two collisions. Let us assume that the potential for state $|2\rangle$ collisions hold a bound state ϵ, with binding energy $B < \Delta$.

Let us now introduce the concept of coupling: the possibility, that is, that a collision between the two particles could change the state of particle 2. In the absence of coupling, a particle of type 1, and one of type 2 in state $|2\rangle$ could be bound in state ϵ for ever. If coupling is introduced, since $B < \Delta$, then it would be energetically favorable for particle 2 to change state, and for the two particles to break-up, implying that ϵ would no longer be a proper bound-state.

From a collisional point of view, consider a particle of type 1 colliding with a particle of type 2 in state $|1\rangle$, at an energy smaller that Δ. In this example, it is possible that that during the scattering event particle 2 will visit state $|2\rangle$ temporarily, though it is energetically impossible it will leave the collision in this state. If the collision energy is close to $\Delta - B$ (the position of state ϵ relative to state $|1\rangle$ threshold), then the time the two particles spend together before breaking up becomes quite long, and we identify a resonance.

2.4 Magnetic Feshbach Resonances in Alkali Gases

In this section we will briefly introduce the physics of ultracold collision of alkali atoms in a magnetic field, from the perspective of an atomic physicist. Because of the scope of this thesis, we will not dwell substantially on this point, but only give a general overview. A more accurate and detailed account is given in [50].

Magnetic Feshbach resonances in alkali atoms, are the consequence of the interplay between the magnetic/hyperfine degrees of freedom, dominant at long-range, and the interatomic interaction, which is diagonal in the electronic spin

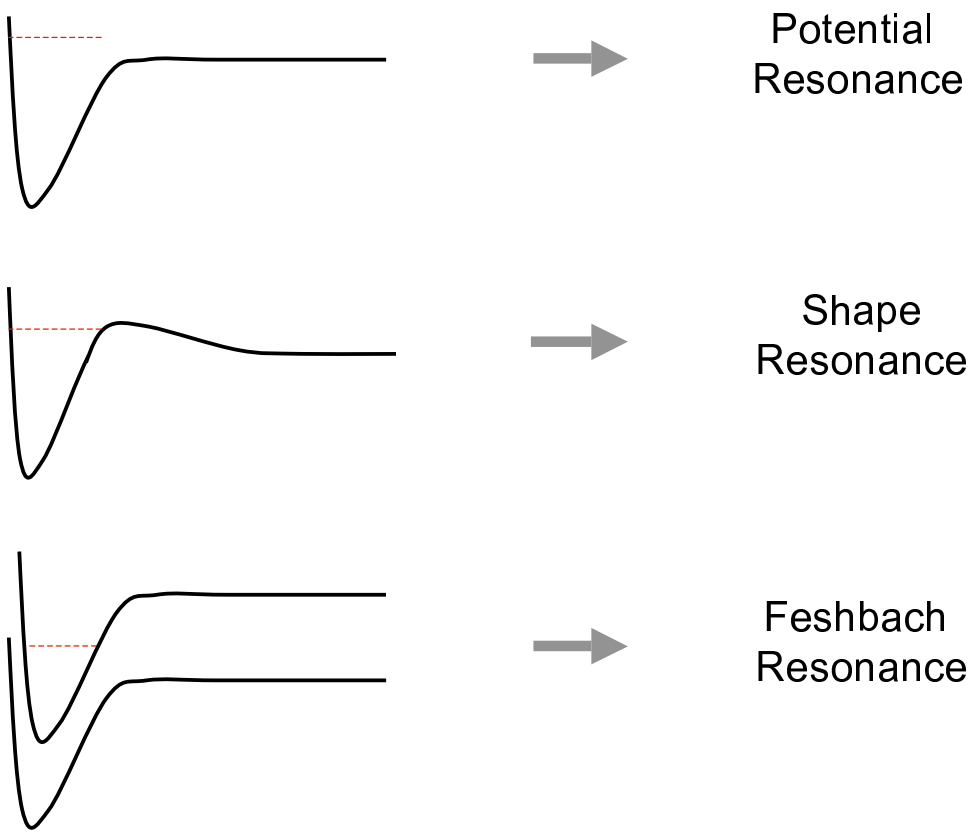

Figure 2.3: Pictorial representation of the three main types of resonances described in the text.

degrees of freedom, and dominates the short-range physics.

The Hamiltonian can be schematically written as

$$H = T(R) + H^M + H^{HF} + V(R), \tag{2.21}$$

where $T(R) = -\frac{1}{2\mu}\frac{\partial}{\partial R} + \frac{l(l+1)}{R^2}$ is the kinetic term in the interparticle coordinate R, $V(R)$ is the interparticle potential, H^M is the Zeeman Hamiltonian, and H^{HF} is the hyperfine Hamiltonian.

We should note that while $V(R) \to 0$ as $R \to \infty$, H^M and H^{HF} are very nearly R-independent, and they persist at $R \to \infty$, thus defining the thresholds of the problem. From this follows that the basis we use to describe the problem must diagonalize these two components of the Hamiltonian. Simultaneously, we will see that this basis does not diagonalize $V(R)$, and these off-diagonal elements will provide the coupling which will lead to the existence of Feshbach resonances.

The operational procedure, which we will describe in more detail below, may be outlined as follows:

- basis $|a\rangle$ diagonalizes $V(r)$
- basis $|b\rangle$ diagonalizes H^{HF}.
- basis $|\tilde{b}\rangle$ diagonalizes $H^{HF} + H^M$.

We need to express everything in basis $|\tilde{b}\rangle$, which are the physically relevant scattering stares at $R \to \infty$; to this end we take the following steps:

(1) Express $H^{HF} + H^M$ in basis $|b\rangle$; this can be done analytically, and leads to a non-diagonal matrix.

(2) Diagonalize numerically this matrix, to obtain the diagonal eigenvalue matrix $\lambda_{\tilde{b}}$, and the eigenvector transformation matrix $U_{b\to\tilde{b}} = \langle b|\tilde{b}\rangle$. This step is known as "field dressing"

(3) Transform $V(R)$ from the $|a\rangle$ basis representation (in which it is diagonal) to the $|b\rangle$ basis; this can also be done analytically, and leads to a non-diagonal matrix

(4) Transform $V(R)$ from the $|b\rangle$ basis representation to the $|\tilde{b}\rangle$ basis representation, using $U_{b\to\tilde{b}}$.

At this point the whole Hamiltonian is expressed in the appropriate long-range basis, and it is possible to run a close coupling scattering calculation.

In the following section we will discuss this procedure in more detail, filling in the missing parts of this outline, and, in particular, the quantum numbers associated with the $|a\rangle$, $|b\rangle$ and $|\tilde{b}\rangle$ basis.

2.4.1 $1 \otimes 1$-Particle Physics

We will begin our discussion by studying the $R \to \infty$ Hamiltonian, to define the operational long-range basis $|\tilde{b}\rangle$. The long-range physics of the problem consists, by definition, of two distant non-interacting atoms. This implies that the most physically relevant representation must be a direct product of single-atom representations. This allows us to treat each atom individually, and then put the two pictures together. We therefore write the magnetic Hamiltonian for atoms 1 and 2 as

$$H_a^M = H^Z + H^{HF} = H_1^Z + H_1^{HF} + H_2^Z + H_2^{HF} \tag{2.22}$$

Assuming without loss of generality that the magnetic field $\mathbf{B} = B\hat{z}$,

$$\begin{aligned} H_a^Z &= -B\left[g_e\mu_e s_z^a + \mu_N g_N^a i_z^a\right] \\ H_a^{HF} &= \left(\vec{f}_a^{\,2} - \vec{s}_a^{\,2} - \vec{i}_a^{\,2}\right) C \end{aligned} \tag{2.23}$$

In these expressions $\vec{s}_a$ and $\vec{i}_a$ are respectively the electron spin and nuclear spin operators of atom a (which refers to either 1 or 2), and $\vec{f}_a = \vec{s}_a + \vec{i}_a$ is the total

spin, while s_z^a, i_z^a and f_z^a are the corresponding $\hat{z}$ projections. Also μ_e and g_e are the electron magnetic moment and g-factor, while μ_N^a and g_N^a are their nuclear counterparts for atom a. Finally $C = \Lambda_a \frac{\Delta_a}{2i_a+1}$, where Δ_a is the hyperfine energy splitting, and $\Lambda_a = sign(\mu_N^a)$. If $\Lambda = 1$, then the hyperfine structure is said to be "standard", otherwise it is said to be "inverted."

With these definitions, we can readily identify the basis which diagonalizes H_a^{HF}, namely $|f_a m_a\rangle$, and we can write

$$\langle f_a' m_a' | H_a^{HF} | f_a m_a \rangle = \Lambda_a \frac{\Delta_a}{2i_a+1} \delta_{f_a, f_a'} \delta_{m_a, m_a'}. \tag{2.24}$$

The matrix H_a^Z in this basis, on the other hand, is not diagonal, and its matrix elements read

$$\begin{aligned}\langle f_a' m_a' | H_a^Z | f_a m_a \rangle = -B \sum_{m_{sa}+m_{ia}=m_a} & ms \left[g_e \mu_e m_{sa} + \mu_N g_N^a m_{ia} \right] \times \\ & \langle f_a m_a | s_a m_{sa}; i_a m i_a \rangle \langle f_a' m_a' | s_a m_{sa}; i_a m i_a \rangle,\end{aligned} \tag{2.25}$$

where $\langle f\ m | s\ m_s; i\ m_i \rangle$ is a Clebch-Gordon coefficient coupling s and i into f.

Diagonalizing the matrix $\langle f_a' m_a' | H_a^{HF} + H_a^Z | f_a m_a \rangle$ generates a set of eigenvalues ϵ_a, and an eigenvector transformation matrix

$$U_{f_a m_a \to \widetilde{f_a m_a}} = \langle f_a m_a | \widetilde{f_a m_a} \rangle. \tag{2.26}$$

It should be noted that $\tilde{f}$ is not a strictly good quantum number in the dressed basis, but given the small magnetic fields generally involved in the experiments (recall that $\tilde{f} \to f$ in zero field), the $\tilde{f}$ state is usually still "recognizable", and the single-particle states are still referred to using $\tilde{f}$.

So far we have worked focusing on a single atom; since $H^Z + H^{HF}$ is separable into 1-atom components. Obtaining a two-atom version of the Hamiltonian is just a matter of taking direct products, so that the basis $|\tilde{b}\rangle$ can be written as $|\widetilde{f_a m_a}\rangle |\widetilde{f_a m_a}\rangle$ (or equivalently$|\widetilde{f_a m_a}; \widetilde{f_a m_a}\rangle$, and the full transformation matrix

becomes

$$U_{f_1 m_1 f_2 m_2 \to \widetilde{f_1 m_1} \widetilde{f_2 m_2}} = U_{f_1 m_1 \to \widetilde{f_1 m_1}} \otimes U_{f_2 m_2 \to \widetilde{f_2 m_2}} = \langle f_1 m_1 | \widetilde{f_1 m_1} \rangle \langle f_2 m_2 | \widetilde{f_2 m_2} \rangle. \tag{2.27}$$

A plot of the hyperfine levels of ^{40}K and ^{87}Rb appears in fig. 2.4, along with a plot of the thresholds for the collision in the $|9/2 - 9/2\rangle|11\rangle$ state.

2.4.2 The Interparticle Potential

Alkali atoms have only a single valence electron, and we are only concerned with their orbital ground state which is an s-shell. It follows that the only electronic degrees of freedom which influence the interatomic interaction is the spin of this electron. In this regime, the interatomic potential $V(R)$ is therefore diagonal in the basis $|IM_I; SM_S>$, so that

$$\langle S'M'_S; I'M'_I | V(R) | SM_S; IM_I \rangle = \delta_{I,I'} \delta_{M_I, M'_I} \delta_{S,S'} \delta_{M_S, M'_S} \, V_S(R) \tag{2.28}$$

where $\vec{S} = \vec{s}_1 + \vec{s}_2$, $\vec{I} = \vec{i}_1 + \vec{i}_2$ and i_1, i_2 are the nuclear spins of the atoms, while $s_1 = s_2 = 1/2$ are the electronic spins.

Although the details of how the actual potentials are derived are beyond the scope of this thesis, and we refer the reader to [51] for more details, we would like to point out that the potentials $V_S(R)$ are not in general entirely ab-initio, as they generally require some tweaking via empirical parameterizations. High-precision Feshbach spectroscopy experiments have been used heavily to determine these parameterizations, with outstanding results, such as [4, 7, 8, 9]. Potential curves for the Rb-K collision were obtained in [52], and are plotted in fig. 2.5.

Our goal is to integrate the above representation of $V(R)$ with our previous representations. To this end we first wish to represent V in the hyperfine basis

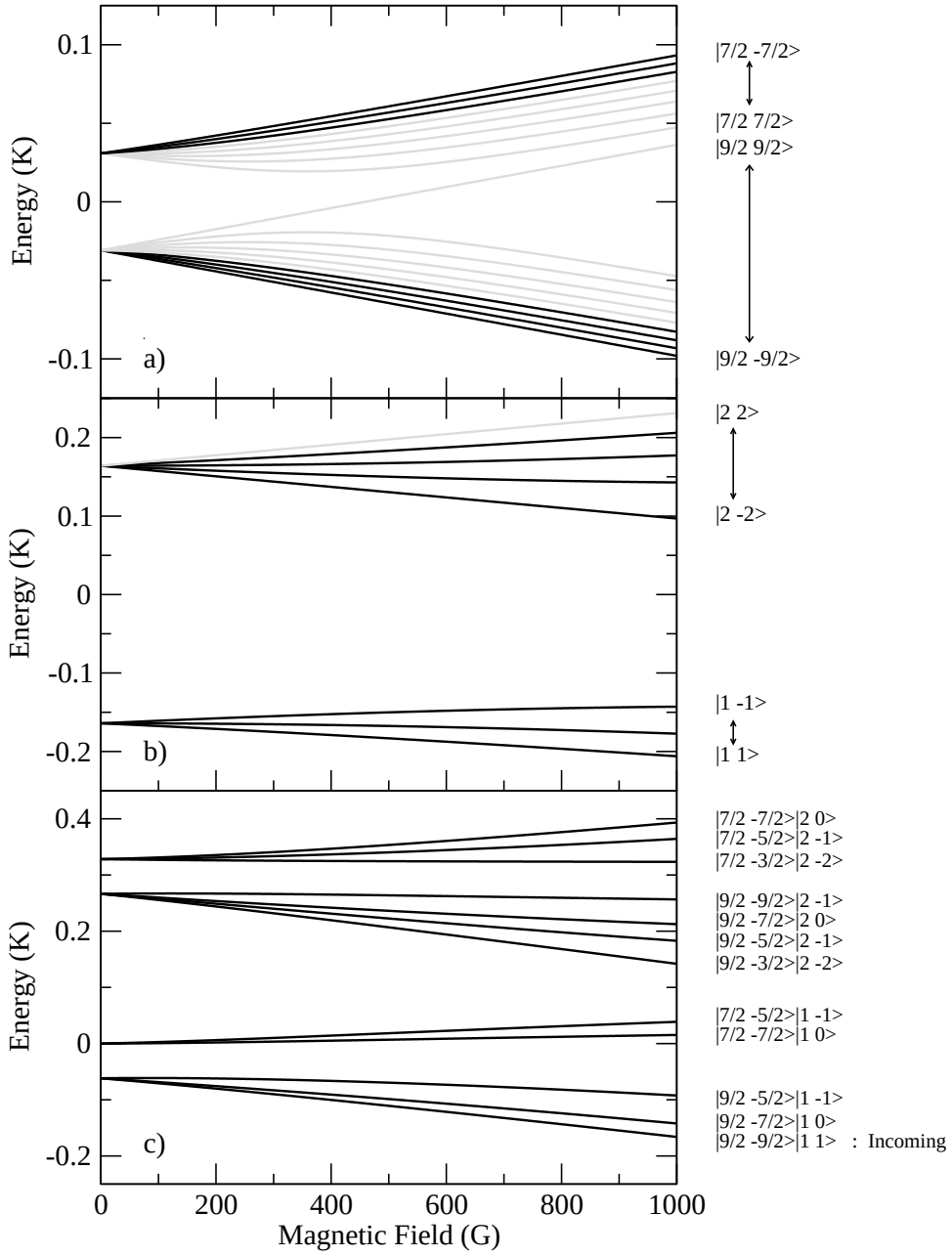

Figure 2.4: a) Hyperfine levels as a function of external magnetic field of ^{40}K in its electronic orbital groundstate. b) Same as a) but for ^{87}Rb. c) Thresholds for a ^{40}K$-^{87}$Rb collision, incoming in the $|9/2 - 9/2\rangle|11\rangle$ channel. Since $m_1 + m_2$ is conserved in the collision, only the states plotted in black in the a) and b) channel participate. It is informative to note the energy scale of the threshold energies, and compare it with the depths of the singlet and triplet potentials in fig 2.5.

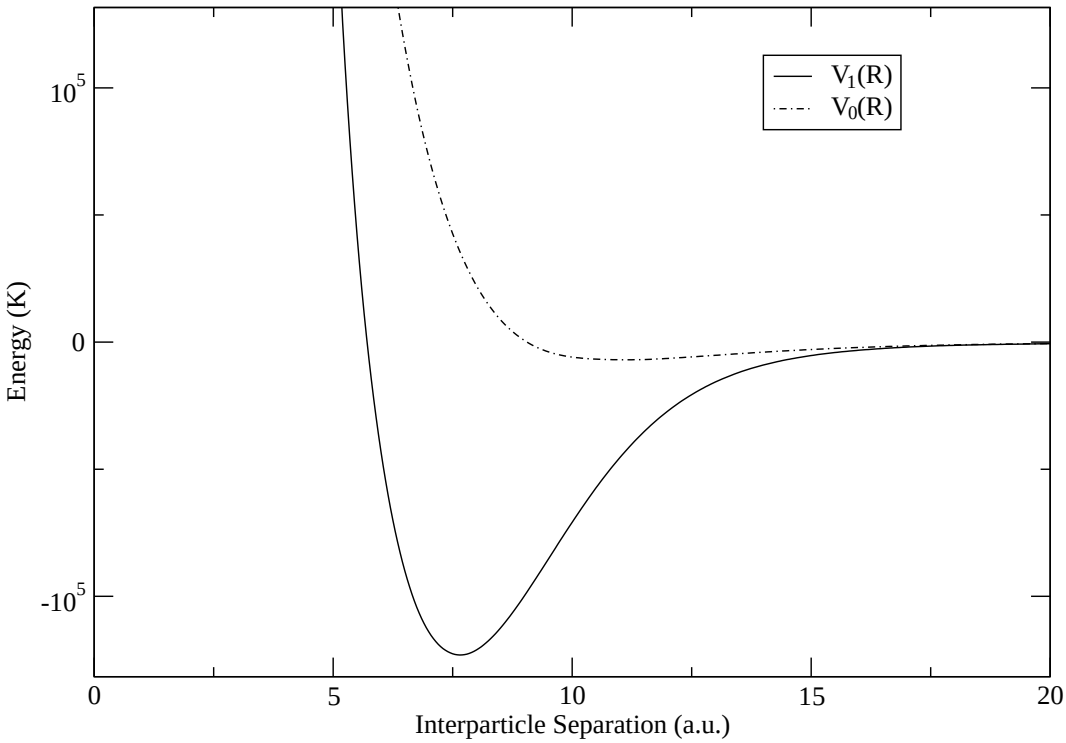

Figure 2.5: Singlet and triplet potential curves for the Rb-K collision. Note the potential depth is of the order of 10^5 Kelvins, while the threshold energies are of the order of hundreds of milliKelvins or less. (see fig 2.4)

with the following basis transformation:

$$\langle f_1' m_1'; f_2' m_2' | V(R) | f_1 m_1; f_2 m_2 \rangle = \sum_{\substack{S,S',M_S,M_S' \\ I,I',M_I,M_I'}} \langle f_1' m_1' f_2' m_2' | S' M_S'; I' M_I' \rangle \times$$
$$\langle S' M_S'; I' M_I' | V(R) | S M_S; I M_I \rangle \langle S M_S; I M_I | f_1 m_1; f_2 m_2 \rangle =$$
$$\sum_S V_S(R) \langle S M_S; I M_I | f_1 m_1; f_2 m_2 \rangle \langle f_1' m_1' f_2' m_2' | S M_S; I M_I \rangle, \tag{2.29}$$

where in the first step we introduced two complete sets of the form $|SM_S; IM_I\rangle\langle SM_S; IM_I|$, and in the second step we used equation 2.28.

To make the final expression in equation 2.29 useful, we need the matrix elements $\langle SM_S; IM_I | f_1 m_1; f_2 m_2 \rangle$, which, it turns out, are well known [53]

$$\langle SM_S; IM_I | f_1 m_2; f_2 m_2 \rangle = \sum_{f,m} \langle SM_S; IM_I | fm \rangle \langle f_1 m_1; f_2 m_2 | fm \rangle$$
$$\sqrt{(2f_1+1)(2f_2+1)(2S+1)(2I+1)} \times \begin{Bmatrix} s_1 & i_1 & f_1 \\ s_1 & i_1 & f_1 \\ s_1 & i_1 & f_1 \end{Bmatrix}. \tag{2.30}$$

Here $\langle SM_S; IM_I | fm \rangle$ and $\langle f_1 m_1; f_2 m_2 | fm \rangle$ are Clebsch Gordon coefficients, and the quantity in curly brackets is an object known as a "nine-J" symbol [53].

From this expression we note that $m_1 + m_2 = m = M_S + M_I$. Since from the equivalent "primed" expression we get that $m_1' + m_2' = m = M_S + M_I$, then we can conclude that $m_1' + m_2' = m_1 + m_2$. This makes perfect physical sense, given the cylindrical symmetry of the problem around the field axis, which we also use as quantization axis.

The final step is to transform the matrix elements in eq.2.29 in the dressed basis. To this end we use the transformation matrices U derived in the previous section, obtaining

$$\langle \widetilde{f_1' m_1'}; \widetilde{f_2' m_2'} | V(R) | \widetilde{f_1 m_1}; \widetilde{f_2 m_2} \rangle = \sum_{\substack{f_1 f_2 f_1' f_2' \\ m_1 m_2 m_1' m_2'}} \langle f_1 m_1 | \widetilde{f_1 m_1} \rangle \langle f_2 m_2 | \widetilde{f_2 m_2} \rangle \times$$
$$\langle f_1' m_1'; f_2' m_2' | V(R) | f_1 m_1; f_2 m_2 \rangle \langle f_1 m_1 | \widetilde{f_1 m_1} \rangle \langle f_2 m_2 | \widetilde{f_2 m_2} \rangle. \tag{2.31}$$

Now that we managed to write the Hamiltonian matrix elements in a physically relevant basis, we need to add the kinetic energy part, whereby our basis becomes $|\widetilde{f_1 m_1}; \widetilde{f_2 m_2}\rangle |LM_L\rangle$. Within our approximation L and M_L are good quantum numbers.

Finally, the last step to take is symmetrization of the wavefunctions, but since we are concerned here with collision between distinguishible particles, we will not require it.

Where necessary, in throughout the thesis we have solved the coupled-channel equations for K-Rb collisions using the log-derivative propagator method described in [54, 55].

Feshbach resonances are very common in multichannel problems with this level of complexity. What truly renders these resonances special is the motion of the thresholds relative to one-another as a function of magnetic field, as depicted in fig 2.4. This causes the resonances to shift in line with the thresholds, which, in many cases, provides a very powerful and direct mean to control the creation of molecuar dimers.

Chapter 3

Two-Body Physics: The Model

In order to describe the many-body properties of the system we wish to employ the powerful tools offered by statistical field theory. To this end we need to rephrase the concepts from the last chapter in the language of field theory, and to develop a simplified model able to retain most of the relevant two-body physics.

In this chapter we present a reasonably well studied field theoretical model of resonant collisions, which we tailor for our specific needs. The model is exactly solvable in the two-body limit, and we show it can reproduce the equations derived in section 2.2.2. We then proceed by testing quantitatively the model by comparing its predictions to the results of (virtually exact) close-coupling calculations.

3.1 The Hamiltonian

We are interested primarily in the effects of resonant behavior on the otherwise reasonably understood properties of the system. To this end we use a model which, in the last few years, has become one of the standards in the literature, and which was used to study the effect of resonant scattering in systems composed of bosons [38, 56, 57], and fermions [58, 59, 60, 61, 62, 63]. Because there is already a significant literature explaining the details involved in the choice of the appropriate model Hamiltonian, we only outline the extent of the approximation

involved in such a choice.

An accurate approach to the problem would have to incorporate several scattering channels, since the resonance in question is a consequence of the intertwined behavior of the complex internal structures of the atoms. In a field theoretical sense, that would imply having to consider vector fields for the bosons and fermions with as many components as there are spin states involved in the interaction, and a non local interaction tensor of adequate size, to account for all coupling between such components. Fortunately, if we assume that the resonances in the system are sufficiently far from each other, such that it is possible to define a "background," or away from resonance behavior, we can focus on only one resonance at a time, which in turn makes it possible for an effective two channel model to describe the resonance.

Furthermore, since the closed channel threshold is energetically unaccessible at the temperatures of interest, we can "integrate out" the closed channel components of the fermion and boson field, in favor of a fermion field which we identify as representative of the motion of one boson and one fermion, and which we dub the "molecular field." In the appropriate limit the molecular field identifies bound states between fermions and bosons.

We emphasize that the molecular field is a theoretical artifice that alleviates the need to treat relative motion of two atoms on the natural scale of the interaction (tens of Bohr radii). However, this model is appropriate for the study of the systems at hand, typically composed of 10^{12} ^{40}K atoms per cubic centimeter, whereby the characteristic length scale associated with the many body system is of the order of the inverse Fermi wavenumber, (thousands of Bohr radii), implying an average interparticle distance, which is given by $\left(\frac{9}{4\pi}\right)^{1/3} \frac{1}{k_F}$, of the same order. Lastly, since the coupling terms in the Hamiltonian represent an effective interaction, we can choose its functional form, and we do so by choosing to deal

with contact interactions, which simplify the calculations immensely.

The resulting Hamiltonian has the following form:

$$H = H_0 + H_I, \tag{3.1}$$

where

$$\begin{aligned} H_0 &= \sum_p \epsilon_p^F \ \hat{a}_p^\dagger \hat{a}_p + \sum_p \epsilon_p^B \ \hat{b}_p^\dagger \hat{b}_p + \sum_p \left(\epsilon_p^M + \nu\right) \ \hat{c}_p^\dagger \hat{c}_p \\ &+ \frac{\gamma}{2V} \sum_{p,p',q} \hat{b}_{p-q}^\dagger \hat{b}_{p'+q}^\dagger \hat{b}_p \hat{b}_{p'} \\ H_I &= \frac{V_{bg}}{V} \sum_{p,p',q} \hat{a}_{p-q}^\dagger \hat{b}_{p'+q}^\dagger \hat{a}_p \hat{b}_{p'} \\ &+ \frac{g}{\sqrt{V}} \sum_{q,p} (\hat{c}_q^\dagger \hat{a}_{-p+q/2} \hat{b}_{p+q/2} + h.c.). \end{aligned} \tag{3.2}$$

Here $\hat{a}_p, \hat{b}_p$, are the annihilator operators for, respectively, fermions and bosons, $\hat{c}_p$ is the annihilator operator for the molecular field [58, 62, 63]; $\gamma = 4\pi a_b/m_b$ is the interaction term for bosons, where a_b is the boson-boson scattering length; and V_{bg}, ν, and g are parameters related to the Bose Fermi interaction, yet to be determined. Also we define single particle energies $\epsilon^\alpha = p^2/2m_\alpha$, where m_α indicates the mass of bosons, fermions, or pairs, and V as the volume of a quantization box with periodic boundary conditions.

3.2 Two Body Scattering Parameters

The first step is to find the values for V_{bg}, ν, g, in terms of measurable parameters. We will, for this purpose, calculate the 2-body T-matrix resulting from the Hamiltonian in eq. 3.2. Integrating the molecular field out of the real time path integral, (see Appendix C for clarifications) leads to the following Bose-Fermi

interaction Hamiltonian

$$H_I^{2body} = \frac{1}{V}\left(V_{bg} + \frac{g^2}{E-\nu}\right)\sum_p \hat{a}_p^\dagger \hat{b}_{-p}^\dagger \hat{a}_p \hat{b}_{-p}. \tag{3.3}$$

This expression is represented in center of mass coordinates, and E is the collision energy of the system. From the above equation we read trivially the zero energy scattering amplitude in the saddle point approximation:

$$T = (V_{bg} - \frac{g^2}{\nu}), \tag{3.4}$$

which corresponds to the Born approximation [1] . We emphasize that this approximation is only valid at exactly zero energy, and it does not, therefore, describe the correct binding energy as a function of detuning, and will be improved in treatment in Sec. 3.3. However, with this approach we obtain an adequate description of the behavior of scattering length as a function of detuning, which allows us to relate the parameters of our theory to experimental observables via the conventional parameterization [58, 56]

$$T(B) = \frac{2\pi}{m_{bf}} a_{bg}\left(1 - \frac{\Delta_B}{(B-B_0)}\right), \tag{3.5}$$

where a_{bg} is the value of the scattering length far from resonance, Δ_B is the width, in magnetic field of the resonance, m_{bf} is the reduced mass, and B_0 is the field at which the resonance is centered.

The identification of parameters between eqns, (3.4) and (3.5) proceeds as follows: far from resonance, $|B - B_0| >> \Delta_B$, the interaction is defined by a background scattering length, via $V_{bg} = \frac{2\pi a_{bg}}{m_{bf}}$. To relate magnetic field dependent quantity $B - B_0$ to its energy dependent analog ν, requires defining a parameter $\delta_B = \partial\nu/\partial B$, which may be thought of as a kind of magnetic moment for the molecules. It is worth noting that ν does not represent the position of the

[1] This is akin to identifying the scattering amplitude $f = a_{sc}$ in the Gross-Pitaevskii equation, where the interaction term would be $\frac{2\pi}{m_{bf}} a_{sc}$

resonance nor the binding energy of the molecules, and that, in general δ_B is a field-dependent quantity, since the thresholds move quadratically with field, because of nonlinear corrections to the Zeeman effect. For current purposes we identify δ_B by its behavior far from resonance, where it is approximately constant. Careful calculations of scattering properties using the model in eq. (3.2), however, leads to the correct Breit-Wigner behavior of the 2-body T-matrix, as we show in section 3.3

Finally we get the following identifications:

$$\begin{aligned} V_{bg} &= \tfrac{2\pi a_{bg}}{m_{bf}} \\ g &= \sqrt{V_{bg}\delta_B\Delta_B} \\ \nu &= \delta_B(B - B_0). \end{aligned} \tag{3.6}$$

3.3 Solution of the Model in the Two-Body Limit

In this section we will abandon the Hamiltonian formalism in terms of the path integral formalism, which is better suited to the perturbative treatment we wish to present. This implies that we will be using the field operators ϕ, ψ, ξ instead of the second quantized operators b, a, c used so far [64].

The perturbative analysis begins by recasting the Hamiltonian in eq. (3.2) in terms of a 2-body action, in center of mass coordinates :

$$S[\psi,\psi^\dagger,\phi,\phi^\dagger,\xi,\xi^\dagger] = S_B[\phi,\phi^\dagger]+S_F[\psi,\psi^\dagger]+S_M[\xi,\xi^\dagger]+S_C[\psi,\psi^\dagger,\phi,\phi^\dagger,\xi,\xi^\dagger], \tag{3.7}$$

where the field ϕ represents the bosons, ψ the fermions, and ξ the fermionic molecules, and where

$$S_B[\phi,\phi^\dagger] \;=\; \int \frac{d\omega}{2\pi} \sum_{\mathbf{p}} (-\hbar\omega + \epsilon_p^B)\; \phi^\dagger_{\omega,\mathbf{p}}\phi_{\omega,\mathbf{p}} +$$

$$
\begin{aligned}
& \frac{1}{2V}\gamma \int \frac{d\omega}{2\pi} \sum_{\mathbf{p},\mathbf{p'q}} \phi^{\dagger}_{\omega,\mathbf{p}-\mathbf{q}} \phi^{\dagger}_{\omega,\mathbf{p'}+\mathbf{q}} \phi_{\omega,\mathbf{p'}} \phi_{\omega,\mathbf{p}} \\
S_F[\psi,\psi^{\dagger}] &= \int \frac{d\omega}{2\pi} \sum_{\mathbf{p}} (-\hbar\omega + \epsilon^F_p)\ \psi^{\dagger}_{\omega,\mathbf{p}} \psi_{\omega,\mathbf{p}} \\
S_M[\xi,\xi^{\dagger}] &= \int \frac{d\omega}{2\pi} \sum_{\mathbf{p}} (-\hbar\omega + \epsilon^M_p + \nu)\ \xi^{\dagger}_{\omega,\mathbf{p}} \xi_{\omega,\mathbf{p}} \\
S_C[\psi,\psi^{\dagger},\phi,\phi^{\dagger},\xi,\xi^{\dagger}] &= \frac{V_{bg}}{V} \int \frac{d\omega}{2\pi} \sum_{\mathbf{p},\mathbf{p'q}} \psi^{\dagger}_{\omega,\mathbf{p}-\mathbf{q}} \phi^{\dagger}_{\omega,\mathbf{p'}+\mathbf{q}} \psi_{\omega,\mathbf{p'}} \phi_{\omega,\mathbf{p}} \\
& \quad + g \int \frac{d\omega}{2\pi} \sum_{\mathbf{pq}} (\xi^{\dagger}_{\omega,\mathbf{p}} \psi_{\omega,\mathbf{q}-\mathbf{p}} \phi_{\omega,\mathbf{p}} + c.c), \qquad (3.8)
\end{aligned}
$$

where $\hbar\omega$ is the frequency associated with the motion of the various fields.

The initial difficulty is that there are two distinct interaction pathways between bosons and fermions: a direct one of the form $|\phi|^2|\psi|^2$, and an indirect molecule-mediated one, of the form $\xi\phi^{\dagger}\psi^{\dagger}$, corresponding respectively to open and closed channel events. In order to proceed, we will introduce an alternate effective molecular field, which will exactly reproduce both these interaction pathways via a single mediated interaction term. This is accomplished by first integrating out the original molecular degree of freedom [64] to get :

$$
S'_C[\psi,\psi^{\dagger},\phi,\phi^{\dagger}] = \int \frac{d\omega}{2\pi}\frac{d\omega'}{2\pi} \sum_{\mathbf{pp'}} \left(V_{bg} + \frac{g^2}{E-\nu} \right) \phi^{\dagger}_{\omega,\mathbf{p}} \psi^{\dagger}_{E-\omega,-\mathbf{p}} \phi_{\omega',\mathbf{p'}} \psi_{E-\omega',-\mathbf{p'}} \qquad (3.9)
$$

where E is the collision energy between the fermions and the bosons. After collecting the background and resonance terms of the interaction, we note that this new direct interaction contains both the resonant and background channels. Next we undergo the inverse transformation to eliminate all direct boson-fermion interactions in favor of interactions mediated by new effective molecules, to obtain:

$$
\begin{aligned}
S''_M[\xi,\xi^{\dagger}] &= -\int \frac{d\omega}{2\pi} \sum_{\mathbf{p}} \left(\frac{V_{bg}}{g^2} + \frac{1}{w - \frac{p^2}{2(m_b+m_f)} - \nu} \right)^{-1} \xi'^{\dagger}_{\omega,\mathbf{p}} \xi'_{\omega,\mathbf{p}} \\
S''_C[\psi,\psi^{\dagger},\phi,\phi^{\dagger},\xi,\xi^{\dagger}] &= \int \frac{d\omega}{2\pi} \sum_{\mathbf{p}} g^2 (\xi'^{\dagger}_{E,\mathbf{0}} \psi_{E-\omega,-\mathbf{p}} \phi_{\omega,\mathbf{p}} + c.c).
\end{aligned}
\qquad (3.10)
$$

Here ξ' represents the new effective (i.e. primed) molecules. The first line of fig. 3.1 shows the diagrams describing the effective resonant collisions between bosons and fermions. Here the solid lines refer to fermions, the dashed lines to bosons, and the double solid-dashed lines to effective molecules.

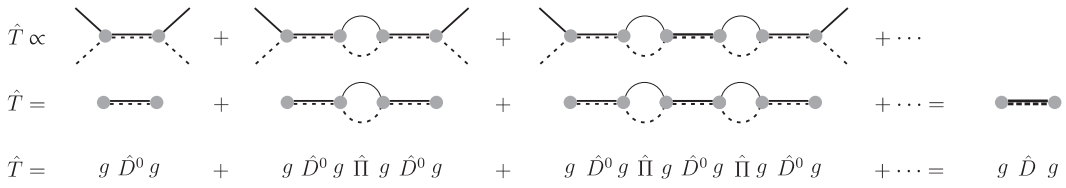

Figure 3.1: Feynman diagrams representing the resonant collision of a fermion and a boson. Solid lines represent fermions, dashed lines bosons, and double solid-dashed lines represent the effective composite fermions.

Since we are looking for poles of the S-matrix, we can disregard the trivial fermion and boson propagators, and proceed, as outlined in fig. 3.1, to calculate the renormalized propagator for ξ', denoted as $\hat{D}$, represented there as a heavy broken line. This object is proportional to the T-matrix of the system, and shares its poles. Using the definition of the retarded molecular self energy $\hat{\Pi}$ given in fig. 3.1, and calling the free molecular propagator $\hat{D}^0$ (again for ξ'), we get the following Dyson series:

$$T = g\hat{D}^0 g + g\hat{D}^0 g\ \hat{\Pi}\ g\hat{D}^0 g + g\hat{D}^0 g\ \hat{\Pi}\ g\hat{D}^0 g\ \hat{\Pi}\ g\hat{D}^0 g + \cdots = g\hat{D}g \tag{3.11}$$

where T is the T-matrix for the collision, and which has formal solution

$$T = g\hat{D}g = \frac{g^2}{(\hat{D}^0)^{-1} - g^2\hat{\Pi}}. \tag{3.12}$$

These quantities take the explicit form

$$\hat{D}^0(E) \ = \left(\frac{V_{bg}}{g^2} + \frac{1}{E-\nu}\right)$$

$$\hat{\Pi}(E) = -i\int \frac{d\omega}{2\pi}\frac{d\mathbf{p}}{(2\pi)^3}\frac{1}{(\hbar\omega - \frac{p^2}{2m_b} + i0^+)(E - \hbar\omega - \frac{p^2}{2m_f} + i0^+)}$$
$$\approx i\frac{m_{bf}^{3/2}}{\sqrt{2}\pi}\sqrt{E} + \frac{m_{bf}\Lambda}{\pi^2}, \tag{3.13}$$

where m_{bf} is the boson-fermion reduced mass, and Λ is an ultraviolet momentum cutoff needed to hide the unphysical nature of the contact interactions; we will dwell more on that shortly. Finally inserting eq. 3.13 into eq. 3.12, we obtain the following expression for the T-matrix:

$$T(E) = \left[\frac{1}{V_{bg} + \frac{g^2}{E-\nu}} + i\frac{m_{bf}^{3/2}}{\sqrt{2}\pi}\sqrt{E} + \frac{m_{bf}\Lambda}{\pi^2}\right]^{-1} \tag{3.14}$$

To show that this expression correctly represents the low-energy two-body T-matrix for resonant scattering, we will compare it to the s-wave ($l = 0$) version of equation 2.18, remembering that $T = 2\pi/m_{bf}f$

$$T(E) = \frac{2\pi}{m_{bf}\sqrt{2m_{bf}}}\left(\frac{\Gamma}{(E - E_r) - i\Gamma\sqrt{E}}\right). \tag{3.15}$$

The quantities Γ and E_r can be extracted from experimental observables, through accurate two-body scattering calculations.

From the parameterization of the zero energy T-matrix in eq.(3.5), and the $E \to 0$ limit of (3.15), we easily derive $\Gamma = \sqrt{2m_{bf}}a_{bf}\delta_B\Delta B$. With these definitions we can relate equations (3.15) and (3.14), to find a regularization scheme for the theory, by substituting the non observable parameters g, ν, and V_{bg} by the Λ dependent (renormalized) quantities $\bar{g}$, $\bar{\nu}$, and $\bar{V_{bg}}$, such that the observable T-matrix will not be itself Λ dependent

Following [58] we compare equations (3.14) and (3.15), in the limit $E \to 0$, where we have (once we include the definitions of the bare quantities)

$$V_{bg} - \frac{(g)^2}{\nu} = \left[\frac{1}{\bar{V_{bg}} - \frac{\bar{g}^2}{\bar{\nu}}} + \frac{m_{bf}\Lambda}{\pi^2}\right]^{-1}. \tag{3.16}$$

Since we have one equation and three unknowns, we will have to consider some physical circumstances, analyzing 3.16 in various limits. The first limit is far from

resonance, where $\nu \to \infty$

$$\bar{V_{bg}} = V_{bg}\left(\frac{1}{1-\frac{m_{bf}\Lambda V_{bg}}{\pi^2}}\right) \tag{3.17}$$

We are now left with the task of defining the resonant quantities, and we have no more leeway to make physically motivated simplifications. The equations which remain are ambiguous, which leaves us with a set of possibilities for the choice of $\bar{g}$ and $\bar{\nu}$. One way is to proceed as follows: insert eq. (3.17) into (3.16), and solve for $\bar{\nu}$, to get

$$\bar{\nu} = \bar{g}^2(1-\frac{m_{bf}\Lambda V_{bg}}{\pi^2})(\frac{m_{bf}\Lambda}{\pi^2}+\frac{\nu}{g^2}). \tag{3.18}$$

From inspecting the above equation we can choose a definition of $\bar{g}$, which will also imply one for $\bar{\nu}$, and we get (reporting also eq(3.17) for completeness)

$$\begin{aligned}
\bar{V_{bg}} &= V_{bg}\left(\frac{1}{1-\frac{m_{bf}\Lambda V_{bg}}{\pi^2}}\right) \\
\bar{g} &= g\left(\frac{1}{1-\frac{m_{bf}\Lambda V_{bg}}{\pi^2}}\right) \\
\bar{\nu} &= \nu + \bar{g}g\frac{m_{bf}\Lambda V_{bg}}{\pi^2}
\end{aligned} \tag{3.19}$$

Using these definitions of $\bar{V_{bg}}$, $\bar{g}$ and $\bar{\nu}$, together with the policy of imposing Λ as the upper limit of momentum integrals, will guarantee that observables will not depend on the choice of Λ, as long as it is chosen to be bigger than momentum scales relevant to experiment.

3.3.1 Poles of the T-Matrix: The Two-body case

As described in section 2.2.2, bound states and resonances of the two-body system are identified in the structure of poles of the T-matrix (eq.3.14). This is illustrated in Figure 3.2, where real and imaginary parts of the poles' energies are plotted as a function of magnetic field. The resonance portrayed in the figure

is the $544.7G$ resonance present in the $|9/2, -9/2\rangle|1, 1\rangle$ state of ^{40}K-^{87}Rb. For $B < 544.7G$ (corresponding to detunings $\nu < 0$) the two-body system possess a true bound state, whose binding energy is denoted by the solid line. In this case, the pole of 3.15 occurs for real energies. This bound state vanishes as the detuning goes to zero, where the resonance occurs.

For positive detunings, $\nu > 0$, on the other hand, the poles are complex, and the inverse of the imaginary part is proportional to the lifetime of the metastable resonant state. In this regime, there is no longer a true bound state, but there may be a scattering resonance, indicated in fig. 3.2 by a thick dashed line. This resonance appears for magnetic fields $B > 544.7$ for this particular resonance, well before the disappearance of the bound state. This is highly dependent upon the value of the background potential. We will see in chapter 5 that for $V_{bg} = 0$, the resonance actually appears at positive detunings. In the case of ^{40}K-^{87}Rb, $V_{bg} < 0$, implying that there is a weak potential resonance in the open channel which interferes with the closed-channel resonance, and causes it to cross the axis at negative detunings. For $V_{BG} > 0$ ([65]) the positive background scattering length is set by a bound state in the open channel, which does not affect the resonance states, but which interferes with the bound state at negative detunings. An in depth analysis of this physics is highly interesting, but is beyond the scope of this thesis.

The thin dashed lines in fig. 3.2 are physically meaningless solutions to the Schrödinger equation, in which the amplitude in the resonant state would grow exponentially in time, rather than decay. These poles do not therefore identify any particular features in the energy-dependent cross section of the atoms, and will not modify the physics of the system.

Finally fig. 3.2 contains data obtained from virtually exact close-coupling calculations (see section 2.3.3), which show the extent of validity of the model.

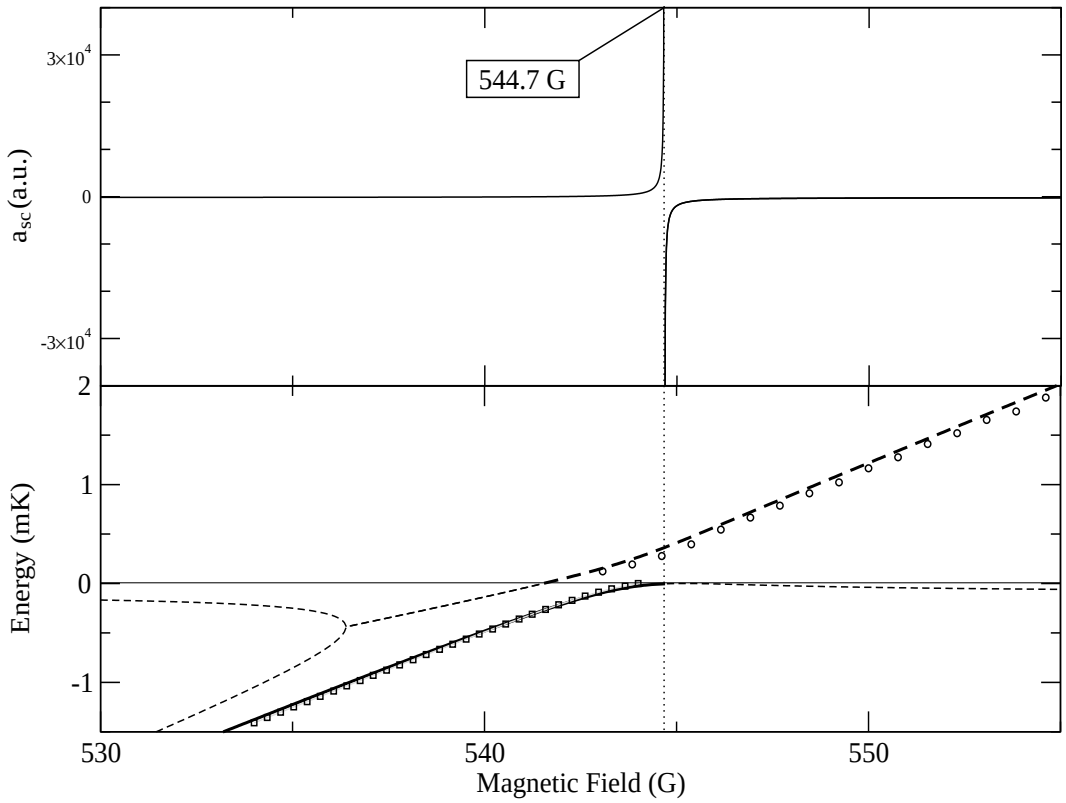

Figure 3.2: The top panel shows the scattering length versus magnetic field for the 544.7 G resonance, present in the $|9/2, -9/2\rangle|1, 1\rangle$ states of the ^{40}K-^{87}Rb collision. The bottom panel shows the poles of the model two-body T-matrix (eq. 3.14) parametrized for the same resonance, as a function of magnetic field. Thick solid and dashed lines denote the real parts of relevant poles, representing bound and resonance states respectively. The thin dashed lines are the real parts of unphysical poles. The empty circles and squares, represent the position of the resonance and the bound state, obtained via a virtually exact close coupling calculation, and are presented to show the level of accuracy of the model.

For the purposes at hand this agreement is sufficient.

It should be noted that the agreement is not as good for positive background scattering length systems, since the open-channel bound state determining this scattering length is not adequately described by the model, which treats the background physics as an essentially zero range interaction. This implies that the relation between the background scattering length and open channel bound-state energy is exactly $E_b = 1/2\mu a_{bg}^2$, while in the physical system this relation depends on the details of the interaction potential. This problem has been addressed in the literature [49], but no treatable field theory has yet been proposed.

$B_0(G)$	$\Delta_B(G)$	$\delta_B(K/G)$	$a_{bg}(a.u.)$
492.49	0.134	3.624×10^{-5}	-176.5
544.7	3.13	1.576×10^{-4}	-176.5
659.2	1.0	2.017×10^{-4}	-176.5

Table 3.1: Parametrization of the three main Feshbach resonances used in this thesis. All Three resonances are in the $|9/2, -9/2\rangle|1, 1\rangle$ states of the $^{40}K -^{87} Rb$ collision

Chapter 4

Mean-Field Theory: The Language

In this chapter we wish to introduce the many-body physics of the system, by first analyzing the mean-field approach. Because of the statistical properties of the system, we will see right away that mean-field theory does not recover the correct two-body physics in the low density limits. In spite of this substantial weakness, however, the approach has several qualitative features which persist even in the improved theory which we will later introduce. Furthermore, since the model is exactly solvable, it will allow us to develop a language which will help us to understand the problem in simpler terms, and to identify some small physical effects, which, when ignored, can greatly simplify the beyond mean-field approach presented in the next chapter.

We will then develop the Hartree-Fock-Bogoliubov equations of motion, as a first attempt to gain beyond mean-field insight. We will observe that the peculiar physical structure of the problem is such that the HFB equations reduce to the mean-field equations, and higher order correlations play an unusually important role in the physics of mixture.

This fact is of itself a novelty: the physics of other resonant systems, composed of either fermions or bosons, is known to be mainly driven by atom-atom correlations, (at least qualitatively). We will show that even some of the most fundamental qualitative physical aspects of resonant Bose-Fermi mixtures require

that at least three-body correlations be considered to be reasonably well understood, implying a peculiar complexity of the system that sets it apart from its Bose-Bose and Fermi-Fermi counterparts.

4.1 Equilibrium Approach

The mean-field theory approach to the resonant Bose-Fermi mixture lends itself very naturally to treatment in the Hamiltonian formalism, and in the next section we will mainly focus on this particular approach. Nonetheless, to create a stronger link to the beyond-mean-field approach of chapter 5 we will also introduce the Green's function formalism, and discuss the similarity between the two approaches. All calculations in this and next Chapters assume a gas in free space, at zero temperature.

4.1.1 The Formalism

Starting with the Hamiltonian described by equation 3.1, we obtain the mean-field Hamiltonian by substituting the boson annihilator $\hat{b}$ by its expectation value $\phi = \langle \hat{b} \rangle$, a complex number. The number operator $\hat{b}_p^\dagger \hat{b}_p$ therefore becomes $|\phi|^2 = N_b$, where N_b is the number of condensed bosons. The grand canonical Hamiltonian therefore becomes

$$\begin{aligned} H &= E_b + \sum_p \left(\epsilon_p^F - \mu_f + V_{bg} n_b\right) \hat{a}_p^\dagger \hat{a}_p + \sum_p \left(\epsilon_p^M + \nu - \mu_m\right) \hat{c}_p^\dagger \hat{c}_p \\ &+ g\sqrt{n_b} \sum_p \left(\hat{c}_p^\dagger \hat{a}_p + h.c.\right), \end{aligned} \tag{4.1}$$

where n_b is the density of condensed bosons, $E_b/V = \gamma n b^2 - \mu_b n b$ is the energy per unit volume of the (free) condensed bosons, a constant contribution to the total energy of the system, and $\mu_{(b,f,m)}$ are the chemical potentials. These are Lagrange multipliers that serve to keep the densities constant as we minimize the

energy to find the ground state. In the following we will drop the volume term, absorbing it in the definition of the creator/annihilator operators, such that the expected value of the number operator represents a density, instead of a number.

Before proceeding with the analysis of this Hamiltonian, we should introduce the set of self-consistent equations we wish to solve. To this end we define the quantities $n^0_{b,(f)}$, representing the total density of bosons (fermions) in the system, at detuning $\nu \to \infty$. At finite detunings some of these atoms will combine into molecules, and the densities will be denoted as $n_{(b,f,m)}$ for bosons, fermions and molecules respectively.

The system, therefore, is composed of six unknowns, namely three densities, and three chemical potentials, which require six equations to solve. These equations, which can be derived by number-conservation constraints and energy minimization arguments, are:

$$n_f + n_m - n_f^0 = 0 \tag{4.2.a}$$

$$n_b + n_m - n_b^0 = 0 \tag{4.2.b}$$

$$n_f = \frac{d\ \Omega}{d\mu_f} \tag{4.2.c}$$

$$n_m = \frac{d\ \Omega}{d\mu_m} \tag{4.2.d}$$

$$\frac{d\Omega}{d\phi} = 0 \tag{4.2.e}$$

$$\mu_b + \mu_f = \mu_m, \tag{4.2.f}$$

where $\Omega = \langle H \rangle / V$ is the Gibbs free energy.

Equations 4.2.a and 4.2.b follow from the simple counting argument that for every molecule created, there is one less free boson and one less free fermion in the gas. Equations 4.2.c, and 4.2.d are simply the Lagrange multiplier constraint equations, equation 4.2.e follows from the mean-field approximation, whereby the bosonic field is simply a complex number, and minimization of the energy can

therefore be done directly. Finally equation 4.2.f, known as the "law of mass action," is just a condition on the multipliers that follows from the fact that to make a molecule it takes one free atom of each kind.

The next step is to write down Ω for the system, by taking the expectation value of the Hamiltonian in equation 4.1, obtaining

$$\begin{aligned}\Omega &= E_b/V + \sum_p \left(\epsilon_p^F - \mu_f + V_{bg} n_b\right) \eta_f(p) + \sum_p \left(\epsilon_p^M + \nu - \mu_m\right) \eta_m(p) \\ &+ 2g\sqrt{n_b} \sum_p \eta_{mf}(p),\end{aligned} \tag{4.3}$$

where $\eta_f(p) = \langle \hat{a}_p^\dagger \hat{a}_p \rangle$ and $\eta_m(p) = \langle \hat{a}_p^\dagger \hat{c}_p \rangle$ are the fermionic and molecular momentum distributions, $\eta_{mf}(p) = \langle \hat{c}_p^\dagger \hat{a}_p \rangle$ is an off-diagonal correlation term arising from the interactions in the system, and the densities are given by $n_{f,m,mf} = \int \frac{dp}{2\pi^2} \eta_{f,m,mf}(p)$. Equations 4.2.a-4.2.f then read

$$n_f + n_m - n_f^0 = 0 \tag{4.4.a}$$

$$n_b + n_m - n_b^0 = 0 \tag{4.4.b}$$

$$n_{f,m,mf} = \int \frac{dp}{2\pi^2} \eta_{f,m,mf}(p) \tag{4.4.c}$$

$$g\ n_{mf} - \mu_b \sqrt{n_b} + \lambda n_b^{3/2} = 0 \tag{4.4.d}$$

$$\mu_b + \mu_f = \mu_m \tag{4.4.e}$$

The remaining task is now to find expressions to calculate the expected values $\eta_{f,m,mf}(p)$. To this end we follow a Bogoliubov-like approach, similar to that described in [35]. The mean-field Hamiltonian is bilinear in all creation/annihilation operators, which means that it can be diagonalized via a change of basis, whereby introducing the operators

$$\begin{aligned}\alpha_p &= A_\alpha a_p + C_\alpha c_p \\ \beta_p &= A_\beta a_p + C_\beta c_p,\end{aligned} \tag{4.5}$$

for some appropriately chosen coefficients $A_{\alpha,\beta}$ and $B_{\alpha,\beta}$, the Hamiltonian will read

$$H' = E_0 + \sum_p \lambda_\alpha(p)\alpha_p^\dagger\alpha_p + \sum_p \lambda_\beta(p)\beta_p^\dagger\beta_p. \tag{4.6}$$

At this point we note that the Hamiltonian is just a separable sum of free-particle Hamiltonians, where the free particles are fermions, with dispersion relations $\lambda_{\alpha,\beta}(p)$. We can readily write down the distribution

$$\eta_{\alpha,\beta}(p) = \Theta(-\lambda_{\beta,\alpha}(p)) \tag{4.7}$$

, where Θ is the step function, and calculate the densities $n_{\alpha,\beta}$. The step function could be replaced by the free Fermi distribution for non-zero temperatures, but the mean-field assumption that all bosons are condensed would no longer hold. Also Note that if these were ordinary free fermions with dispersion $p^2/2m - \mu$, equation 4.7 would reduce to the standard zero-temperature Fermi distribution. We will see below that $\lambda_{\alpha,\beta}(p)$ are dispersion relations of quasi-particles, which are a mixture of atoms and molecules.

Below we show how these ideas, together with equation 4.2.a - 4.2.f, give us the tools we require to calculate the observable atomic and molecular densities as a function of the chemical potentials.

To illustrate more explicitly the diagonalization procedure we define the vectors

$$A = \begin{pmatrix} a_p \\ c_p \end{pmatrix} \quad A^\dagger = \begin{pmatrix} a_p^\dagger & c_p^\dagger \end{pmatrix}, \tag{4.8}$$

and

$$B = \begin{pmatrix} \alpha_p \\ \beta_p \end{pmatrix} \quad B^\dagger = \begin{pmatrix} \alpha_p^\dagger & \beta_p^\dagger \end{pmatrix}, \tag{4.9}$$

whereby the Hamiltonian can be written as $A^\dagger\hat{H}A$, and $B^\dagger\hat{H}'B$, where

$$\hat{H} = \begin{pmatrix} \left(\epsilon_p^F - \mu_f + V_{bg}n_b\right) & g\sqrt{n_b} \\ g\sqrt{n_b} & \left(\epsilon_p^M + \nu - \mu_m\right) \end{pmatrix}, \tag{4.10}$$

and

$$\hat{H}' = \begin{pmatrix} \lambda_\alpha(p) & 0 \\ 0 & \lambda_\beta(p) \end{pmatrix}. \tag{4.11}$$

Diagonalizing $\hat{H}$, we get the two eigenvalues

$$\lambda_{\alpha,\beta}(p) = \frac{h_f(p) + h_m(p)}{1} \pm \frac{1}{2}\sqrt{4g^2 n_b + (h_m(p) - h_f(p))^2}, \tag{4.12}$$

where we have defined $h_f(p) = \left(\epsilon_p^F - \mu_f + V_{bg} n_b\right)$, and $h_m(p) = \left(\epsilon_p^M + \nu - \mu_m\right)$, and the unitary eigenvector matrix

$$U = \begin{pmatrix} A_\alpha & B_\alpha \\ A_\beta & B_\beta \end{pmatrix}. \tag{4.13}$$

The transformation in eq. 4.5 can then be written as $A = U^\dagger B$, and its inverse $B = UA$.

Our goal now is to write the densities $\eta_{m,f,mf}(p)$ in terms of the known densities $\eta_{\alpha,\beta}(p)$. In component notation, (where $A_i = a_p$, etc.), we can write

$$\langle A_i^\dagger A_l \rangle = \langle B_j^\dagger U_{ji} (U^\dagger)_{lj} B_k \rangle = U_{lj} U_{ij}^* \langle B_j^\dagger B_j \rangle, \tag{4.14}$$

where we have used the fact that since the Hamiltonian is diagonal in the B basis, then $\langle B_j^\dagger B_k \rangle = \langle B_j^\dagger B_j \rangle \delta_{jk}$.

Using this formalism we get the relations:

$$\begin{aligned} \eta_f(p) &= |A_\alpha|^2 \eta_\alpha(p) + |B_\alpha|^2 \eta_\beta(p) \\ \eta_f(p) &= |A_\beta|^2 \eta_\alpha(p) + |B_\beta|^2 \eta_\beta(p) \\ \eta_{fm}(p) &= A_\alpha^* A_\beta \eta_\alpha(p) + B_\alpha^* B_\beta \eta_\beta(p). \end{aligned} \tag{4.15}$$

Using these expressions in conjunction with eqs. 4.4.a-4.4.e will then allow us to compute the equilibrium properties of the system.

4.1.2 Analysis and Results

For concreteness, in this section, as well as in some of the following ones, we will consider a free gas of fermionic ^{40}K atoms, with a density of $8.2 \times 10^{14} cm^{-3}$, corresponding to the Thomas-Fermi density of 10^6 such atoms in the center of a $100Hz$ spherical trap. The coupling term $g\sqrt{n_b}$ in equation 4.10 is the perturbative expansion parameter for the problem, and since it has units of energy, it must be compared with the characteristic non-perturbed energy of the gas, which in this case is E_f. Also since in the perturbative expansions it always appear squared (see eq. 3.11), we can define the unitless small parameter for the system as $\epsilon_{SM} = g^2 n_b / E_f^2 = g^2 n_f / E_f^2 r_{bf}$, where r_{bf} is the boson to fermion density ratio. For the $492G$ resonance in table 3.1, we have $\epsilon_{SM} = 6.35 \times 10^{-2} r_{bf}$, and since we will be mostly concerned with values of r_{bf} generally smaller than 10 (10^6 ^{87}Rb atoms correspond to a bosonic density in the center of the same $100Hz$ trap about six times larger than the fermionic one i.e $r_{bf} = 6$), the small parameter is of order 10^{-1}, appropriate for perturbative treatment.

Figure 4.1 shows the quasi-particle energy levels $\lambda_{\alpha,\beta}(k_f)$, as a function of detuning. On the leftmost and rightmost part of the graph we see that the two lines asymptote to the detuning (mean field molecular energy) and 0 (atomic internal energy). Looking in the region near the resonance we see that the two lines avoid crossing each other, and from the form of the Hamiltonian in equation 4.10 we can easily deduce that the avoiding is due to the coupling term $g^2 n_b$, which, for a specified resonance, implies that the size of the crossing is proportionally related to the density of condensed bosons in the gas.

If we consider a gas with more fermions than bosons, we easily see that on the left side of the plot, both states are populated, and there exist a well defined atomic Fermi surface, as well as a well defined molecular Fermi surface. However,

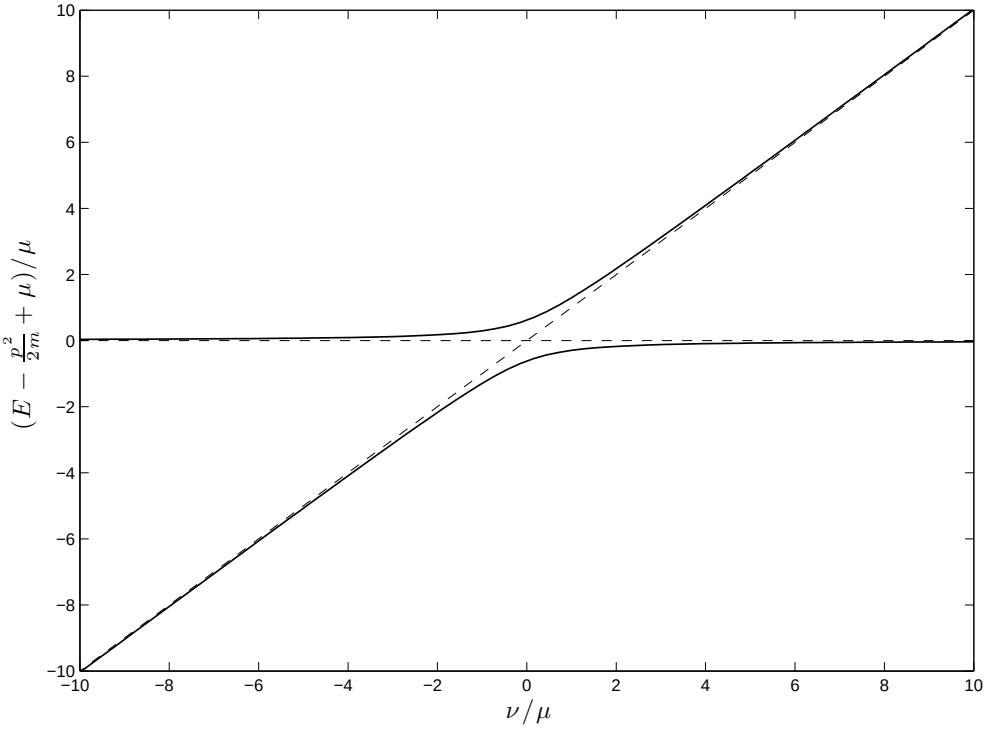

Figure 4.1: The thick solid lines represent the "renormalized" mean-field energy levels $\lambda_{\alpha,\beta}(k_f)$, while the thin dashed lines represent their bare counterparts.

if the density of bosons is much larger than the density of fermions, the crossing may be so large, that the higher state is energetically inaccessible, and only the bottom state is ever populated, such that a single Fermi surface is ever populated. This implies that the atoms on the large positive detuning side of the resonance "morph" into molecules as the detuning is shifted, to the negative size, and it is no longer strictly appropriate to talk about atoms or molecules separately in this regime.

To illustrate this difference, we start by an example problem, in which we turn off the interactions (i.e. $g, V_{bg}, \gamma \to 0$). Using this simplified system, we study an example of a gas with two Fermi surfaces, $r_{bf} = 0.6$, and one with one Fermi surface, with $r_{bf} = 6$. Results appear respectively in figures 4.2 and 4.3, where we plot the chemical potentials and populations as a function of detuning.

At zero temperature, the chemical potential in a Fermi gas, represents its Fermi energy. Analyzing the top panel of figure 4.2, starting from the positive detuning region, we see that the molecular and fermionic chemical potentials coincide, which is reasonable, since the chemical potential for a condensate vanishes at zero temperature. Plotted in the graphs are also the internal energies of fermions and molecules, which for the noninteracting gas are equal to 0 and ν respectively. In the large positive detuning regime, the only Fermi surface present is the fermionic one, since $\mu_f > 0$ (and 0 is the internal energy of the fermionic atoms), while $\mu_m < \nu$, which implies that it is energetically not favorable to create a molecule. As the detuning diminishes, and becomes smaller than 1 (region marked "a" in the graph), it starts to "cut" into the energetically favorable regime, so that creating low-momentum molecules becomes favorable to high momentum atoms. This reduces the number of atoms present in the gas, and causes $\mu_f = \mu_m$ to diminish. This process continues until there are no bosons left (region marked

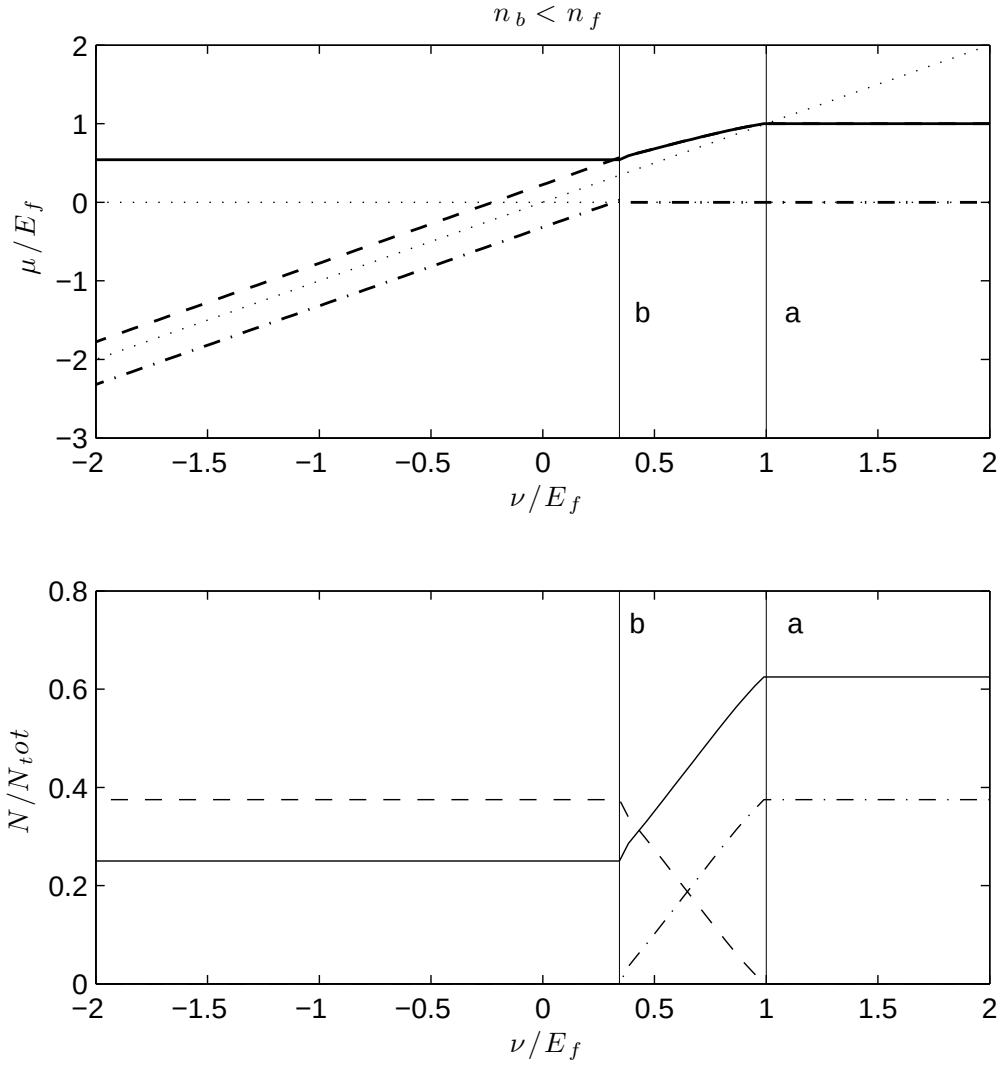

Figure 4.2: Equilibrium chemical potentials (top panel) and populations (bottom panel) as a function of detuning for a non interacting gas with $r_{bf} = .6$. The solid lines represent fermions, dashed lines molecules, and dashed-dotted lines bosons. The dotted lines in the top panel represent the bare molecular and fermionic internal energies, respectively ν and 0. The vertical lines labeled a) and b) are discussed in the text, and represent the detuning at which molecular formation begins and ends, respectively

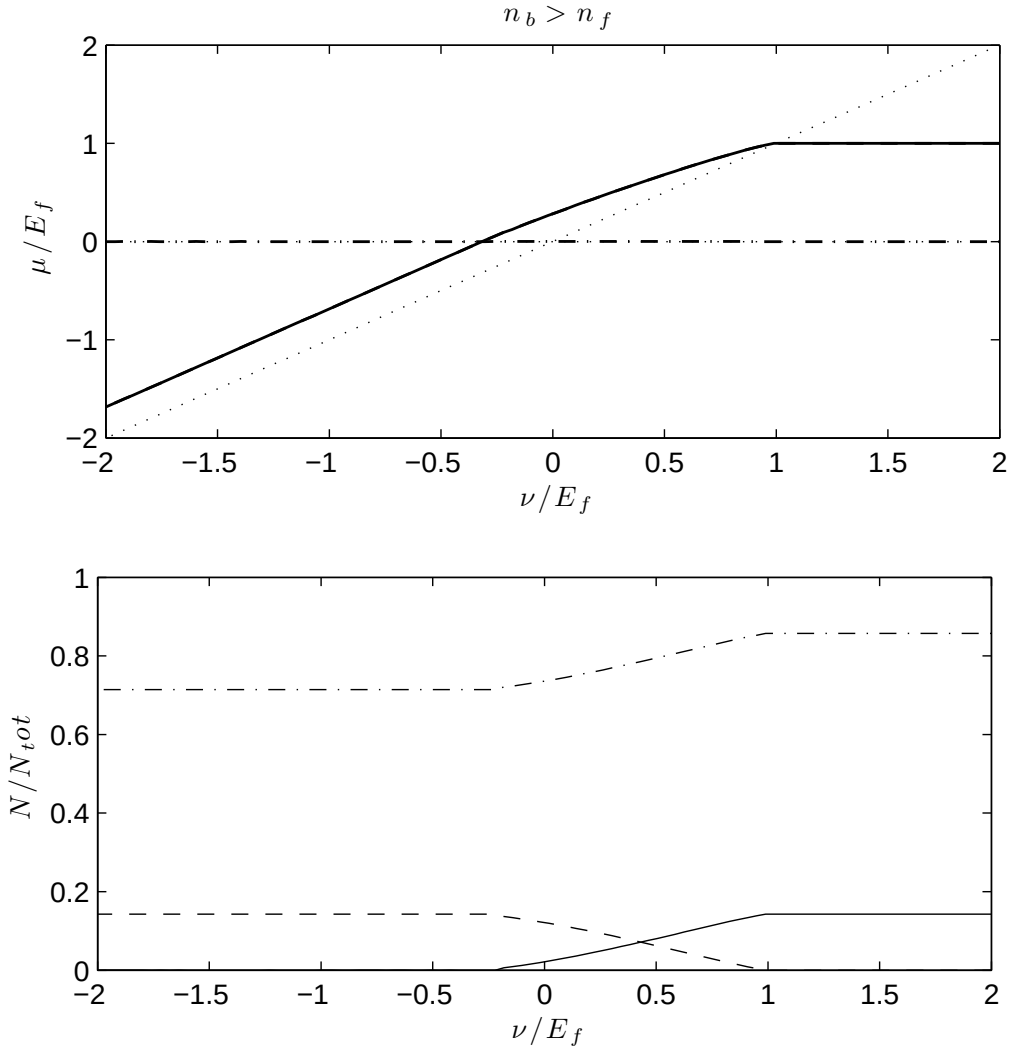

Figure 4.3: Equilibrium chemical potentials (top panel) and populations (bottom panel) as a function of detuning for a non interacting gas with $r_{bf} = 6$. The solid lines represent fermions, dashed lines molecules, and dashed-dotted lines bosons. The dotted lines in the top panel represent the bare molecular and fermionic internal energies, respectively ν and 0.

"b" in the graph), and no more molecules can be formed. Since there are no bosons left in the gas, the bosonic chemical potential can become negative, and this allows μ_f and μ_m to separate, so that two separate Fermi seas are created: a molecular one, from ν to μ_m, and an atomic one, from 0 to μ_f.

The case of only one Fermi surface, is represented in figure 4.3. Like the previous case, no molecules are generated until the detuning cuts into the atomic Fermi gas. Since there are enough bosons to turn all the fermions into molecules, the atomic and molecular chemical potentials move in unison. When they cross zero, then no more fermions can exist in the gas, since $\mu_f < 0$ (the atomic internal energy), and $\mu_m > \nu$, (the molecular internal energy), making molecules the only energetically accessible state.

Since, under standard experimental conditions, in the center of the trap the bosonic density is larger than the fermionic one, we only analyze the one Fermi-surface case in the mean-field approximation. Figure 4.4, shows the equilibrium chemical potentials for the system obtained via a self-consistent solution of equations 4.16 and 4.4.a-4.4.e.

The first main difference which appears when comparing the graph in figs 4.4 with its non-interacting equivalent in fig 4.3, is the fact that $\mu_b > 0$, causes a split between the molecular and fermionic chemical potential. At first sight this may suggest the existence of two Fermi surfaces, as it was the case in fig 4.3. The reason why μ_b is nonzero, is a consequence of equation 4.4.d, whereby the boson-boson interaction energy generates a shift. In physical terms, this means that there is an energy cost in maintaining bosons unpaired, and therefore we need to take this into account in the kinematic analysis, by realizing that while in the noninteracting case pairing becomes energetically favorable when ν crosses μ_f, in the interacting case this happens when ν crosses $\mu_f + \mu_b$. Therefore the only consequence of this interaction energy is to shift the molecular population

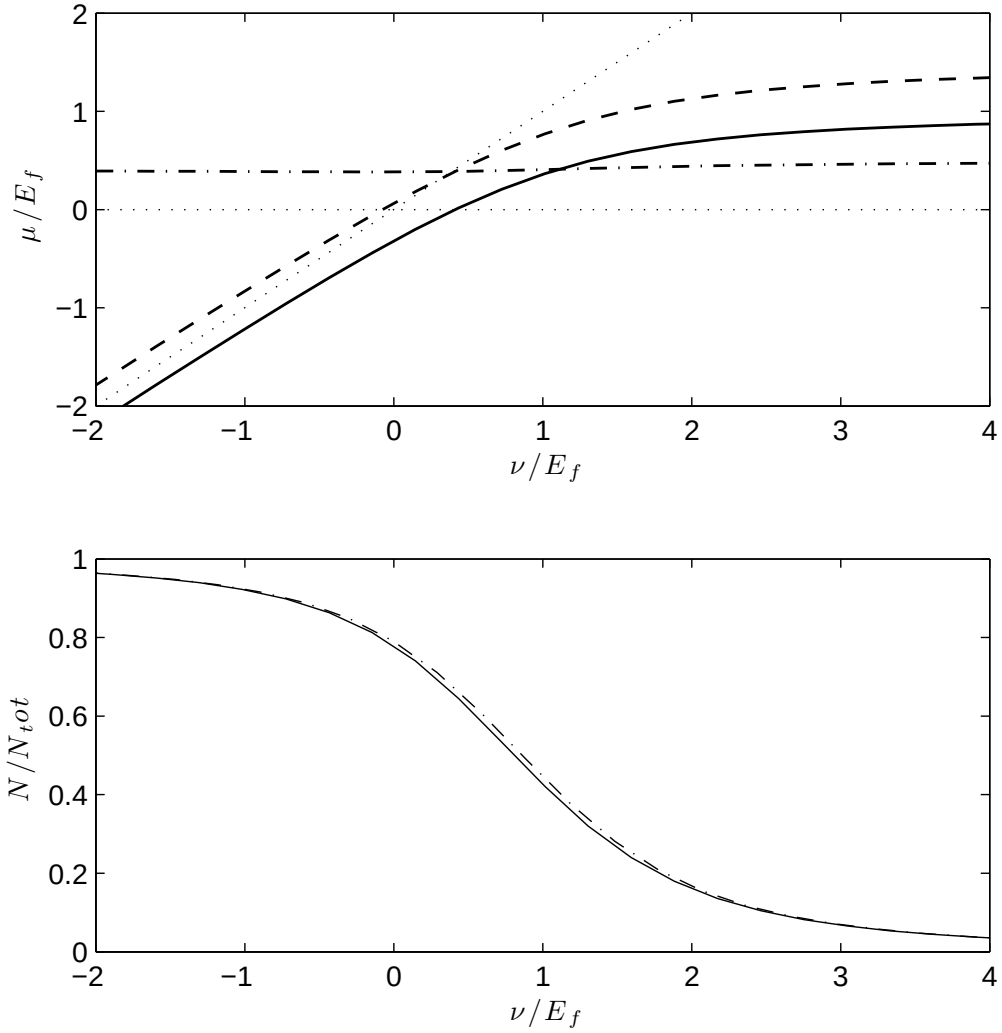

Figure 4.4: Mean-field equilibrium chemical potentials (top panel) and molecular fraction (bottom panel) as a function of detuning. In the top panel, solid lines represent fermions, dashed lines molecules, and dashed-dotted lines bosons. In the bottom panel, the solid line represents the full mean-field result, while the dashed-dotted line represents results obtained using the approximations in described in the text.

curve up and to the left by exactly and amount μ_b (see bottom panel of fig 4.4).

Another substantial difference between the interacting and noninteracting case, is that molecule creation takes place in a much narrower range of detunings in the noninteracting case. This can be understood by the fact that the avoided crossing makes for a gentler sloping internal molecular energy than the bare detuning. This will be emphasized even further when we will discuss the beyond mean-field case, where the molecular binding energy slopes even more gently.

The last goal of this section is to introduce some approximations to facilitate the beyond mean-field approach to the problem. These approximations have been tested numerically, and they give corrections of the order of .1% or less in calculated molecular populations for all regimes of interest here.

- V_{bg} can be disregarded
- As per the arguments above, the interaction γn_b^3 is included by appropriately shifting the detuning, and the molecular potential.
- $\langle \eta_b f(p) \rangle$ (analogous to the boson polarization operator in the Green function formalism) can also be disregarded, since its contribution to μ_b is much smaller than that of γn_b^3.

A comparison plot of the full calculation and the approximate calculation of the molecular population as a function of detuning appear in the second panel of figure 4.4. With exception of the last item, and some aspects of the first, we are unable to directly test the validity of these approximations in the generalized beyond mean-field theory which we introduce in the next chapter. However, we have reason to believe that this approximations will be valid also, since, as we will see, the generalized mean field theory is, after all, a mean-field theory at heart.

4.2 Non Equilibrium Approach

Having discussed the equilibrium mean-field properties of the system we will now develop the Hartree-Fock-Bogoliubov equations of motion, as a first attempt to gain beyond-mean-field insight. We will then notice that the peculiar physical structure of the problem is such that the HFB equations reduce to the mean-field equations, and higher order correlations play a peculiarly important role in the physics of mixture.

4.2.1 The Formalism

We now move on to derive the Heisenberg equations of motion for the many body system. The way this is done is to find equations of motion for correlation functions, $f_s(x_1, ...x_s)$, which represent the probability of finding s particles at positions $x_1, ..., x_s$. As it turns out, the equation of motion for the correlation function f_1 will depend on the function f_2, which in turn will depend on f_3, and so on all the way to f_N, where N is the total number of particles in the system. This is known as a Bogoliubov-Born-Green-Kirkwood-Yvon (BBGKY) hierarchy [66]. In practice we will be concerned with momentum space correlation functions, but the idea is the same.

Given the large number of particles in the system, it is impossible to calculate equations of motion for all correlation functions, and we need to invoke an approximation. In practice, correlation functions are often calculated only up to two-body correlations, $s = 2$. This is justified under the assumption that interactions are suitably "weak." Higher-order correlations are included in an approximate way by considering, not the actual atomic constituents, but rather combinations called quasiparticles. The quasiparticles are defined to be noninteracting, so that their higher-order correlation functions can be written in terms of

second order correlation functions [64].

Using this qualitative idea we proceed to develop a more formal understanding. In statistical field theory, given an operator $\mathcal{O}$, and Hamiltonian H, we define the thermal average of $\mathcal{O}$ with respect to H as $\langle\mathcal{O}\rangle_H = 1/ZTr\left\{\mathcal{O}e^{-\beta H}\right\}$, where $\beta = (k_B T)^{-1}$ is the inverse temperature, and $Z = Tr\left\{e^{-\beta H}\right\}$ is the partition function. In this framework, the 1-particle correlation function is defined as the thermal average of the number operator, with respect to the Hamiltonian of the system.

In the quasiparticle representation, we define the annihilation operator for quasiparticles as a', reminding ourselves that it is a complicated function of $a, a^\dagger, b, b^\dagger, c, c^\dagger$. In momentum space, the 1-particle correlation function in this representation, will then be $\langle a'_{p1} a'_{p2}\rangle_{H_{qp}}$, where H_{qp} is the (noninteracting) quasiparticle Hamiltonian.

Now we introduce the real approximation, namely that the quasi-particles can be written as linear combinations of all possible products of two operators (except for averages involving one fermionic and one bosonic operator, which are easily shown to vanish). The procedure is then to find the Heisenberg equations of motion for these pairs of operators, and then average over the quasi-particle Hamiltonian

$$i\hbar\frac{\partial}{\partial t}\langle\mathcal{O}\rangle_{H_{qp}} = \langle[\mathcal{O}, H]\rangle_{H_{qp}}, \tag{4.16}$$

which, being Gaussian, allows us to invoke Wick's theorem to decompose all higher order correlations in 1-particle correlations, thus truncating the BBGKY hierarchy.

4.2.2 The Equations of Motion

Before generating Heisenberg equations, we need to take a little care in the treatment of the Bose field, to properly treat the condensed part. To this end we perform the usual separation of mean field and fluctuations of the Bose field, substituting b_0 (the zero-momentum component of the Bose gas) with a c-number $\phi = \langle b_0 \rangle_{H_{qp}}$, and identifying it with the condensate amplitude, while $\langle b_{p\neq 0} \rangle_{H_{qp}} = 0$ are the fluctuations. We insert these definitions in the Hamiltonian in eq. (3.2), then proceed to calculate commutators.

Since we wish to consider a homogeneous gas, the correlation functions $f_1(x, x')$ can be written in terms of a relative coordinate $y = x - x'$. Thus in momentum space $f_1(p)$ is the probability to find a particle with momentum p in the gas, or in other words it is the momentum distribution of the system.

Having taken all appropriate commutators, and applied Wick's theorem, (for more details on the procedure see [67], or Appendix B for the derivation of a sample equation.), we obtain the following self consistent set of equations of motion for the system:

$$
\begin{aligned}
i\hbar\frac{\partial}{\partial t}\phi &= V_{bg}\rho_F\phi + \gamma\left(2\phi\tilde{\rho}_B + \Delta_B\phi^*\right) + g\rho^*_{MF} + \gamma|\phi|^2\phi && \text{(4.17.a)}\\
\hbar\frac{\partial}{\partial t}\tilde{\eta_B}(p) &= 2\gamma\,\Im m\left[\kappa_B(p)(\phi^{*^2} + \Delta^*_B)\right] && \text{(4.17.b)}\\
i\hbar\frac{\partial}{\partial t}\kappa_B(p) &= \left[\epsilon^B_P + 2V_{bg}\rho_F + 4\gamma(|\phi|^2 + \tilde{\rho_B})\right]\kappa_B(p) + \\
&\qquad \gamma(2\tilde{\eta_B}(p) + 1)(\phi^2 + \Delta_B) && \text{(4.17.c)}\\
\hbar\frac{\partial}{\partial t}\eta_F(p) &= -2g\,\Im m(\phi\eta_{MF}(p)) && \text{(4.17.d)}\\
i\hbar\frac{\partial}{\partial t}\kappa_F(p) &= \left[\epsilon^F_p + 2V_{bg}(\tilde{\rho_B} + |\phi|^2)\right]\kappa_F(p) && \text{(4.17.e)}\\
\hbar\frac{\partial}{\partial t}\eta_M(p) &= 2g\,\Im m(\phi\eta_{MF}(p)) && \text{(4.17.f)}\\
i\hbar\frac{\partial}{\partial t}\kappa_M(p) &= \left[\epsilon^M_P + \nu\right]\kappa_M(p) && \text{(4.17.g)}
\end{aligned}
$$

$$i\hbar\frac{\partial}{\partial t}\eta_{MF}(p) = \left[\epsilon_p^F - \epsilon_p^M - \nu + V_{bg}(\tilde{\rho_B} + |\phi|^2)\right]\eta_{MF}(p) - g\phi^*\left(\eta_F(p) - \eta_M(p)\right) \quad (4.17.h)$$

$$i\hbar\frac{\partial}{\partial t}\kappa_{MF}(p) = \left[\epsilon_p^F + \epsilon_p^M + \nu + V_{bg}(\tilde{\rho_B} + |\phi|^2)\right]\kappa_{MF}(p) - g\left[\phi\kappa_F(p) + \phi^*\kappa_M(p)\right], \quad (4.17.i)$$

where $\tilde{\eta_B}(p) = \langle b^\dagger_{p\neq 0} b_{p\neq 0}\rangle_{H_{qp}}$ is the momentum distribution of non-condensed bosons, and $\tilde{\rho}_B = \int \frac{dp}{2\pi^2} p^2 \tilde{\eta_B}(p)$ is the density of non-condensed bosons; $\kappa_B(p) = \langle b_{p\neq 0} b_{p\neq 0}\rangle_{H_{qp}}$ is the anomalous distribution of bosonic fluctuations, and $\Delta_B = \int \frac{dp}{2\pi^2} p^2 \kappa_B(p)$ the anomalous density. Similarly $\eta_{F,M}(p)$ are the fermionic and molecular distributions, $\rho_{M,F}$ the densities, and $\kappa_{F,M}(p)$, and $\Delta_{F,M}$ the anomalous molecular and fermionic distributions and densities. Finally $\eta_{MF}(p) = \langle c_p^\dagger a_p\rangle_{H_{qp}}$ and $\kappa_{MF}(p) = \langle c_p a_p\rangle_{H_{qp}}$ are the normal and anomalous distribution for molecule-fermion correlation, with the associated densities ρ_{MF} and Δ_{MF}.

4.2.3 Analysis and Results

Equations (4.17.a-4.17.i) describe the complete self-consistent set of HFB equations for the resonant BF mixture. Inspection of these equations, however, allows us to simplify the set quite dramatically, without sacrificing almost any of the physics thereby contained. First, we notice that the evolution of the anomalous fermionic densities $\kappa_{MF}(p)$, $\kappa_F(p)$, and $\kappa_M(p)$ is entirely decoupled from the evolution of all other quantities, and can therefore be considered separately. This implies that, since we are mainly interested in the evolution of the normal densities, we can eliminate without approximation all the anomalous ones.

The next thing we notice is that the evolution of the normal and anomalous bosonic averages is completely independent of the resonant interaction, and is controlled only by the background interactions between bosons and with fermions. For typical background interaction strengths, and cold enough temperatures, it is

well established that the role of noncondensed bosons is minor, and the system is well described at the Gross-Pitaevskii level of approximation.

We can therefore write the following reduced set of equations:

$$
\begin{aligned}
i\hbar\frac{\partial}{\partial t}\phi &= (V_{bg}\rho_F + \gamma|\phi|^2)\phi + g\rho^*_{MF} && \text{(4.18.a)}\\
\hbar\frac{\partial}{\partial t}\eta_F(p) &= -2g\ \Im m(\phi\eta_{MF}(p)) && \text{(4.18.b)}\\
\hbar\frac{\partial}{\partial t}\eta_M(p) &= 2g\ \Im m(\phi\eta_{MF}(p)) && \text{(4.18.c)}\\
i\hbar\frac{\partial}{\partial t}\eta_{MF}(p) &= \left[\epsilon^F_p - \epsilon^M_p - \nu + V_{bg}|\phi|^2\right]\eta_{MF}(p) - \\
&\qquad g\phi^*\left(\eta_F(p) - \eta_M(p)\right). && \text{(4.18.d)}
\end{aligned}
$$

Together with the prospect of simulating time dependent experiments, such a set of equations allow us to calculate many characteristics of the system, which we could use to understand further physics or, more importantly at this stage, to test the theory against our knowledge of the system in various limits.

A relevant quantity we can calculate to this end is the binding energy of the molecules. This can be done by an instantaneous jump of the detuning from large and positive values, where we know the equilibrium distributions very well, to some other arbitrary value. The system thus perturbed oscillates at a specific characteristic frequency, which is identified as the (unique) pole of the HFB many body T-matrix of the system. For negative detunings, as shown below, this pole corresponds to the binding energy of the molecules, dressed by the interactions in the system.

Figure 4.5 shows a representative example of time evolution of the condensate population (number conservation guarantees that all three populations oscillate with the same frequency) under the conditions described above. In this particular example, at time t=0 the detuning is suddenly shifted a magnetic field

detuning of approximatively $0.1G$. The response of the population shows an envelope function, indicated by the gray shaped area, that arises from nonlinearities in the equations of motion. The inset shows that under this envelope is a well defined sinusoidal oscillation.

The nearly monochromatic character of the response is made clearer by Fourier transforming the time-dependent population. The Fourier transform shown in the second panel of Fig 4.5 is strongly peaked at $5.4 \times 10^{-6} K$. Similarly, the position of the peak in the frequency spectrum, for different final detunings, should map the molecular binding energy as a function of magnetic field.

Figure 4.6 shows the results obtained by this method. This plot represents the binding energy of the molecules, dressed by the interactions in the system. This dressing is expected to be weaker for smaller densities of atoms and molecules. In this limit, we should thus recover the two-body molecular binding energy, obtained via coupling calculations (solid line in fig 4.6), and which, as described in chapter 3 can be well approximated by our model.

Instead we see that the pole behavior approaches the bare detuning (dashed line in fig 4.6), indicating that the renormalization of the binding energy obtained at the presented level of approximation is inadequate to correctly include the two-body physics. This behavior is in sharp contrast to the Bose-Bose resonant interaction, where the correct binding energy is preserved at the HFB level [38]. This is also true for the Fermi-Fermi case [68].

This discrepancy is due to the fact that the creation of molecules requires the formation of correlations between bosons and fermions, which, as shown in the following, cannot exist if the density matrix is assumed to be Gaussian. Specifically what is required is a more careful consideration of the noncondensed bosons.

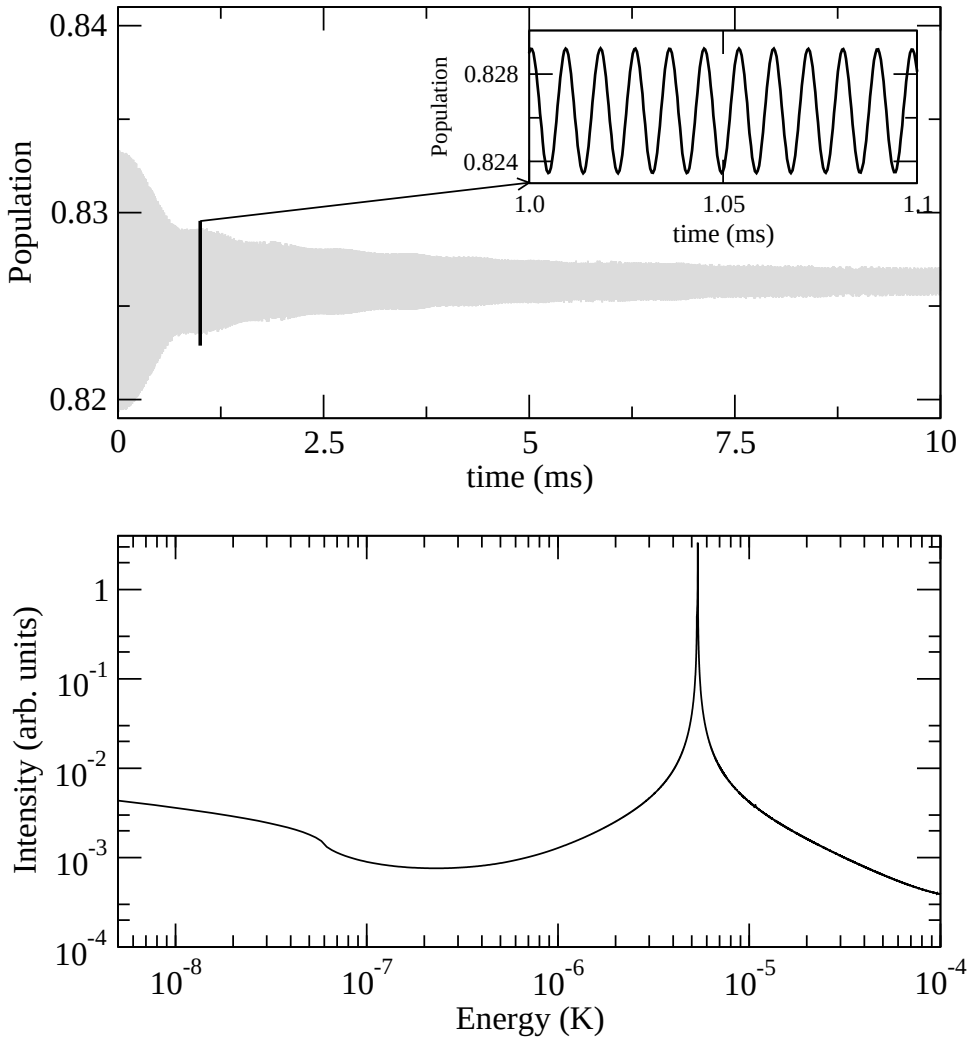

Figure 4.5: The top panel represents the time evolution of the population of condensed atoms after detuning is suddenly shifted from infinitely positive to -5.1 K ($-.1G$ magnetic detuning) around the $659.2G$ resonance in $^{87}Rb -^{40} K$ described in table 3.1. The bottom panel shows the absolute value of Fourier transform of said time evolution. The main peak in this graph represents the computed value of the binding energy, which we see is about $5.410^{-6}K$. The system under consideration is composed of fermionic densities of $10^{15}cm^{-3}$, for a constant density ratio of six bosons per fermion.

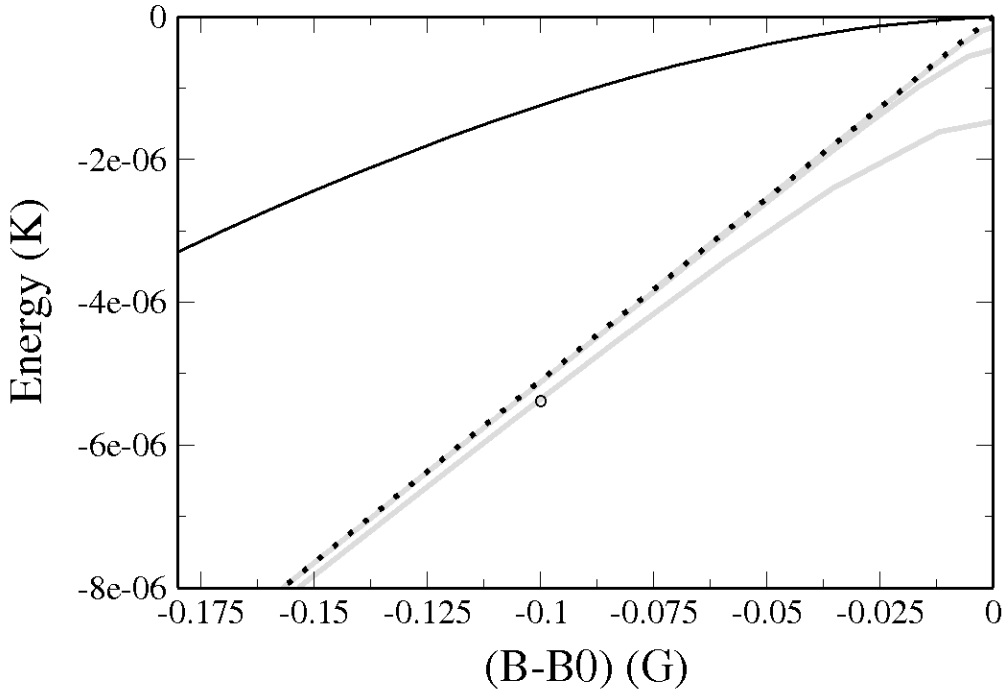

Figure 4.6: Plot representing the poles of the scattering t-matrix for the 659.2G resonance in ^{87}Rb-^{40}K described in table 3.1. The dotted line represents the "bare" molecular detuning as a function of field, as defined in the text. The solid black line is the correct binding energy of the molecular state, obtained by means of full close coupling calculations, while the gray solid lines are the eigenenergies obtained from equations 4.18.a-4.18.d, for different atomic densities. From top to bottom on the right the grey lines refer to fermionic densities of $10^{13}cm^{-3}$,$10^{14}cm^{-3}$, and $10^{15}cm^{-3}$, for a constant density ratio of five bosons per fermion. We note that for lower and lower densities the calculated binding energy incorrectly approaches the bare detuning instead of the correct two-body binding energy.

4.3 The Importance of Noncondensed Bosons

The reason for the failure of the HFB theory is not immediately clear from the theory itself. To bring out the inadequacy of this theory in the dilute limit, in Chapter 5, we recast the problem in an alternative perturbative form that can reproduce the correct behavior in the two-body limit. This path integral approach will also lay bare the role of noncondensed bosons.

What we will see in the upcoming analysis may be qualitatively understood in the following simple terms. A molecule in the gas can decay into a pair of "virtual" (i.e. non energy conserving) atoms, which can then meet again and reform the molecule. These events modify the behavior of the molecule, and an appropriate treatment of these virtual excitations is therefore necessary to correctly include the two-body properties of the molecules in the many-body theory. In particular, the molecules can decay forming a virtual non condensed boson, and the contribution of this set of events to the physics of the molecules turns out to be very important. An appropriate theory would therefore consider the coupling of the molecules to non condensed bosons explicitly, which implies that one has to include in the equations of motion three-point averages, such as $\langle c_q^\dagger a_{-p+q/2} b_{(p+q/2)}\rangle$. Since the HFB theory disregards three-point averages, it only contains molecule-atom-atom couplings of the form $\langle c_q^\dagger a_q\rangle\phi_0$, where molecules can only decay forming a condensed boson.

It is straightforward to see that the HFB theory treats 3-body correlation functions differently depending on the quantum statistics of the constituents. For a Bose-Bose mixture, the correlation function is approximated (schematically) by

$$\langle bbm^\dagger\rangle \approx \langle m^\dagger\rangle\langle b(-q)b(q)\rangle + 2\langle b\rangle\langle bm^\dagger\rangle, \tag{4.19}$$

where b is a boson and m is a molecule. The first term of the right of this expression allows explicitly for virtual bosonic pairs of arbitrary momentum, provided that

the molecular field $\langle m \rangle$ accounts for most of the molecules, which is assumed to be the case. Similarly, in a mixture of distinct fermions, the correlation function reads

$$\langle f_1 f_2 m \rangle \approx \langle m \rangle \langle f_1(q) f_2(-q) \rangle, \tag{4.20}$$

and the same argument applies, since the molecules are bosons.

For the Bose-Fermi mixture, on the other hand, the correlation function would be approximated by

$$\langle b f m \rangle \approx \langle b \rangle \langle f m \rangle + \langle f \rangle \langle b m \rangle + \langle m \rangle \langle b f \rangle. \tag{4.21}$$

The required virtual atom-atom pairs would arise from the third term on the right-hand-side of this expression. However, these molecules are fermions, which have no mean field, $\langle m \rangle = 0$. The only surviving term is then the first one, which accounts only for condensed bosons, and somehow correlates the fermionic atoms to the fermionic molecules. This is only an indirect way to get the bosons and fermions correlated.

Chapter 5

Beyond Mean Field

In chapter 4 we reached the conclusion that the mean-field approach to the resonant Bose-Fermi system does not properly account for the correct two-body physics of the system. In this chapter we wish to improve on this, by introducing a generalization to mean-field theory, via an appropriate renormalization of the molecular propagator, which is able to reproduce the correct two-body physics in the low-density limit. To accomplish this, we will have to abandon the Hamiltonian treatment of the previous chapter, in favor of a perturbative approach based on the Green's function formalism, much as was done for two bodies in chapter 3.

We begin this treatment, by first describing the effect of the many-body medium on the collisional properties of the constituents. We will find that the kinematic implications of Pauli blocking play an important role in the physics of the stability of the molecules. We then proceed by introducing a generalized mean-field theory, which we solve self-consistently to calculate equilibrium molecular densities and distribution in the gas, as a function of detuning.

5.1 Scattering in the Medium

The behavior of the atom pairs in a resonant BF mixture depends subtly on the momentum of the pairs. Roughly speaking, as discussed in chapters 2 and 3 for a single, free pair of atoms, a true molecular bound state exists on one side

of the resonance, denoted as the "negative detuning" side. On the other, "positive detuning," side, the pair is not rigorously bound but may exhibit resonant scattering. (see fig. 3.2). For free molecules this demarcation at zero detuning between bound and resonant states is clearly independent of the pair's center-of-mass momentum. In the many-body environment, however, this situation changes dramatically. We will show that slowly moving molecules can be stable against decay even on the positive detuning side of resonance. The reverse is also true: pairs that are moving fast enough will become unstable and exhibit only resonances on the negative detuning side, even though their two-body analog would be completely stable. This unusual behavior is connected to the fact that the pairs are themselves fermions, and must obey the correct Fermi statistics. This is of course different from the case of either a boson-boson or fermion-fermion resonance, where the pairs are always bosons.

In this section we will consider only one aspect of BF mixture near FR, namely how the stability of a composite fermionic molecule will be affected by the many-body medium. To do this we will assess the poles of the many-body T-matrix of a molecular pair propagating in the many-body medium. All the calculations in this section refer to the $659.2G$ resonance in $^{87}Rb-^{40}K$ described in table 3.1

5.1.1 Poles of the T-Matrix: The Two-body Case Revisited

The mean-field analysis in section 4.1.2 led us to conclude that the role of V_{bg} close to resonance is negligible with regards to the many-body properties of the system. In this section we present once more the analysis of section 3.3.1, and modify it to include this approximation, to establish a closer connection to the many-body analysis which follows. In this light, as $V_{bg} \to 0$, after the appropriate

renormalization, equation 3.14 becomes

$$T_{2B}(E) = -\frac{2\pi\hbar}{m_{bf}} \frac{1}{-a^{-1} + r_0 m_{bf} E - i\sqrt{2m_{bf}E}}, \tag{5.1}$$

where $r_0 = -2\pi/m_{bf}^2 g^2$ is the effective range of the interaction resulting from the underlying model. The main difference in the pole structure, as anticipated in section 3.3.1, is that the resonant state crosses threshold for the positive detuning $\nu = \mu < g^4 m_{bf}^3/4\pi^2$, where we have introduced the chemical potential μ to provide a direct link to the many-body analysis which will follow.

At the same detuning, there emerges a positive imaginary part of the pole energy (dashed line), which denotes the energy width of the resonance. Interestingly, for detunings $0 < \nu/\mu < g^4 m_{bf}^3/4\pi^2$, the poles of (5.1) are purely imaginary, and the imaginary part is negative. These poles stand for physically meaningless solutions to the Schrödinger equation, in which the amplitude in the resonant state would grow exponentially in time, rather than decay. These poles do not therefore identify any particular features in the energy-dependent cross section of the atoms. There is a characteristic detuning scale on which these events occur. This scale is given by the width parameter $\gamma^2 = g^2 M_{bf}^{3/2}/\sqrt{2}\pi$ [60], also indicated in the figure.

5.1.2 Poles of the T-Matrix: The Many-body Case

In a many-body environment, the T-matrix and its poles depend on the center-of-mass momentum. The importance of taking into account this dependence was demonstrated in [69] for the BCS-BEC crossover at $T \neq 0$ when non-condensed fermion pairs lead to pseudogap effects above T_c and non BCS- behavior below. The influence of the many- body medium on a Feshbach resonance between two fermions was demonstrated in [70] for a composite boson as well. In the BF mixture the composite object is a fermion, so its momentum dependence cannot

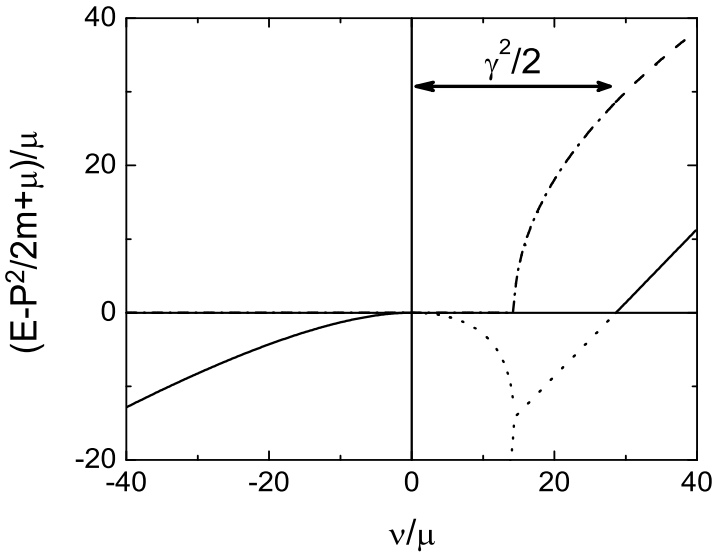

Figure 5.1: Complex poles of the two-body T-matrix, as a function of detuning. Solid and dashed lines denote the real and imaginary parts of physically relevant poles, respectively. The dotted and dash-dotted lines are real and imaginary parts of unphysical poles, respectively.

be omitted even for $T = 0$. Thus the T-matrix near the FR in a BF medium must be considered as a function of densities of both the Bose and Fermi subsystems as well as the center-of-mass motion of a given BF pair. We have found that T-matrix poles and residues are quite sensitive to all these ingredients.

The T-matrix $\hat{T}$ of the system in the many-body medium is defined, similarly to the two-body version case discussed in chapter 3 by the Lippmann-Shwinger equation:

$$\hat{T} = \hat{g}\hat{D}\hat{g^\dagger} = \hat{g}\hat{D^0}\hat{g^\dagger} + \hat{g}\hat{D^0}\hat{g^\dagger}\hat{G_B}\hat{G_F}\hat{T}, \tag{5.2}$$

where $\hat{D}$ is the renormalized molecular Green function, and $\hat{G_{B/F}}$ is the boson/fermion renormalized Green function. These quantities are defined in terms of their many-body non-interacting counterparts

$$\begin{aligned} \hat{D^0} &= \frac{1}{\omega - \xi^M(\mathbf{p}) + i\eta\ sign(\xi(\mathbf{p}))} \\ \hat{G^0}_F &= \frac{1}{\omega - \xi^F(\mathbf{p}) + i\eta\ sign(\xi(\mathbf{p}))} \\ \hat{G^0}_B &= \frac{1}{\omega - \xi^B(\mathbf{p}) + i\eta}, \end{aligned} \tag{5.3}$$

where $\xi^{M,F,B}(\mathbf{p}) = \epsilon_p^{M,F,B} - \mu_{M,F,B}$, and the role of η is described in depth in appendix A), by the self-consistent set of equations

$$\begin{aligned} \hat{D} &= \hat{D^0} + \hat{D^0}\hat{\Pi}\hat{D} \\ \hat{G_B} &= \hat{G_B^0} + \hat{G_B^0}\hat{g}\hat{G_F}\hat{D}\hat{g^\dagger}\hat{G_B} \\ \hat{G_F} &= \hat{G_F^0} + \hat{G_F^0}\hat{g}\hat{G_B}\hat{D}\hat{g^\dagger}\hat{G_F} \end{aligned}$$

where $\hat{\Pi}$ is the molecular self energy. All quantities are functions of the energy E and center-of-mass momentum P of the molecules. The complete solution to these equations is beyond current computational capabilities, except perhaps by Monte Carlo methods.

We therefore make a few simplifying assumptions, namely we account for propagation of the atomic fermions and bosons using their free Green functions

only (i.e., setting $\hat{G_F} \approx \hat{G_F^0}$ and $\hat{G_B} \approx \hat{G_B^0}$). An important consequence of these choices is that the many-body T-matrix is approximated by its ladder series, which means that $\hat{\Pi} \approx g\hat{G_B^0}\hat{G_F^0}g^\dagger$ analogously to that introduced chapter 3, but obtained integrating the free Green functions in eq. 5.3. This standard approximation has the property of being exact in the two-body limit, where Eq. 5.1 satisfies 5.2. This implies that the two-body physics is accounted for exactly in the many-body problem.

Another appealing characteristic of this approach is that the molecular self energy Π can be calculated exactly [71], leading to the following expression

$$\begin{aligned}\Pi(E,P) = \tfrac{g^2}{\pi^2} m_{bf}\Lambda - \tfrac{g^2}{4\pi^2} m_{bf} k_f - \tfrac{g^2}{8\pi^2}\left(\tfrac{m_b k_f^2}{P} - \tfrac{m_{bf}^2 P}{m_b} - \tfrac{m_b D}{P}\right) \\ \ln\left(\tfrac{(k_f + P\ m_{bf}/m_b)^2 - D}{(k_f - P\ m_{bf}/m_b)^2 - D}\right) + \tfrac{g^2}{4\pi^2} m_{bf}\sqrt{D}\ \ln\left(\tfrac{(k_f+\sqrt{D})^2 - (P\ m_{bf}/m_b)^2}{(k_f - \sqrt{D})^2 - (P\ m_{bf}/m_b)^2}\right),\end{aligned} \tag{5.4}$$

where $D = \sqrt{2m_{bf}(E - P^2/2(m_f + m_b) + \mu)}$, and Λ is the ultraviolet cutoff introduced in chapter 3, which in the $V_{bg} \to 0$ approximation used here can be regularized by a shift in the detuning $\nu \to \nu - \frac{g^2}{\pi^2} m_{bf}\Lambda$.

Further approximations include considering a homogeneous system where the density of the fermionic subsystem is much larger than that of the bosonic one, whereby the avoided crossing between atomic and molecular state introduced in chapter 4 becomes approximately a real crossing. This condition is introduced for the purposes of this section, to allow us to isolate the effects of Pauli blocking on the collision physics, and will be relaxed later, when we study the equilibrium properties of the system.

The set of equations we obtain with these approximations is therefore

$$T(E) = g^2 D(E), \tag{5.5}$$

where $D(E)$ is the pair propagator defined by:

$$D(E) = D^0(E) + D^0(E)\Pi(E)D(E), \tag{5.6}$$

$$\Pi(E) = g^2 G_B^0(E) G_F^0(E),$$

which lead to

$$T(E,P) = \frac{g^2}{E - \frac{P^2}{2m} - \nu + \mu - \Pi(E,P)}, \tag{5.7}$$

where $m = m_f + m_b$ is the molecular mass.

In order to understand the stability of a BF molecule, we study the structures of the poles and residues of the T-matrix in Eq. (5.7). To determine numerically the poles, we consider this equation as a system of two nonlinear equations for real and imaginary parts of the internal energy, $E - P^2/2(m_f + m_b) + \mu$. The resulting nonlinear system of equations always has some unphysical solutions which can be rejected by the following analysis: i) the residues for physical solutions, which represent the distribution of population in that state (see appendix A) must be less than unity; ii) for the imaginary solutions the relative momentum, $D = \sqrt{2m_{bf}(E - P^2/2m + \mu)}$ in Eq. (5.4), should dwell on the lower half of the complex momentum plane, to ensure that resonances decay with time [72]; iii) the sum rule (5.11, see below) should be fulfilled including both the discrete and continuum parts.

As an example, we have calculated the poles of (5.7) for a dual species gas with fermion density 10^{13} cm^{-3} and boson density 10^{14} cm^{-3}. The results are shown in Figure 5.2 for two representative center-of-mass momenta P of the molecules. (Note the different scale from Figure 5.1). Unphysical poles are not shown in this figure. These results are cast as a kind of "binding energy," by subtracting the center-of-mass kinetic energy, and adding the chemical potential μ. They can therefore be compared directly to the two-body results in Fig. 5.1.

The structure of these poles is quite different near resonance, although we stress that far from resonance ($\nu \gg \gamma^2/2$) they return to the two-body values. A main difference from the two-body case is that now there may exist physical poles

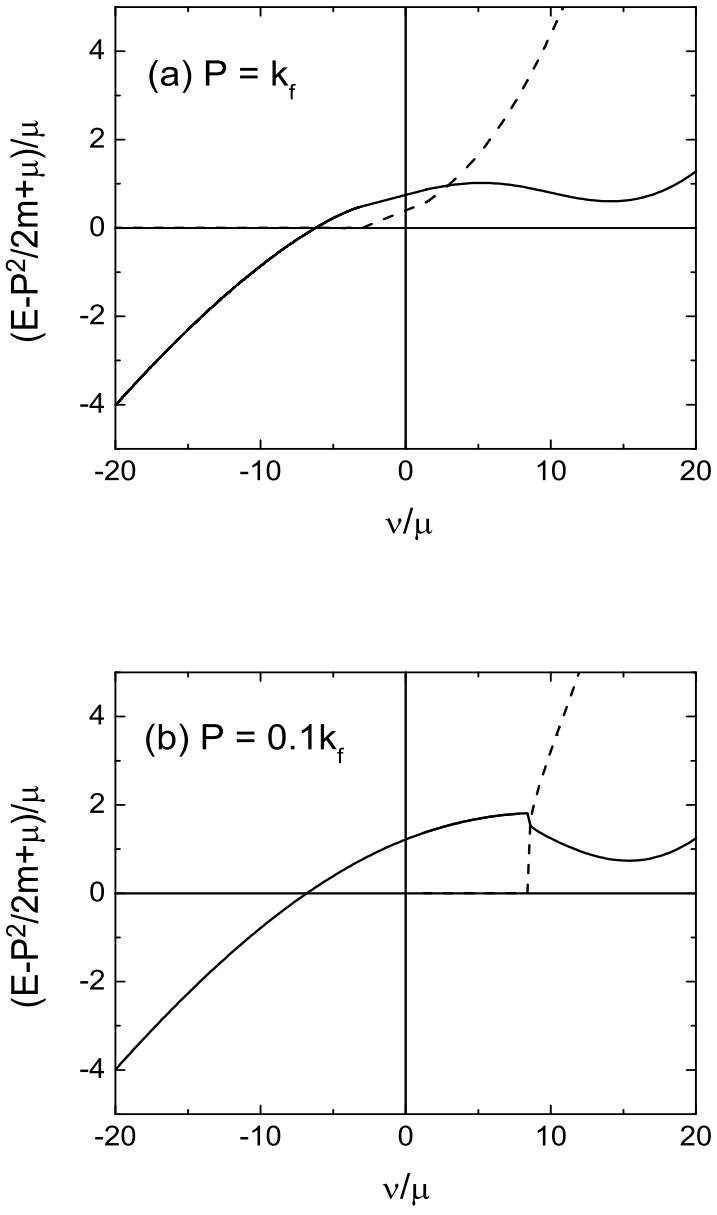

Figure 5.2: Complex poles of the many-body T-matrix, as a function of detuning. Solid and dashed lines denote the real and imaginary parts of physically relevant poles. In (a) the center-of-mass momentum of the molecule is $P = k_f$, i.e., equal to the Fermi momentum of the atomic gas. In (b), this momentum is $P = 0.1k_f$.

for any detuning across the resonance, depending on momentum. The appearance of poles depends, however, on the center-of-mass momentum P of two atoms. If $P \gg 2k_f$, the two-body physics will not be influenced much and the poles structure will be as it is in Fig. 5.1. We have verified this numerically, but have not shown it in this thesis.

Figure 5.2(a) shows the case where the center-of-mass momentum of the atom pair is equal to the Fermi momentum of the atomic gas, $P = k_f$. The criterion of molecular stability is set by the vanishing of the imaginary part of the pole. Figure 5.2(a) shows that the imaginary part remains zero until $\nu/\mu \sim -5$, after which the pair becomes unstable. Thus, for detunings $-5 \leq \nu/\mu \leq 0$, some of the molecules that would have been stable become de-stabilized in the many-body environment. They may still be rather long-lived, however. In the limit of very large momenta, $P \gg 2k_f$, we find that the pole structure returns to the two-body value. This makes sense, since a very rapidly-moving molecule does not interact strongly with the gas at all. In particular, for $P \geq 2k_f$, we find that a "gap" reappears, in which no physical poles exist for some range of positive detuning. In the $P \to \infty$ limit, this gap returns to its two-body value, $\gamma^2/2$.

Figure 5.2(b) shows an alternative case in which the molecular momentum is much smaller than the atomic Fermi momentum, $P = 0.1k_f$. In this case, the imaginary part of the pole only differs from zero at positive detunings, $\nu/\mu > 8$. Therefore, quite the opposite to the $P = k_f$ case, here the molecules that would have been unstable are stabilized by the presence of the many-body environment. Roughly, this is due to Pauli blocking of the fermionic atoms into which the molecules would dissociate. If such an atom already occupies the state into which the molecule would drop its atom, then the process is forbidden. We discuss this further below. For any molecule with $P \leq 2k_f$, there exist physical poles at all detunings. Thus positive-detuning molecules are always present in the BF

mixture.

5.1.3 Conditions for molecular stability

To make a more global picture of whether molecules are stable or not for a given detuning, we can consider the spectral function for atom pairs. In general, when the molecular propagator possesses an imaginary part, this part alludes to the decay rate of the pair due to interactions with the rest of the gas, in the same sense that the oscillator strength of an atom alludes to its decay rate by spontaneous emission. Following a standard approach (see appendix A), the spectral function is defined as

$$\rho(P,E) = -\frac{1}{\pi} ImD(P,E). \tag{5.8}$$

In the case of a true, bound molecular state, the spectral function reduces to a delta function at the energy of the state E_0:

$$\rho(P,E) = 2\pi Z(P)\delta(E - E_0), \tag{5.9}$$

where the coefficient is given by the "spectral weight" function

$$Z(P) = \frac{1}{1 - dRe(\Pi(P,E))/dE|_{E_0}}. \tag{5.10}$$

Just as for an oscillator strength, the discrete and continuum parts of the spectral density must satisfy a sum rule:

$$Z(P) + \int dE\rho(E,P) = 1 \tag{5.11}$$

for each momentum P. We have explicitly verified the sum rule in each case we computed, as a test of the numerical procedure, and to distinguish between physical and unphysical poles of the T-matrix.

As mentioned above, the spectral weight Z is associated with a specific pole E_0 of the T-matrix, an energy level of the system, and represents its population.

Therefore, if Z vanishes, so does the probability of finding stable molecules in the gas. To this end, Figure 5.1.3 plots contours of the function $Z(P)$ as a function of detuning ν and center-of-mass momentum P of the atom pairs. These calculations are performed for fermion density $n_f = 10^{13}$ cm^{-3}. The contour of $Z = 0$ thus represents the borderline between conditions where molecules exist and are stable (to the left of this line) and where they are unstable to decay (to the right of this line, in the white region of the graph).

Figure 5.1.3 thus shows that: i) molecules are still stable for a continuum of positive detuning when P is small; ii) molecules that *would have been* stable at negative detuning may not be such stable at intermediate momenta P (although at small negative detuning they may possess small widths); and iii) in the limit $P \rightarrow \infty$, the borderline between stable and unstable again returns to zero detuning.

Thus far, these are exact results, at least within the simplifying approximations made above. Once this is done, the effective dissociation energy of the molecules within the medium is determined. The relation between the molecule's total energy at dissociation and the molecule's momentum is then easily determined from kinematics, plus simple considerations on the Pauli blocking of the atomic fermions. For example, consider the case where the molecule's kinetic energy is greater than twice the atomic Fermi energy, i.e., $P^2/2(m_f + m_b) \geq 2 \times k_f^2/2m$. At the same time, the molecule is assumed to be exactly at its dissociation threshold, so that it could live equally well as a molecule or as two free atoms. Upon dissociating, each atom would carry away half the energy, so in particular the fermionic atom is at the top of the Fermi sea, and this dissociation is not prevented by the Pauli exclusion principle. The total energy of the molecule at its dissociation threshold is then determined simply by the molecular kinetic energy, and no contribution is required from the molecular binding energy. Thus, if B represents the internal energy of the pairs relative to threshold, bound

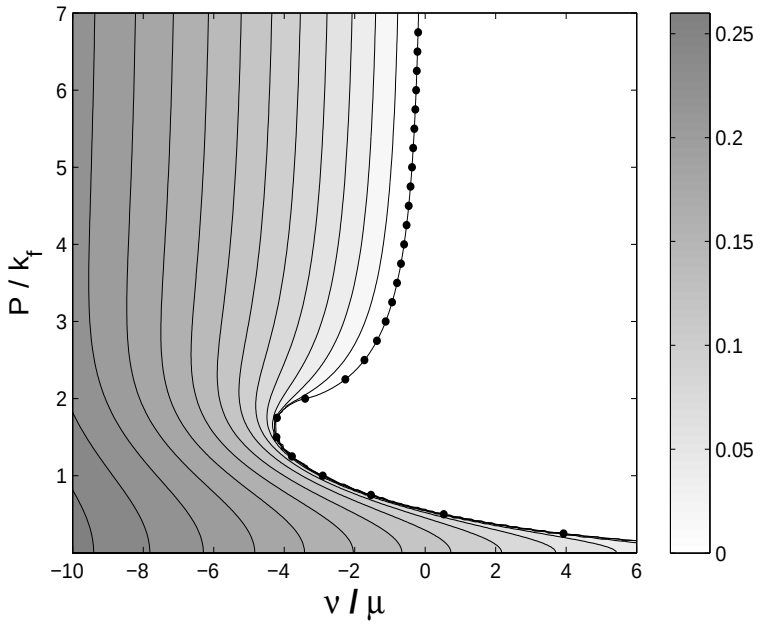

Figure 5.3: Contours of molecular population under various combinations of molecular center-of-mass momentum P and detuning ν. The uppermost contour identifies the detuning at which bound molecules first appear for a given momentum P. Numbers indicate contours with a equal molecule fraction. The dots represent the result obtained analytically for the critical detuning, Eq. (5.16).

molecules are possible when

$$B \leq 0 \quad \text{for} \quad P \geq \sqrt{\frac{2(m_b + m_f)}{m_f}} k_f. \tag{5.12}$$

Alternatively, suppose the molecules have less than twice the atomic Fermi energy, $P^2/2(m_f + m_b) \leq 2 \times k_f^2/2m$. Now it is no longer guaranteed that the molecules can automatically decay in the many-body environment, since the fermion's kinetic energy may lie below the Fermi level of the atomic gas. In such a case, the molecule can sustain a *positive* internal energy without dissociating, simply due to Pauli blocking. To decide how high this binding energy can be, we examine the conservation of energy and momentum in the dissociation process:

$$\mathbf{P} = \mathbf{p}_f + \mathbf{p}_b \tag{5.13}$$

$$\frac{P^2}{2(2m)} + B = \frac{p_b^2}{2m_b} + \frac{p_f^2}{2m_f}. \tag{5.14}$$

Here $\mathbf{p}_f$, $\mathbf{p}_b$, and $\mathbf{P}$ are the momenta of the atomic fermions, atomic bosons, and molecules, respectively. To ensure that the atomic fermion emerges with the maximum possible kinetic energy, we consider the case where $\mathbf{P}$ and $\mathbf{p}_f$ point in the same direction. To ensure that $p_f > k_f$, where k_f is the atomic Fermi momentum, along with (5.14), implies that molecules are stable when

$$B \leq \frac{(m_f P - (m_b + m_f)k_f)^2}{2m_b\ m_f(m_b + m_f)} \quad \text{for} \quad P \leq \sqrt{\frac{2(m_b + m_f)}{m_f}} k_f. \tag{5.15}$$

Figure 5.4 shows the internal energy of the molecules evaluated at the stability boundary, as described above, as a function of center-of-mass momentum. The solid line in this figure is determined numerically from the $Z = 0$ contour of Fig. 5.1.3. Subtracting the kinetic energy contribution and chemical potential from the pole of the T-matrix evaluated on the contour, we obtain the molecular internal energy. Also shown, as dots, are the kinematic estimates (5.12,5.15).

Analytical expressions for the detuning at the boundary as a function of center-of-mass momentum, plotted as dots in Fig. 5.1.3, are readily obtainable

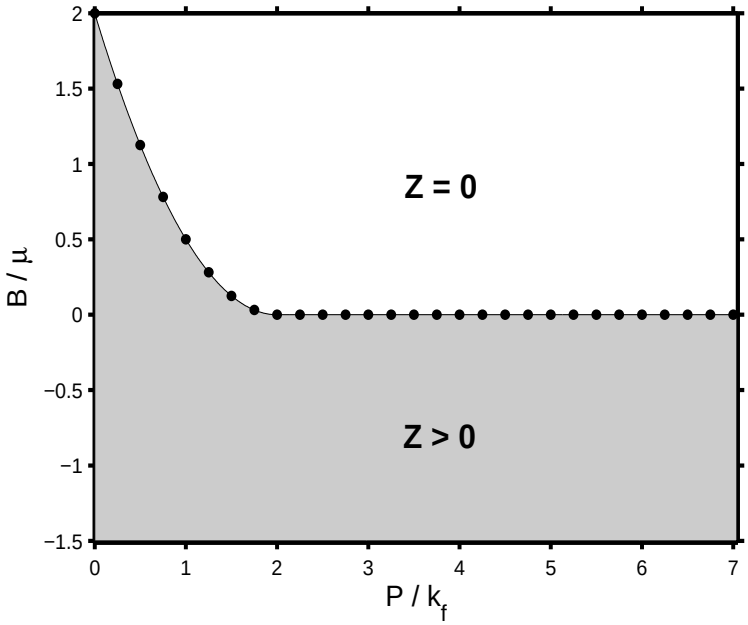

Figure 5.4: The internal energy that a molecule of center-of-mass momentum P/k_f would require to overcome Pauli blocking and dissociate. The shaded area represents numerical calculations, and the dots represent the analytical kinematic arguments in Eqs. (5.12,5.15).

analytically, with similar accuracy by inspecting the denominator of Eq. (5.7). The total energy of the molecule, measured from the chemical potential, is, in fact, given by the pole of (5.7). In general this energy can be written as $E_0 = \frac{P^2}{2(m_f+m_b)} - \mu + B$, where B is a complicated function of all the parameters. However, since E_{tot} is a pole of (5.7), then $E_0 = \frac{P^2}{2(m_f+m_b)} - \mu + \nu + \Pi(E_0, P)$, so

$$\nu_{crit} = B - \Pi\left(\frac{P^2}{2(m_f+m_b)} - \mu + B, P\right). \tag{5.16}$$

Plugging the stability boundary value of B from Eqs. (5.12,5.15) into this formula leads to an analytic, albeit complicated, expression for the critical detuning as a function of cente-of-mass momentum.

5.2 Many-Body Physics

Having described the effect of the many-body medium on the resonant collision physics, we now proceed to an equilibrium analysis of the system. In chapter 4, we introduced the mean-field theory for the gas; here we will introduce a generalized version of that same theory, which will properly take into account for the intricacies of the resonant two-body physics.

We begin this discussion by introducing the mean-field theory approach in the language of Green-Functions, within the limits of the three approximations we tested in the previous chapter, namely

- $V_{bg} \to 0$
- $\gamma n_b^3 \to 0$
- $\langle \eta_b f(p) \rangle \to 0$.

The self-consistent Dyson equations that describe this system are:

$$\begin{aligned} G_F^{MF}(E,P) &= G_F^0(E,P) + g^2 n_b \; D^0(E,P) \; G_F^{MF}(E,P) \\ D^{MF}(E,P) &= D^0(E,P) + g^2 n_b \; G_F^0(E,P) \; D^{MF}(E,P). \end{aligned} \tag{5.17}$$

The processes which these equations describe, depicted diagrammatically in fig 5.5, are simply the facts that a free fermion may encounter a condensed bosons on its path and associate with it creating a molecule, or that a free molecule may split into a fermion and a condensed boson. The self-consistency ensures that these processes may be repeated coherently an infinite number of times. The omission of the bosonic renormalization equation $\phi^{MF} = n_b^0 + g^2 n_b \; G_F^0(E,P) \; D^0(E,P)$, whereby a boson sitting in the condensate may pick-up a fermion to create a molecule, is a restatement of the third of the approximations described above.

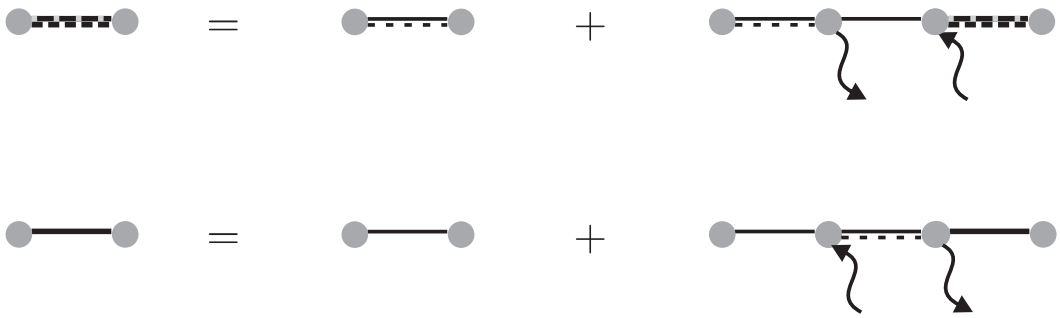

Figure 5.5: Feynman diagrams included in the mean-field theory. Thin (thick) solid lines represent free (renormalized) fermions, thin double dashed-solid lines represent free molecules, and thick double dashed lines represent renormalized molecules. The little lightning bolts represent condensed bosons, whereby the arrow indicates whether they are taken from or released into the condensate.

Solutions to these equations take the form

$$\begin{aligned} G_F^{MF}(E,P) &= \frac{1}{G_F^0(E,P)^{-1} - g^2 n_b \; D^0(E,P)} \\ D^{MF}(E,P) &= \frac{1}{D^0(E,P)^{-1} - g^2 n_b \; G^0(E,P)}. \end{aligned} \tag{5.18}$$

Plugging in the definitions of $G_F^0(E,P)$ and $D^0(E,P)$ from eq 5.3 and solving for the poles, we notice that we get exactly the mean-field eigenvalues $\lambda_{\alpha,\beta}(p)$ from chapter 3, appropriately modified to include the three approximations above-mentioned.

Another interesting property of this theory, is that it is perfectly symmetric

with respect to interchange of G_F and D, which implies that both renormalized Green functions have the same poles, and the same residues, which means that we can, for example, study the properties of the fermions by only looking at the molecules. This is not completely striking, since, given that the condensed bosons are relatively inert, every molecules corresponds exactly to a missing fermion, and vice-versa.

The simple discussion above, in terms of the fundamental processes included in the theory, highlight numerous limitations, but one is particularly striking, namely that we only allow molecules to decay into a free fermion and a condensed boson, disregarding the possibility that the bosonic byproduct may be noncondensed. The fundamental mean-field assumption is that the gas is at zero temperature, and therefore the noncondensed population should be negligible at equilibrium. Furthermore, if a molecule is made by a zero-momentum boson and a fermion from the Fermi sea, dissociating into a noncondensed boson implies that the outgoing fermion would have momentum lower than the Fermi momentum, and will need to be "fit" into quite a tightly packed Fermi sea, an event which Pauli blocking makes quite unlikely.

In this light, we should therefore feel relatively confident about the fact that if a molecule does indeed decay yielding a non-condensed boson, it should be in order to recapture it right-away, in a virtual process such as that described in fig. 3.1. It is only convenient that these events are exactly the kind of events which will correctly renormalize the binding energy of the molecules, leading to a theory which will reproduce the exact two-body resonant physics.

The Dyson equation describing this theory are:

$$\begin{aligned} G_F^{GMF}(E,P) &= G_F^0(E,P) + g^2 n_b \; D(E,P) \; G_F^{GMF}(E,P) \\ D^{GMF}(E,P) &= D(E,P) + g^2 n_b \; G_F^0(E,P) \; D^{GMF}(E,P). \end{aligned} \tag{5.19}$$

where D is the renormalized molecular propagator from equation 5.7. A diagrammatic representation of this theory appears in fig. 5.6, and the solution to these equations are:

$$\begin{aligned} G_F^{GMF}(E,P) &= \frac{1}{G_F^0(E,P)^{-1} - g^2 n_b \; D(E,P)} \\ D^{GMF}(E,P) &= \frac{1}{D(E,P)^{-1} - g^2 n_b \; G^0(E,P)}. \end{aligned} \tag{5.20}$$

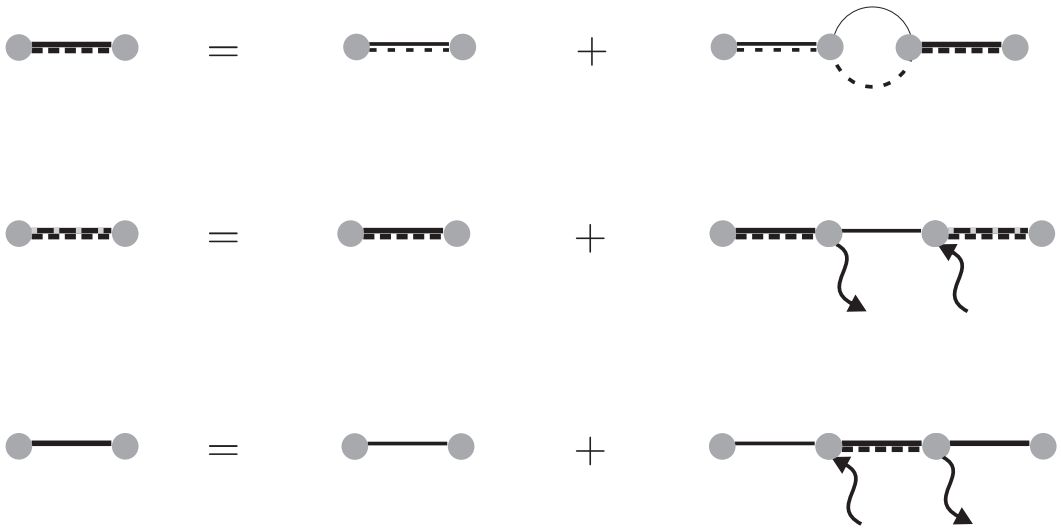

Figure 5.6: Feynman diagrams included in the generalized mean-field theory. Like in the mean field case (fig 5.5), thin (thick) solid lines represent free (renormalized) fermions, thin double dashed-solid lines represent free molecules, and thick double dashed lines represent renormalized molecules. The little lightning bolts represent condensed bosons, whereby the arrow indicates whether they are taken from or released into the condensate. The novelty here in the inclusion of the 2-body dressed molecules from fig. 3.1.

These equations preserve the symmetrical nature of the mean-field theory described above, and also the two avoiding states structure discussed in the previous chapter. This is demonstrated in figure 5.7, where we reproduce the $P = k_f$ pole of D from fig 5.1, and the corresponding poles for the generalized mean-field theory. As in figure 4.1 we note the splitting in two energy levels, avoiding eachother around $\nu = 0$. The fundamental difference in this case is that the molecular

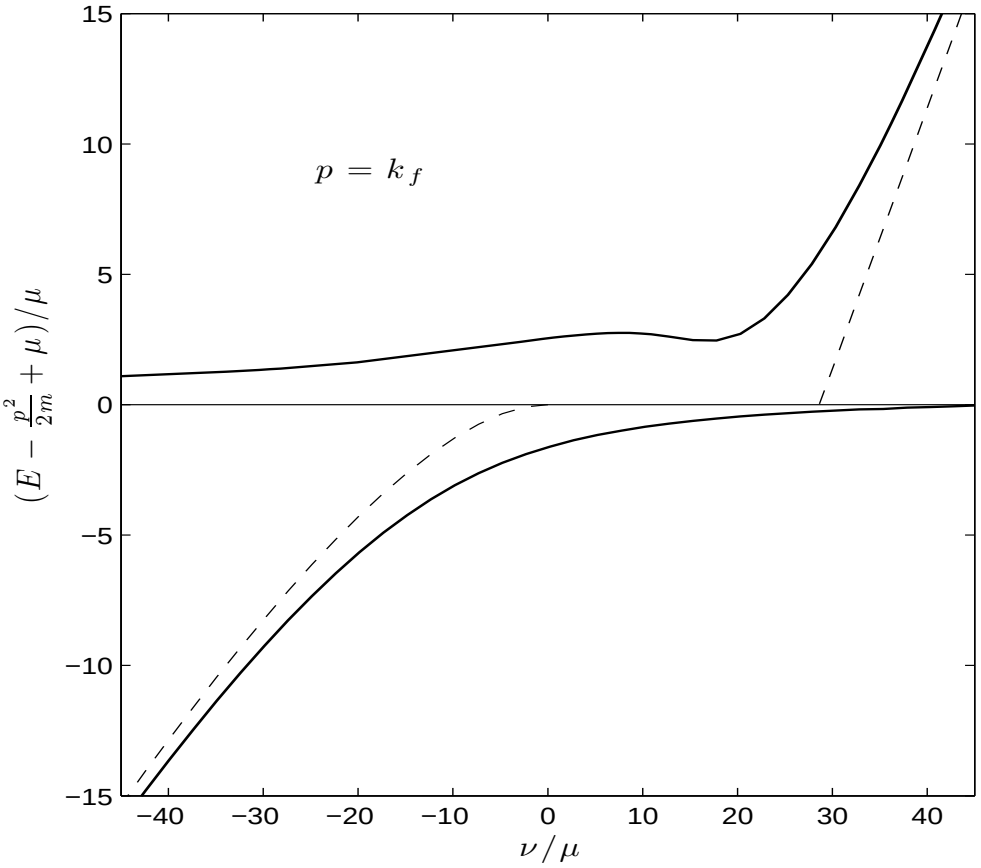

Figure 5.7: The thick lines represent the poles of $D^{GMF}(k_f)$, and correspond to molecular and fermionic energies. The dashed lines represent the molecular two-body poles, corresponding to the molecular binding and resonant energies. Comparison with the top panel of fig 5.2 highlights the fact that, as in the mean-field theory case, the effect of the interaction with the condensate is to create an avoided crossing between the atomic and molecular states.

curve does not asymptote to the bare detuning, but rather to the correct molecular binding and resonance energies.

Studying the equilibrium properties of the system is now a matter solving the self-consistent set of equations 4.4.a-4.4.e, remembering to disregard η_{mf} and λ. To do this we first need to extract the distributions $\eta_{f,m}$ from the Green functions D^{GMF} and G_F^{GMF}; to avoid taking a distracting detour here, we refer the reader to appendix A.

As in the previous section, we will consider a mixture composed free gas of fermionic ^{40}K atoms, with a density of $8.2 \times 10^{14} cm^{-3}$, and a gas of condensed ^{87}Rb bosons with density 4.9×10^{15} (corresponding to the respective Thomas-Fermi densities of 10^6 atoms of either species in the center of a $100Hz$ spherical trap).

As mentioned in Chapter 4, the generalized mean-field theory presented here is very similar, in spirit, to the simple mean-field theory presented there. The real difference between the two, is simply a shift in the molecular internal energy structure, in line with the two-body results of Chapter 3. This means that the difference between the two approaches will be quantitiatve only, and that the interpretation of the results can be done in the same exact way as we did in section 4.1.2.

Figure 5.8 shows the equilibrium molecular population as a function of detuning, for the $492.5G$ resonance, where, for the conditions mentioned above, the mean-field parameter $\epsilon_{SM} = g^2 n_b / E_f^2 \approx .38$ is indeed perturbative. In this regime, the agreement between mean-field and generalized mean-field is quite good, unlike the example in fig. 5.9, where the mean-field parameter is $\epsilon_{SM} = 38.7$. The difference in this latter example is due to the fact that the actual molecular bound-state energy is actually higher than the bare detuning, by an amount proportional to ϵ_{SM}. Using the chemical potential arguments analogous to the ones used in sec.

4.1.2, this can be shown to hinder molecular formation.

5.3 Non-Equilibrium Mean-Field Theory Revisited

In section 4.2, we outlined the limitations of the non-equilibrium theory, by claiming that to obtain the correct two-body physics in the low-density limit it would be necessary to include three point and possibly higher correlations. While this fact is indeed true, we showed in the previous section that for experimentally reasonable parameters, there exists a regime where mean-field theory accurately describes the equilibrium properties.

In and of itself, this argument does not necessarily guarantee that the non-equilibrium approach will also be accurate, however the results do encourage us to push forward, though the results should be taken with an appropriate amount of caution.

In the following we wish to study molecular formation via a time dependent ramp of the magnetic field across the resonance. To this end we use two approaches: the first consists of propagating equations 4.18.a-4.18.d, ramping the detuning linearly in time from a large positive value to a large negative one, and plotting the final molecular population as a function of detuning ramping rate R. The second approach consists in noticing that if $\nu(t)$ is a linear function of time, then the mean-field Hamiltonian (eq. 4.10) is ideally suited to a Landau-Zener treatment, whereby the final molecular population as a function of detuning can be readily written as

$$n_m/min(n_b, n_f) = 1 - e^{\frac{-R}{\tau}} \tag{5.21}$$

Here $n_m/mim(n_b, n_f)$ is the fraction of possible molecules formed, and $R = 1/\frac{\partial B}{\partial t}$ is the inverse ramp rate, and the exponential time constant is given by $\tau = \frac{\hbar\delta_B}{g^2 n_b} = \frac{m_{bf}}{ha_{bg}n_b\Delta_B}$, where a_{bg} is the background scattering length, m_{bf} the reduced mass, h

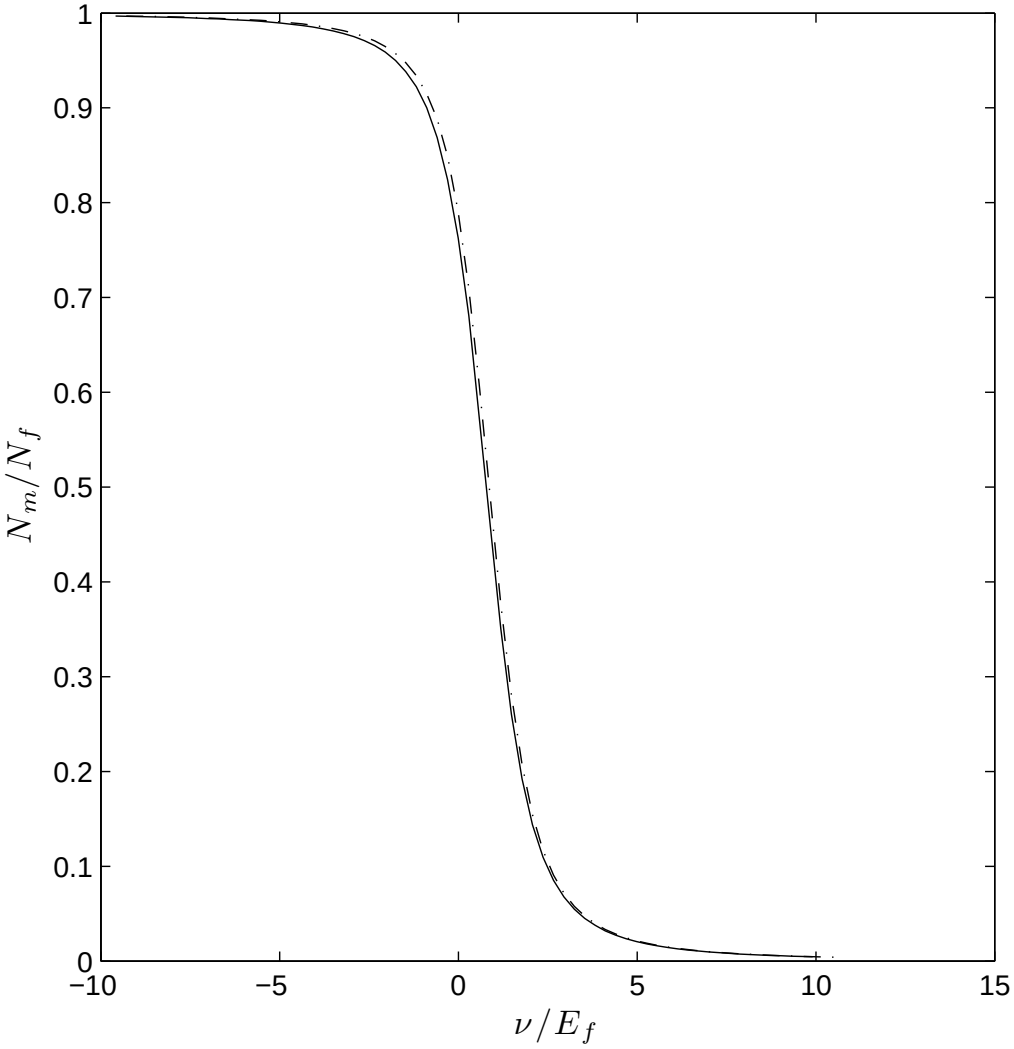

Figure 5.8: Equilibrium molecular population as a function of detuning for the narrow $492.49G$ resonance. The solid line represents results obtained via the generalized mean-field theory presented in the text, while the dashed-dotted line represents the mean-field results.

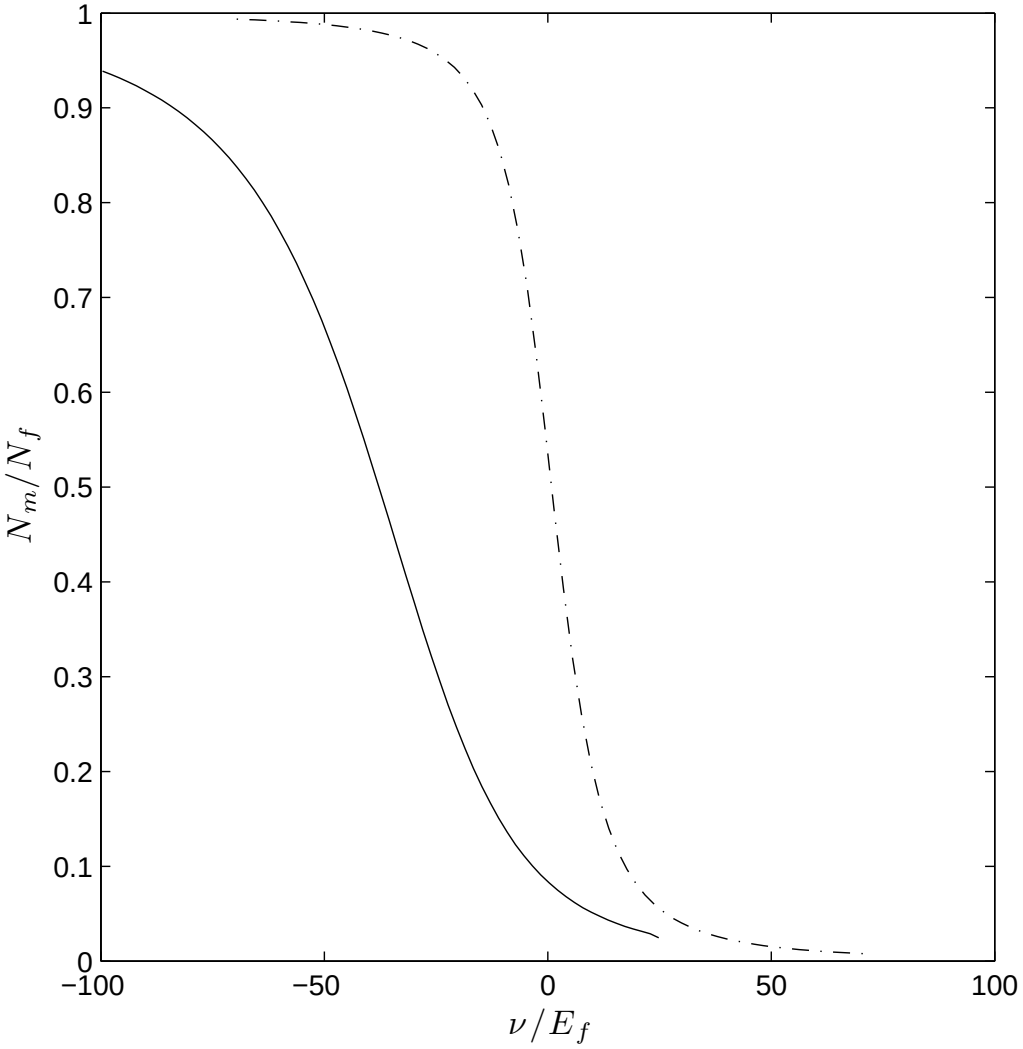

Figure 5.9: Equilibrium molecular population as a function of detuning for the wider $544.7G$ resonance. The solid line represents results obtained via the generalized mean field theory presented in the text, while the dashed-dotted line represents the mean field results.

is Plank's constant, and Δ_B is the magnetic field width of the resonance.

Remarkably, the τ does not depend on the fermionic density. This is an artifact due to fact that in mean-field theory the momentum states of the fermionic gas are uncoupled, except via the depletion of the condensate. Since in the Landau-Zener approach the depletion is assumed small, it follows that the various fermionic momentum states are considered independent, and that the probability of transition of the gas is equal to the probability of transition of each individual momentum state. This approximation is only valid for narrow resonances, such as the $492.5G$ resonance in table 3.1.

The two approaches described above agree virtually exactly, and the results for an example set of parameters is shown in fig 5.10. We note from the bottom panel of the figure, that the Landau-Zener model agrees with the numerical simulations even when $n_b < n_f$. This is quite surprising, since the width of the crossing is proportional to density of leftover bosons, and we expect that this number will change substantially as the bosonic population is depleted via the formation of molecules. This type of time dependent crossing should not be properly described by the Landau-Zener formula. However, monitoring the time evolution of the molecular population as a function of time shows that the majority of the transfer takes place quite abruptly somewhat after crossing the zero-detuning region, whereby the change in bosonic density does not modify the energy levels substantially.

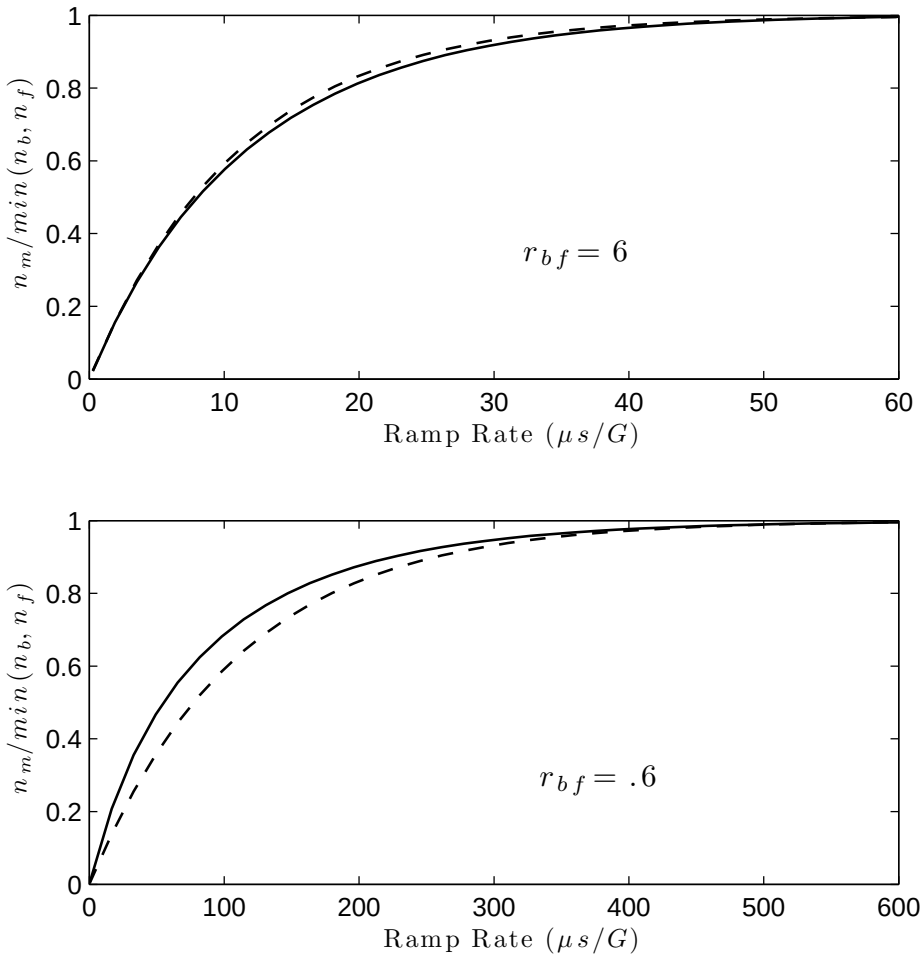

Figure 5.10: Transition probability into molecular state via a magnetic-field ramp across the $492.5G$ Feshbach resonance. The solid lines are obtained via numerical solutions of equations 4.18.a-4.18.d, while the dashed lines represent the Landau-Zener equivalent. In the top panel the gas is composed of more bosons than fermions $r_{bf} = 6$, while in the bottom panel the opposite is true $r_{bf} = .6$

Chapter 6

Conclusion

In this thesis, we developed and solved a generalized mean-field theory describing an ultracold atomic Bose-Fermi mixture in the presence of an interspecies Feshbach resonance. The "generalized" attribute refers to the fact that we had to modify the simple mean-field treatment obtained by neglecting bosonic fluctuations, to include the correct two-body physics.

We also attempted to give a reasonably self-consistent account of the two-body physics involved, and attempted to bridge the often obscure gap between it and the many-body field-theoretical treatment.

The theory presented, as any mean-field theory, presents undeniable limitations. Nevertheless, any useful many-body treatment must start from a well conceived mean-field theory, which we provide herein.

In light of these remarks, necessary future directions of this work may include the generalization to finite temperature, and the inclusion of a trap, initially in a local-density approximation. These advances would be essential to check for empirical confirmation (or lack there of) of the theory.

Bibliography

[1] J. Bardeen, L. N. Cooper, and J. R. Schrieffer. Phys. Rev., 108(5):1175–1204, Dec 1957.

[2] S.N. Bose. Z. Phys, 26:178–181, 1924.

[3] A. Einstein. Physik- Mathematik, pages 261–267, 1924.

[4] M. Greiner, C.A. Regal, and D.S. Jin. Nature, 426(6966):537–540, 2003.

[5] M. Bartenstein, A. Altmeyer, S. Riedl, S. Jochim, C. Chin, J.H. Denschlag, and R. Grimm. Physical Review Letters, 92(12):120401, 2004.

[6] MW Zwierlein, CA Stan, CH Schunck, SMF Raupach, AJ Kerman, and W. Ketterle. Physical Review Letters, 92(12):120403, 2004.

[7] E.A. Donley, N.R. Claussen, S.T. Thompson, and C.E. Wieman. Nature, 417:529–533, 2002.

[8] S. Inouye, J. Goldwin, M. L. Olsen, C. Ticknor, J. L. Bohn, and D. S. Jin. Phys. Rev. Lett., 93(18):183201, Oct 2004.

[9] Francesca Ferlaino, Chiara D'Errico, Giacomo Roati, Matteo Zaccanti, Massimo Inguscio, Giovanni Modugno, and Andrea Simoni. Phys. Rev. A, 73(4):040702, Apr 2006.

[10] CA Stan, MW Zwierlein, CH Schunck, SMF Raupach, and W. Ketterle. Physical Review Letters, 93(14):143001, 2004.

[11] C. Ospelkaus, S. Ospelkaus, L. Humbert, P. Ernst, K. Sengstock, and K. Bongs. Physical Review Letters, 97(12):120402, 2006.

[12] R. Roth and H. Feldmeier. Physical Review A, 65(2):21603, 2002.

[13] R. Roth. Physical Review A, 66(1):13614, 2002.

[14] G. Modugno, G. Roati, F. Riboli, F. Ferlaino, R.J. Brecha, and M. Inguscio. Science, 297(5590), 2002.

[15] H. Hu and X.J. Liu. Physical Review A, 68(2):23608, 2003.

[16] X.J. Liu, M. Modugno, and H. Hu. Physical Review A, 68(5):53605, 2003.

[17] L. Salasnich, S.K. Adhikari, and F. Toigo. Physical Review A, 75(2):23616, 2007.

[18] P. Pedri and L. Santos. Two-Dimensional Bright Solitons in Dipolar Bose-Einstein Condensates. Physical Review Letters, 95(20):200404, 2005.

[19] Sadhan K. Adhikari. Physical Review A (Atomic, Molecular, and Optical Physics), 70(4):043617, 2004.

[20] HP Büchler and G. Blatter. Physical Review A, 69(6):63603, 2004.

[21] R. Kanamoto and M. Tsubota. Physical Review Letters, 96(20):200405, 2006.

[22] S.K. Adhikari. Physical Review A, 72(5):53608, 2005.

[23] A. Albus, F. Illuminati, and J. Eisert. Physical Review A, 68(2):23606, 2003.

[24] M. Lewenstein, L. Santos, MA Baranov, and H. Fehrmann. Physical Review Letters, 92(5):50401, 2004.

[25] R. Roth and K. Burnett. Physical Review A, 69(2):21601, 2004.

[26] A. Sanpera, A. Kantian, L. Sanchez-Palencia, J. Zakrzewski, and M. Lewenstein. Physical Review Letters, 93(4):40401, 2004.

[27] K. Günter, T. Stöferle, H. Moritz, M. Köhl, and T. Esslinger. Physical Review Letters, 96(18):180402, 2006.

[28] MJ Bijlsma, BA Heringa, and HTC Stoof. Physical Review A, 61(5):53601, 2000.

[29] H. Heiselberg, CJ Pethick, H. Smith, and L. Viverit. Physical Review Letters, 85(12):2418–2421, 2000.

[30] DV Efremov and L. Viverit. Physical Review B, 65(13):134519, 2002.

[31] L. Viverit. Physical Review A, 66(2):23605, 2002.

[32] F. Matera. Physical Review A, 68(4):43624, 2003.

[33] AP Albus, SA Gardiner, F. Illuminati, and M. Wilkens. Physical Review A, 65(5):53607, 2002.

[34] D.W. Wang. Physical Review Letters, 96(14):140404, 2006.

[35] S. Powell, S. Sachdev, and H.P. Büchler. Physical Review B, 72(2), 2005.

[36] A. Storozhenko, P. Schuck, T. Suzuki, H. Yabu, and J. Dukelsky. Physical Review A (Atomic, Molecular, and Optical Physics), 71(6):063617, 2005.

[37] Eddy Timmermans, Paolo Tommasini, Mahir Hussein, and Arthur Kerman. Phys. Rep., 315:199, 1999.

[38] S. J. J. M. F. Kokkelmans and M. J. Holland. Phys. Rev. Lett., 89(18):180401, Oct 2002.

[39] S. J. J. M. F. Kokkelmans, J. N. Milstein, M. L. Chiofalo, R. Walser, and M. J. Holland. Phys. Rev. A, 65(5):053617, May 2002.

[40] Y. Ohashi and A. Griffin. Phys. Rev. Lett., 89(13):130402, Sep 2002.

[41] RA Duine and HTC Stoof. Journal of Optics B: Quantum and Semiclassical Optics, 5(2):S212–S218, 2003.

[42] E.M. Lifshitz and L.P. Pitaevskii. Statistical Physics part 2. Butterworth-Heinemann, 1996.

[43] C Zener. C. Proc. R. Soc. London A, 137(696), 1932.

[44] L.D. Landau. Phys. Z. Sowjetunion, 1(89), 1932.

[45] D.C.E. Bortolotti, A.V. Avdeenkov, C. Ticknor, and J.L. Bohn. Journal of Physics B: Atomic, Molecular, and Optical Physics, 39(1):189–203, 2006.

[46] A.V. Avdeenkov, D.C.E. Bortolotti, and J.L. Bohn. Physical Review A, 74(1):12709, 2006.

[47] J.J. Sakurai. Modern Quantum Mechanics. Addison-Wesley, 1994.

[48] L.D. Landau and E.M. Lifshitz. Quantum mechanics: non-relativistic theory. Pergamon Press, 1977.

[49] B. Marcelis, E. G. M. van Kempen, B. J. Verhaar, and S. J. J. M. F. Kokkelmans. Phys. Rev. A, 70(1):012701, Jul 2004.

[50] James Burke. Ph.D. Thesis. University of Colorado, 1999.

[51] G. Herzberg. Spectra of diatomic molecules. Van Nostrand Reinhold, 1950.

[52] M. Marinescu and H. R. Sadeghpour. Phys. Rev. A, 59(1):390–404, Jan 1999.

[53] D.M. Brink and G.R. Satchler. Angular momentum. Oxford, 1994.

[54] DE Manolopoulos, MH Alexander, RE Wyatt, C.P. Lett, M. D'Mello, DC Clary, J.C. Phys, RB Walker, JC May, SE Down, et al. J. Chem. Phys, 85:6425–6429, 1986.

[55] BR Johnson. J. Comput. Phys, 13(3), 1973.

[56] RA Duine and HTC Stoof. Physics Reports, 396(3):115–195, 2004.

[57] Thorsten Köhler, Thomas Gasenzer, and Keith Burnett. Phys. Rev. A, 67(1):013601, Jan 2003.

[58] M. Holland, S. J. J. M. F. Kokkelmans, M. L. Chiofalo, and R. Walser. Phys. Rev. Lett., 87(12):120406, Aug 2001.

[59] GM Falco and HTC Stoof. Physical Review Letters, 92(13):130401, 2004.

[60] AV Andreev, V. Gurarie, and L. Radzihovsky. Physical Review Letters, 93(13):130402, 2004.

[61] Y. Ohashi and A. Griffin. Physical Review A, 67(3):33603, 2003.

[62] A.V. Avdeenkov. Journal of Physics B Atomic Molecular and Optical Physics, 37(1):237–246, 2004.

[63] AV Avdeenkov and JL Bohn. Physical Review A, 71(2):23609, 2005.

[64] J.W. Negele and H. Orland. Quantum Many-Particle Systems. Addison-Wesley, 1988.

[65] D.C.E. Bortolotti. unpublished, 2006.

[66] K. Huang. Statistical Mechanics. Wiley, New York, 1987.

[67] NP Proukakis and K. Burnett. National Institute of Standards and Technology, Journal of Research, 101(4):457–469, 1996.

[68] Holland. private communication, 2005.

[69] J. Stajic, JN Milstein, Q. Chen, ML Chiofalo, MJ Holland, and K. Levin. Physical Review A, 69(6):63610, 2004.

[70] GM Bruun and CJ Pethick. Physical Review Letters, 92(14):140404, 2004.

[71] AP Albus, SA Gardiner, F. Illuminati, and M. Wilkens. Physical Review A, 65(5):53607, 2002.

[72] R.G. Newton. Scattering Theory of Waves and Particles. Courier Dover Publications, 2002.

[73] J. Ranninger and S. Robaszkiewicz. Physica B, page 468, 1985.

[74] R. Friedberg and TD Lee. Physical Review B, 40(10):6745–6762, 1989.

[75] Eddy Timmermans, Paolo Tommasini, Mahir Hussein, and Arthur Kerman. Phys. Rep., 315:199, 1999.

[76] M. Holland, J. Park, and R. Walser. Phys. Rev. Lett., 86(10):1915–1918, Mar 2001.

[77] ML Chiofalo, S. Kokkelmans, JN Milstein, and MJ Holland. Physical Review Letters, 88(9):90402, 2002.

[78] T. Loftus, C. A. Regal, C. Ticknor, J. L. Bohn, and D. S. Jin. Phys. Rev. Lett., 88(17):173201, Apr 2002.

[79] Cindy A. Regal, Christopher Ticknor, John L. Bohn, and Deborah S. Jin. Nature, 424:47, July 2003.

[80] NR Claussen, S. Kokkelmans, ST Thompson, EA Donley, E. Hodby, and CE Wieman. Physical Review A, 67(6):60701, 2003.

[81] M. Zaccanti, C. D'Errico, F. Ferlaino, G. Roati, M. Inguscio, and G. Modugno. Arxiv preprint cond-mat/0606757, 2006.

[82] C. Ospelkaus et al. Arxiv preprint cond-mat/0606781, 2006.

[83] AA Abrikosov. Methods of Quantum Field Theory in Statistical Physics. Dover Publications, 1975.

[84] A.L. Fetter and J.D. Walecka. Quantum Theory of Many-Particle Systems. McGraw-Hill, 1971.

[85] G.D. Mahan. Many-Particle Physics. Springer, 2000.

Appendix A

Green Function Methods for Fermions

In this Appendix we briefly introduce some of the Green function techniques that we found useful in our calculations.

A.1 Free Green functions

We start from the Green function for a gas of free fermions, which is given, in the frequency-momentum representation by

$$G^0(w, \mathbf{q}) = \frac{1}{\omega - \xi(\mathbf{p}) + i\eta \ sign(\xi(\mathbf{p}))}, \tag{1.1}$$

where $\xi(\mathbf{p}) = \mathbf{p}^2/2m - \mu$. The momentum distribution, at equilibrium, is given by

$$n(\mathbf{p}) = -i \lim_{\eta \to 0^+} \int \frac{d\omega}{2\pi} e^{i\omega\eta} G^0(w, \mathbf{q}), \tag{1.2}$$

Here the limit comes from the equilibrium condition; the frequency, in the Green function definition, is the fourier space equivalent of time, whereby the real time green function represents the evolution of the system from from time t to t', and the observables obtained this way, represent expected values of the kind $\langle\psi(t)|\mathcal{O}|\psi(t')\rangle$. However, since we want equilibrium conditions, we need to take the limit $t \to t'$, which is non trivial, since G^0 is defined by a green function equation of the form $\mathcal{L}\ G^0(t - t') \propto \delta(t - t')$, where $\mathcal{L}$ is some linear operator, and which higlights a peculiar behaviour in the limit we desire. However, since we

know on physical grounds that observables, such as the momentum distribution, must be defined and well behaved at equilibrium, then by first taking the expectation value integral, and then the limit, we can circumvent the problem. In eq. 1.2 this implies we cannot quite get rid of the fourier transform exponent $e^{i\omega(t-t')}$ until after the ω integral.

To perform the integral in 1.2, we exploit the fourier exponent, by noting that since η is positive, $e^{i\omega\eta} \to 0$ as $\omega \to +i\infty$, so that the integral is identical to a contour integral over the path defined by the real ω axis, closed in the upper complex ω plain by an infinite radius semicircle, which, as we have just seen, gives no contribution to the integral. We can now integrate using the residue theorem.

We note that the integrand in 1.2 has a simple pole at $\omega = \xi(\mathbf{p}) - i\eta\, sign(\xi(\mathbf{p}))$. Thus, if $\xi(\mathbf{p}) > 0$, then the pole is in the lower complex plane, and the integral vanishes, and if $\xi(\mathbf{p}) > 0$, then the pole is in the upper complex plane, with residue 1. Using the residue theorem, and summarizing these results we finally get

$$n(\mathbf{p}) = \Theta(-\xi(\mathbf{p})), \tag{1.3}$$

which we recognize as the zero temperature fermi distribution.

A.2 Interacting Green functions

According to Dyson's equation, the green function for an interacting system has the form

$$G(w, \mathbf{q}) = \frac{1}{\omega - \xi(\mathbf{p}) - \Sigma(\omega, \mathbf{p})}, \tag{1.4}$$

where $\Sigma(\omega, \mathbf{p})$ is an arbitrarily complicated function summarizing all the interactions in the system, which is known as self energy.

The prescription to find Σ is quite straightforward, and it consists of adding all amputated connected feynman diagrams for the system. The fact that, in general, the number of such diagrams is infinite, makes this task virtually impossible.

Nonetheless, eq. 1.4 is very powerful, since it allows one to include the effect of infinite subsets of the total number of diagrams in the system, by only having to explicitly calculate a few representative ones.

An alternative standard approach, leads to the exact result (NOTE: Abrikosov [83] measures energy from μ, here we measure from 0, which is more standard)

$$G(\omega, \mathbf{p}) = \int_0^\infty d\omega' \left[\frac{A(\omega, \mathbf{p})}{\omega - \omega' + i\eta} + \frac{B(\omega, \mathbf{p})}{\omega + \omega' - i\eta} \right], \tag{1.5}$$

Where A and B are, again, arbitrary complicated functions, though they are known to be finite.

To understand A and B more closely, we need to introduce the following well known identity:

$$\lim_{\nu \to 0} \frac{1}{x \pm i\nu} = \mathcal{P}\frac{1}{x} \mp i\pi\delta(x), \tag{1.6}$$

where $\mathcal{P}$ is a Cauchy principal value, which represents the contribution due to a discontinuity in a Riemann sheet (branch cut), and the delta function represents the contribution due to the pole.

Applying 1.6 to 1.5 we get

$$Re\ G(\omega, \mathbf{p}) = \mathcal{P} \int_0^\infty d\omega' \left[\frac{A(\omega, \mathbf{p})}{\omega - \omega' + i\eta} + \frac{B(\omega, \mathbf{p})}{\omega + \omega' - i\eta} \right] \tag{1.7}$$

$$Im\ G(\omega, \mathbf{p}) = \begin{cases} -\pi A(\omega, \mathbf{p}) & if \quad \omega > 0 \\ \pi B(-\omega, \mathbf{p}) & if \quad \omega < 0 \end{cases} \tag{1.8}$$

Finally, eq. 1.2 represents a fundamental property of green functions, and it can be generalized to interacting systems simply substituting G^0 with G. Applying it to eq. 1.5, and performing the ω integral first, we get

$$n(\mathbf{p}) = \int_0^\infty d\omega' B(\omega, \mathbf{p}) = \int_{-\infty}^0 d\omega \frac{-1}{\pi} Im\ G(\omega, \mathbf{p}). \tag{1.9}$$

Introducing the function $\rho(\omega, \mathbf{p}) = -2ImG(\omega, \mathbf{p})$, generally called spectral function, the above equation can be written as

$$n(\mathbf{p}) = \int \frac{d\omega}{2\pi} \rho(\omega, \mathbf{p}) \Theta(-\omega). \tag{1.10}$$

An important property of the spectral function is that for all $\mathbf{p}$,

$$\int \frac{d\omega}{2\pi}\rho(\omega,\mathbf{p}) = 1. \tag{1.11}$$

This can be understood as a sum rule in the following sense: if we wish to calculate the number of holes in the system, we would take the $\eta \to 0^-$ limit in equation 1.2. The distribution would then have been $n_{holes}(\mathbf{p}) = 1 - n(\mathbf{p}) = \int_0^\infty d\omega' A(\omega',\mathbf{p})$, so that $1 = \int_0^\infty d\omega' \left[A(\omega',\mathbf{p}) + B(\omega',\mathbf{p})\right] = \int \frac{d\omega}{2\pi}\rho(\omega,\mathbf{p})$.

Using eq.1.4, toghether with the definition of ρ, we can write

$$\rho(\omega,\mathbf{p}) = \frac{-2Im\Sigma(\omega,\mathbf{p})}{\left[\omega - \xi(\mathbf{p}) - Re\Sigma(\omega,\mathbf{p})\right]^2 + \left[Im\Sigma(\omega,\mathbf{p})\right]^2}. \tag{1.12}$$

Furthermore, if Σ were to be real, or if, eqivalently, the pole of the green function were to be real, for some momentum $\mathbf{p}$, then taking the limit $Im\Sigma \to 0$ of 1.4, and using eq,1.6, we get

$$\rho(\omega,\mathbf{p}) = 2\pi\delta(\omega - \xi(\mathbf{p}) - Re\Sigma(\omega,\mathbf{p})), \tag{1.13}$$

which can be simplified, using the properties of the delta function, to

$$\rho(\omega,\mathbf{p}) = 2\pi Z(\mathbf{p})\delta(\omega - \omega_0(\mathbf{p})), \tag{1.14}$$

where Z, known as spectral weight is given by

$$Z(\mathbf{p}) = \frac{1}{\left|1 - \frac{\partial}{\partial\omega}Re\Sigma(\omega,\mathbf{p})\right|_{w=\omega_0(\mathbf{p})}}, \tag{1.15}$$

and $\omega_0(\mathbf{p})$ is the pole of the green function, defined by

$$\omega_0(\mathbf{p}) - \xi(\mathbf{p}) - \Sigma(\omega_0(\mathbf{p}),\mathbf{p}) = 0. \tag{1.16}$$

The momentum distribution in this case is thus given by

$$n(\mathbf{p}) = Z(\mathbf{p})\int \delta(\omega - \omega_0(\mathbf{p}))\Theta(-\omega) = Z(\mathbf{p})\Theta(-\omega_0(\mathbf{p})). \tag{1.17}$$

Appendix B

Derivation of Mean-Field Equation of Motion

In this appendix we will present a sample derivation of one of the equations of motion, namely that for $\langle \delta^\dagger \delta \rangle$.

Starting with the Hamiltonian in coordinate space

$$\begin{aligned} H = \quad & \int dx\ \psi^\dagger(x) T^F(x) \psi(x) + \\ & \int dx\ \phi^\dagger(x) T^B(x) \phi(x) + \\ & \int dx\ \xi^\dagger(x) T^M(x) \xi(x) + \\ & \frac{1}{2}\,\gamma \int dx\ |\phi(x)|^4 + \\ & V_{bg} \int dx\ |\phi(x)|^2 |\psi(x)|^2 + \\ & g \int dx\ (\xi^\dagger(x)\phi(x)\phi(x) + c.c) \end{aligned} \tag{2.1}$$

, where $T^\alpha(x)$ is the kinetic energy of molecules, bosons or fermions.

We then write the bosonic field in terms of its average and fluctuations around it $\phi(x) = \phi_0(x) + \delta(x)$, where ϕ_0 is a complex number. Inserting this expression in the Hamiltonian, we get the following

$$\begin{aligned} H \quad & = E_0 + \int dx\ \psi^\dagger(x)(T^F(x) + V_{bg}|\phi_0(x)|^2)\psi(x) + \\ & \int dx\ \delta^\dagger(x) T^B(x) \delta(x) + \int dx\ \xi^\dagger(x) T^M(x) \xi(x) + \\ & \gamma \int dx\ (4|\phi_0(x)|^2 |\delta(x)|^2 + \phi_0^*(x)^2 \delta(x)\delta(x) + \end{aligned}$$

$$
\begin{aligned}
&\phi_0(x)^2\delta^\dagger(x)\delta^\dagger(x)) + \\
&\int dx\ \left(\phi_0^*(x)\delta(x) + \phi_0(x)\delta^\dagger(x)\right) \times \\
&\qquad \left(\frac{\gamma}{2}|\phi_0(x)|^2 + V_{bg}|\psi(x)|^2\right) + \\
&\gamma\int dx\ \left(\phi_0^*(x)\delta^\dagger(x)\delta(x)\delta(x) + c.c\right) + \\
&\frac{\gamma}{2}\int dx\ \delta^\dagger(x)\delta^\dagger(x)\delta(x)\delta(x) + \\
&V_{bg}\int dx\ |\delta(x)|^2|\psi(x)|^2 + \\
&g\int dx\ \left[\xi(x)^\dagger\left(\phi_0(x) + \delta(x)\right)\phi(x) + c.c\right],
\end{aligned}
\tag{2.2}
$$

where E_0 is a constant which depends on ϕ_0, and its relevant for its motion, but does not contribute to that of $\delta^\dagger\delta$.

The next step is to calculate the commutator $[\delta^\dagger(z)\delta(z'), H]$, and to take its average, thereby obtaining

$$
\begin{aligned}
\langle[\delta^\dagger(z)\delta(z'), H]\rangle = \quad & \left(T^B(z') - T^B(z)\right)\langle\delta^\dagger(z)\delta(z')\rangle + \\
& \gamma\left[2|\phi_0(z')|^2\langle\delta^\dagger(z)\delta(z')\rangle + \phi_0^2(z)\langle\delta^\dagger(z)\delta^\dagger(z')\rangle -\right. \\
& \left. 2|\phi_0(z)|^2\langle\delta^\dagger(z)\delta(z')\rangle - \phi_0^{*2}(z')\langle\delta(z)\delta(z')\rangle\right] + \\
& \phi_0(z')\left(\gamma\langle\delta^\dagger(z')\rangle|\phi_0(z')|^2 + V_{bg}\int dx\ \langle\delta^\dagger(z')\psi^\dagger(x)\psi(x)\rangle\right) - \\
& \phi_0^*(z)\left(\gamma\langle\delta(z)\rangle|\phi_0(z)|^2 + V_{bg}\int dx\ \langle\delta(z)\psi^\dagger(z)\psi(z)\rangle\right) + \\
& \gamma\int dx\ \left[\phi_0^*(x)(\langle\delta^\dagger(z)\delta(z')\delta^\dagger(x)\delta(x)\delta(x)\rangle\right. \\
& -\langle\delta^\dagger(x)\delta(x)\delta(x)\delta^\dagger(z)\delta(z')\rangle) + \\
& \phi_0(x)(\langle\delta^\dagger(z)\delta(z')\delta^\dagger(x)\delta^\dagger(x)\delta(x)\rangle \\
& \left. -\langle\delta^\dagger(x)\delta^\dagger(x)\delta(x)\delta^\dagger(z)\delta(z')\rangle)\right] + \\
& \gamma\left(\langle\delta^\dagger(z)\delta^\dagger(z')\delta(z')\delta(z')\rangle - \langle\delta^\dagger(z)\delta^\dagger(z)\delta(z)\delta(z')\rangle\right) + \\
& V_{bg}\left(\langle\delta^\dagger(z)\delta(z')\psi^\dagger(z')\psi(z')\rangle - \langle\delta^\dagger(z)\delta(z')\psi^\dagger(z)\psi(z)\rangle\right) +
\end{aligned}
$$

$$g\left(\langle\xi(z')\psi^{\dagger}(z')\delta^{\dagger}(z)\rangle - \langle\xi^{\dagger}(z)\psi(z)\delta(z')\rangle\right). \tag{2.3}$$

The next step is to apply Wick's theorem to correlation functions of three or more operators. This implies that all correlation functions of odd order will vanish.We then get

$$\begin{aligned}\langle[\delta^{\dagger}(z)\delta(z'),H]\rangle = \quad & \left(T^{B}(z') - T^{B}(z)\right)\langle\delta^{\dagger}(z)\delta(z')\rangle + \\ & \gamma\left[2|\phi_0(z')|^2\langle\delta^{\dagger}(z)\delta(z')\rangle + \phi_0^2(z)\langle\delta^{\dagger}(z)\delta^{\dagger}(z')\rangle - \right. \\ & \left. 2|\phi_0(z)|^2\langle\delta^{\dagger}(z)\delta(z')\rangle - \phi_0^{*2}(z')\langle\delta(z)\delta(z')\rangle\right] + \\ & \gamma\left(\langle\delta^{\dagger}(z)\delta^{\dagger}(z')\rangle\langle\delta(z)\delta(z')\rangle + 2\langle\delta^{\dagger}(z')\delta(z')\rangle\langle\delta^{\dagger}(z)\delta(z')\rangle - \right. \\ & \left. 2\langle\delta(z)\delta^{\dagger}(z)\rangle\langle\delta^{\dagger}(z)\delta(z')\rangle - \langle\delta^{\dagger}(z)\delta^{\dagger}(z)\rangle\langle\delta(z)\delta(z')\rangle\right) \\ & V_{bg}\left(\langle\delta^{\dagger}(z)\delta(z')\rangle\langle\phi^{\dagger}(z')\phi(z')\rangle - \langle\delta^{\dagger}(z)\delta(z')\rangle\langle\phi^{\dagger}(z)\phi(z)\rangle\right) +\end{aligned} \tag{2.4}$$

In free space, ϕ_0 becomes a constant, and all two point correlations, which are functions of z,z', become functions of z-z', so that in momentum space they become functions of a single momentum.

Appendix C

Gaussian Integrals

When we use the words "integrate out" in the text, we are referring to performing one of the following integrals.

- Bosons

$$\int \mathcal{D}[\phi(\mathbf{x}), \phi^\dagger(\mathbf{x})] e^{Tr\left[\ -\phi^\dagger(\mathbf{x})\ G^{-1}(\mathbf{x},\mathbf{x}')\ \phi(\mathbf{x}')\ +J^\dagger(\mathbf{x})\ \phi(\mathbf{x})\ +\ J(\mathbf{x})\ \phi^\dagger(\mathbf{x})\ \right]} = \frac{2\pi i}{[det\ G^{-1}(\mathbf{x},\mathbf{x}')]} e^{Tr\left[\ J^\dagger(\mathbf{x})\ G(\mathbf{x},\mathbf{x}')\ J(\mathbf{x})\ \right]}$$

$$\frac{1}{[det\ G^{-1}(\mathbf{x},\mathbf{x}')]} = e^{-Tr\left[\ ln\ G^{-1}(\mathbf{x},\mathbf{x}')\ \right]}$$

- Fermions

$$\int \mathcal{D}[\psi(\mathbf{x}), \psi^\dagger(\mathbf{x})] e^{Tr\left[\ -\psi^\dagger(\mathbf{x})\ G^{-1}(\mathbf{x},\mathbf{y})\ \psi(\mathbf{y})\ +J^\dagger(\mathbf{x})\ \psi(\mathbf{x})\ +\ J(\mathbf{x})\ \psi^\dagger(\mathbf{x})\ \right]} = \Big[det\ G^{-1}(\mathbf{x},\mathbf{y})\Big]\, e^{Tr\left[\ J^\dagger(\mathbf{x})\ G(\mathbf{x},\mathbf{y})\ J(\mathbf{x})\ \right]}$$

$$\Big[det\ G^{-1}(\mathbf{x},\mathbf{y})\Big] = e^{Tr\left[\ ln\ G^{-1}(\mathbf{x},\mathbf{y})\ \right]}$$

In the above expressions, ϕ refers to a bosonic field, while ϕ refers to a fermionic (Grassman) field. Details of how these formulas are derived are very well explained in chapter 1 of [64].

Appendix D

Reduced Units

In this section we wish to introduce a set of natural units which we found useful to approach the problem. In particular we chose as fundamental energy unit the Fermi energy E_f of the atomic Fermi gas at $\nu \to \infty$. As a length scale we chose the inverse of the Fermi wavenumber k_f, and as time we chose the "Fermi period" $\tau_f = h/E_f$. In terms of these units the various quantities of interest can be converted from standard units to reduce units by multiplying by the respective factors in the table below.

Physical Quantity	Multiplicative Factor
mass	E_f/k_f^2
density	$1/k_f^3$
4-point coupling (V_{bg}, γ)	$k_f^{3/2}/E_f$
3-point coupling (g)	k_f^3/E_f

For magnetic field we define the unit via the product $\delta_B B = \nu$, which has units of energy.